ELASTICITY THEORIES FOR CATIONIC LIPID AND DNA COMPLEXES

Corey S. O'Hern

A DISSERTATION

in

DEPARTMENT OF PHYSICS AND ASTRONOMY

Presented to the Faculties of the University of Pennsylvania in Partial Fulfillment of the Requirements for the Degree of Doctor of Philosophy

1999

Tom Lubensky

Supervisor of Dissertation

Nigel Lockyer

Graduate Group Chairperson

ACKNOWLEDGEMENTS

Obtaining a Ph.D. in physics at Penn was a difficult task. Research consumed most of my energy. Oftentimes, instead of enjoying a Saturday with Jennifer, I forced myself to work. Jennifer's understanding and ability to occasionally dislodge me from physics have made the years in Philadelphia more enjoyable. In fact, getting a Ph.D. would have been unbearable without her. Jennifer is far more important than my degree. I thank her for supporting my career and look forward to an exciting time in Los Angeles. I also thank Mom and Dad; they are my greatest advocates. Semi-annual trips to Merritt Island rejuvenate me and remind me that there is more to life than physics. Having Grandma in Lancaster has also been a blessing; I thank her for being a part of my life.

Choosing Tom Lubensky as my advisor at Penn was an excellent decision. His open-door policy allowed close collaboration, which is one of the more enjoyable aspects of physics research. Tom is one of the most intelligent and hardest-working physicists I know. I also thank Randy Kamien for his friendship and mentorship. He gave crucial advice when I was preparing job talks in the Fall of 1998. I also thank Dave Pettey for his keen physics and financial insight and Dave Moroz for preventing me from being too naive. I thank Mike Cohen for tennis matches and his E&M expertise. Finally, I thank Dave Egolf for introducing me to physics at Duke and look forward to collaborating with him in the future.

ABSTRACT

ELASTICITY THEORIES FOR CATIONIC LIPID AND DNA COMPLEXES

Corey S. O'Hern

Tom Lubensky

DNA and certain species of cationic and neutral lipids self-assemble into lamellar complexes when mixed in water. X-ray scattering experiments have determined that these complexes are highly organized with DNA molecules located in the galleries between lipid bilayers. Within each gallery, DNA molecules form a two-dimensional (2D) smectic lattice. We model the lipid and DNA complexes as three-dimensional stacks of weakly-coupled 2D smectic lattices and study the phase diagram of this model as a function of temperature. The various phases are distinguished by the strength of the translational and orientational correlations between neighboring smectic lattices. For example, it is possible for a columnar phase to form at low temperature with long-range translational correlations between smectic lattices. In the columnar phase, the DNA molecules form a 2D crystal lattice in the plane perpendicular to their column axes, and there is a nonzero shear modulus for sliding neighboring lattices relative to each other. As temperature is increased, thermal fluctuations may induce a second-order phase transition to the *sliding columnar* phase. This phase is characterized by strong in-plane smectic correlations, a vanishing shear modulus for sliding lattices across each other, and a nonvanishing orientational rigidity for rotat-

ing lattices relative to each other. Thus, neighboring lattices are able to slide but not rotate relative to each other without energy cost. We calculate several important structural properties of the sliding columnar phase, for instance, the sliding columnar density-density correlation and structure functions. The sliding columnar correlation function is unique in that in-plane correlations are weaker than any power-law and decay with separation r as $\exp[-\ln^2 r]$. We also calculate the energy cost for edge dislocations in the sliding columnar phase and show that, at the longest lengthscales, a dislocation unbinding transition from the columnar to the nematic lamellar phase precludes the columnar to sliding columnar phase transition. However, if further-neighbor orientational interactions between smectic lattices are permitted, there is a temperature range where the sliding columnar phase is thermodynamically stable.

Contents

List of Figures

List of Tables

Chapter 1

Introduction

1.1 Components of Cationic Lipid and DNA Complexes

Cationic lipid (CL) and DNA complexes are composed of linear DNA molecules and both cationic and neutral lipid molecules. DNA consists of a sequence of base pairs or nucleotides that are stacked in a helical fashion and connected to one another by two sugar-phosphate backbones. This sequence of base pairs carries the genetic information for each organism. For the experiments discussed in this thesis, the density of DNA is small enough that the helical nature of DNA is not important. Recent experiments on the complexes have used DNA extracted from the λ-phage virus with a contour length $l_{\rm DNA} \approx 16\mu m$[26, 28, 29]. At long lengthscales, DNA can be thought of as a long, semi-flexible polymer with a persistence length $\xi_p = 500$Å. In solution, polymers make a random walk with step size ξ_p, and thus the mean-square head-to-tail displacement is much smaller than the contour length. The phosphate groups along the backbones are negatively charged with one charge per 1.7Å. Since

DNA is highly charged, many positive counterions are confined to a small region near the DNA molecule. This counterion confinement, termed Manning condensation, reduces the effective charge density of DNA in solution by a factor of 0.24. (See [25] for general references on Manning condensation.)

CL-DNA complexes are also composed of lipid molecules. Lipids are amphiphilic molecules with one or several hydrophobic hydrocarbon tails and a water soluble head. The amphiphilic nature of the lipids causes them to form bilayer structures in water which shield the tails from the water. Lipid bilayers are made by superimposing two lipid layers tail to tail. In this configuration, the tails are buried and the heads are exposed to water. The shape of the bilayer structure depends on the packing configuration of the tails. For instance, spherical liposomes form when the tails adopt a wedge shape and take up much more lateral area than the heads. The cationic and neutral lipids used in the above experiments form spherical liposomes with diameter approximately 700Å when mixed in water.

1.2 Motivation

The structural properties of CL-DNA complexes have received attention recently from both the biochemistry and physics communities. Much of the interest from the biochemistry community stems from the fact that CL-DNA complexes are now used in gene therapies against genetic diseases such as cystic fibrosis[7, 8]. CL-DNA

complexes are non-viral vectors that transport DNA into the cell nucleus. They are often preferred over viral vectors because the complexes do not invoke an unwanted immune response. Researchers are now able to build positively charged liposomes which envelope the DNA and transport it across the negatively charged outer cell wall and nuclear membrane. Once it crosses the nuclear membrane, the extra-cellular DNA can replace defective or missing genes. Two technical barriers confronting gene therapy are transporting extra-cellular DNA to the nucleus and coaxing the cell into expressing the therapeutic DNA sequence. These barriers are formidable and gene expression rates are low. The hope is that researchers will eventually be able to design CL-DNA complexes with material properties that lead to the highest rate of gene expression.

The physics community is interested in understanding the structure of CL-DNA complexes because they are new soft materials composed of both polymers and lipid bilayers. The structural properties and phase behavior of systems composed of either polymers or lipid bilayers have been studied extensively in the past[17, 27], however, relatively little is known about mixtures of the two. Researchers have recently performed X-ray scattering and light microscopy experiments to probe the internal structure of CL-DNA complexes from micron to Angstrom length scales[26, 28, 29]. They found that DNA and lipids self-assemble into micron-sized aggregates with local liquid-crystalline order. The focus of this thesis is first to enumerate the possible

equilibrium phases for CL-DNA complexes and then to determine the structural properties of each phase. The equilibrium phases will possess varying degrees of positional and orientational order with the most ordered phases occurring at low temperature and more disordered occurring at high temperatures.

1.3 X-ray Scattering Experiments

Researchers have determined from optical microscopy that DNA and cationic liposomes form micron-sized liquid-crystalline spherulites when they are mixed in water[26, 28, 29]. They surmised that both DNA and lipid were located within the spherulites by alternating the fluorescent labeling modes (YOYO Blue labeled DNA and Texas Red labeled cationic liposomes). Large spherulites of DNA and lipid form when both DNA and cationic liposomes release their counter-ions to solution, and the negatively charged DNA molecules condense on the cationic liposomes. The counter-ion release results in a large reduction in the free energy due to the increase in entropy of the counterions. The formation of the spherulites was studied as a function of the mass ratio of lipid to DNA, L/D, where L is the total mass of the lipid including both cationic and neutral species and D is the total mass of DNA. Near the isoelectric point, where the total charge of the DNA is equal to the total charge of the lipid, the spherulites are charge neutral and form chain-like structures due to Van der Waals attractions. Away from the isoelectric point, the complexes are highly

charged and thus repel each other.

The Angstrom-scale local structure of the complexes was probed using small-angle X-ray scattering. Scattering experiments measure the structure function $I(\mathbf{q})$, which is the Fourier transform of the density-density correlation function. If the spherulites possess periodic positional order, $I(\mathbf{q})$ will be peaked at wavenumbers equal to reciprocal lattice vectors. The structure functions from three-dimensional crystals and columnar liquid-crystal phases possess delta-function Bragg peaks since thermal fluctuations do not destroy long-range positional order. However, the displacement fluctuations in one- and two-dimensional crystals diverge with system size, and, as a result, peaks in $I(\mathbf{q})$ decay much more slowly with $\mathbf{q}$. For instance, quasi-Bragg peaks for a 1D crystal existing in three spatial dimensions (or a 3D smectic liquid-crystal) decay as a power-law[1].

The X-ray scattering experiments were performed by groups at the University of California, Santa Barbara (UCSB)[26, 28, 29] and the Munich Technical University[3, 33]. Both groups mixed cationic liposomes with linear DNA in pure water, measured the scattering function at the isoelectric point, and tuned the mass ratio of neutral to cationic lipid $\nu = m_0/m_+$ to change the structural parameters of the complexes. Since

$$\frac{L}{D} = \frac{m_+ + m_0}{m_-} = \frac{m_+}{m_-}\left(1+\nu\right), \tag{1.1}$$

where m_- is the mass of DNA, ν and L/D can be varied without moving away

from the isoelectric point, $m_+/m_- = \text{const}$. However, the two groups used different cationic and neutral lipid species and performed the experiments in different temperature regimes. For instance, the UCSB group studied the high-temperature regime where the complexes are less ordered, and the Munich group studied a wide range of temperatures including the low-temperature regime where the complexes are more ordered because thermal fluctuations and topological defects are suppressed.

1.3.1 High-Temperature Regime

We first discuss the X-ray scattering experiments performed at room temperature by the UCSB group. These researchers used liposomes composed of cationic DOTAP (dioleoyl-trimethylammonium-propane) and neutral DOPC (dioleoyl-phosphatidylcholine). The cationic liposomes had a charge density $\sigma \approx e/100\text{Å}^2$ and a bilayer thickness of $\delta_m \approx 40\text{Å}$. Their main result is summarized in Fig. 1.1 obtained from Ref. [28], which shows four structure functions with L/D decreasing from top to bottom. Two types of peaks are found in each $I(q)$: one type is narrow and occurs at $q_{00n} = 2\pi n/a$, where n is an integer and $a \approx 65\text{Å}$ is the lamellar spacing; the second type is broad, has fewer reflections, and its primary reflection occurs at $q_0 \equiv q_{DNA} = 2\pi/d$, where d is the spacing between DNA molecules. The lamellar peaks are quasi-Bragg peaks corresponding to 3D smectic ordering of the lipid bilayers. However, the lineshape of these peaks differs significantly from the standard 3D

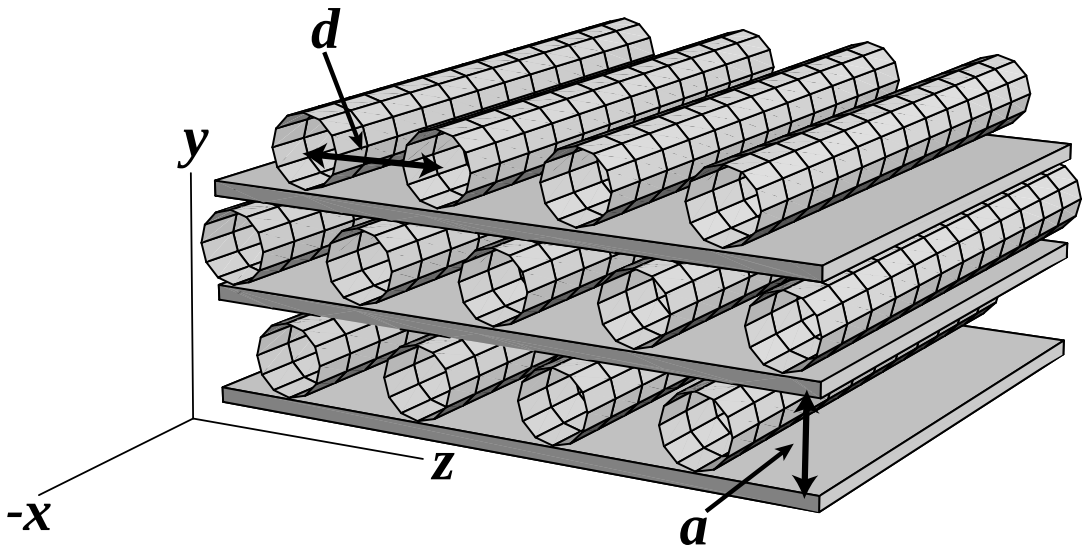

Figure 1.1: Small-angle X-ray scattering intensities from the charge-neutral CL-DNA complexes studied in Ref. [28]. The scattering intensities are shown as a function of the mass ratio of lipid to DNA L/D, with L/D decreasing from top to bottom. The sharp quasi-Bragg peaks arising from the lamellar structure do not vary with L/D, however, the much broader peaks arising from interactions between DNA strands shift to larger q as L/D is decreased. The inset shows a second DNA reflection in the $L/D = 5.5$ scan.

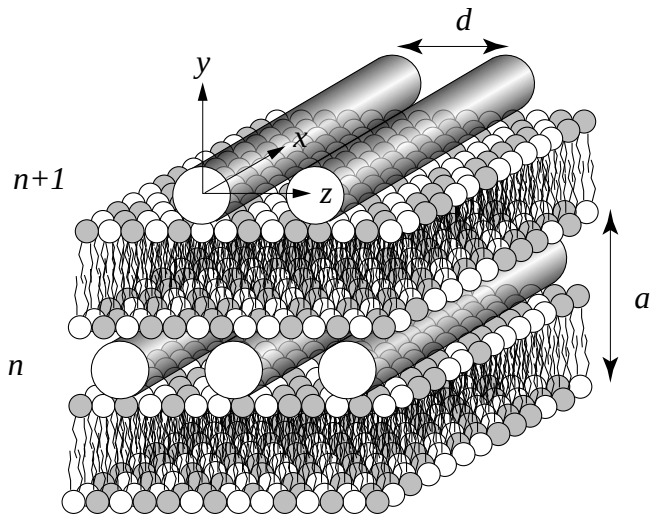

Figure 1.2: Schematic representation of CL-DNA complexes. Parallel strands of DNA form 2D smectic lattices with lattice spacing d in galleries between lipid bilayers with spacing a. Charged and neutral lipid heads are, respectively, shaded and unshaded. DNA strands are aligned parallel to the x axis and the y axis is normal to the lipid planes.

smectic Caillé form[1] because the bending rigidity of the lipid bilayers is anisotropic, i.e. the bending rigidity is greater along the direction of the DNA molecules[28]. The broad DNA peaks imply that there are divergent positional fluctuations and that the DNA molecules are confined to two dimensions.

The X-ray scattering results suggest the following picture for the internal structure of DNA-lipid complexes. The lipids form bilayer membranes that stack in the lamellar structure shown in Fig. 1.2. In the galleries between lipid bilayers, parallel DNA strands are arranged on one-dimensional lattices with spacing d. The lamellar spacing a is the sum of the membrane thickness δ_m and a water gap δ_w between two neighboring bilayers. $\delta_m \approx 40$Å was determined from X-ray scattering in the absence

of DNA. Thus, the water gap $\delta_w \approx 25$Å is large enough to accommodate a single DNA molecule with $2r_{DNA} = 20$Å and a hydration layer. The peaks in $I(q)$ corresponding to the lamellar spacing are relatively insensitive to changes in the mass ratio of neutral to cationic lipid ν. However, the DNA spacing increases (q_0 decreases) linearly with ν in the range 25Å$< d <$ 60Å. d scaling with ν is consistent with the constraint of charge neutrality of the complex, i.e. DNA molecules spread out as cationic lipids become more dilute.

The UCSB group first attempted to fit the structure function to a collection of decoupled 2D smectics. The DNA strands within each gallery form a 2D smectic liquid-crystal with periodic positional order along the z-direction and fluid-like order in the x-direction. The harmonic free energy for a collection of 2D smectics with vanishing correlations in the y-direction is

$$F = \frac{1}{2} \sum_n \int d^2r \left[B_2 (\partial_z u_z^n)^2 + K_2 (\partial_x^2 u_z^n)^2 \right], \tag{1.2}$$

where B_2 is the compression modulus,

$$K_2 = \frac{T\xi_p}{2d} \tag{1.3}$$

is the bending modulus, and $u_z^n(\mathbf{r})$ is the z-displacement of the molecule in gallery n with in-plane position $\mathbf{r} = (x, z)$. A term proportional to $(\partial_x u_z^n)^2$ is missing from Eq. 1.2 because a constant $\partial_x u_z^n$ corresponds to a uniform tilt of the 2D smectic layers, and uniform rotations do not cost energy. Note that this free energy does not

couple fluctuations of the bilayers to z-displacements of the DNA columns and does not couple z-displacements of DNA columns in different galleries.

From Eq. 1.2, one can calculate the density-density correlation function in real space

$$S(\mathbf{r}) = \exp\left[iq_0(u_z^0(\mathbf{r}) - u_z^0(0))\right] \tag{1.4}$$

and then Fourier transform to find the structure function. In the harmonic approximation, $S(\mathbf{r}) = \exp[-q_0^2 g_u(\mathbf{r})]$, where the position fluctuations $g_u(\mathbf{r}) \equiv \frac{1}{2}\langle(u_z^0(\mathbf{r}) - u_z^0(0))^2\rangle$ are calculated from equipartition. We find

$$\begin{aligned} g_u(\mathbf{r}) &= T\int \frac{d^2q}{(2\pi)^2}\frac{1-\cos[\mathbf{q}\cdot\mathbf{r}]}{B_2 q_z^2 + K_2 q_x^4} \\ &= \frac{T}{2B_2}\sqrt{\frac{|z|}{\pi\lambda}}\left[\exp\left[\frac{-x^2}{4\lambda|z|}\right] + \frac{1}{2}\sqrt{\frac{\pi}{\lambda|z|}}|x|\mathrm{erf}\left(\frac{|x|}{2\sqrt{\lambda|z|}}\right)\right], \end{aligned} \tag{1.5}$$

where $\lambda = \sqrt{K_2/B_2}$. Note that in two dimensions, mean-square displacement fluctuations diverge as a power-law with system size, and thus the correlation function is short-ranged. To see this explicitly, set $z = 0$ in the above equation. In this case, $S(x,0) = \exp[-x/\xi_x]$ with $\xi_x = \lambda B_2 d^2/\pi^2 T$. Also, when $x = 0$ $S(0,z) = \exp[-\sqrt{z/\xi_z}]$ with

$$\xi_z = \left(\frac{B_2 d^2}{2\pi^{3/2}T}\right)^2 \lambda. \tag{1.6}$$

Correlations are stronger in the z-direction due to the periodic positional order.

The prepared samples were not single crystals and consisted of many subdomains with randomly oriented smectic layer normals. Thus, a powder-average over the angle

ϕ in the xz plane was necessary. The 2D powder-averaged structure function for this model is given by

$$I(q) = \frac{1}{2\pi}\int_{-\pi}^{\pi} d\phi \int d^2 r S(\mathbf{r}) e^{-i(\mathbf{q}-q_0\hat{z})\cdot\mathbf{r}} e^{-\mathbf{r}^2\pi^2/L^2}, \tag{1.7}$$

where L is the average size of a subdomain and $\mathbf{q} = (q_x, q_z)$. The Gaussian factor, $\exp[-\mathbf{r}^2\pi^2/L^2]$, provides a finite-size correction that disfavors subdomains with size greater than L. The fitting parameters d, L, and B_2 were then used to fit Eq. 1.7 to the DNA peak. However, Eq. 1.7 did not fit the data. When the theoretical curves were forced to match the data on the left side of the peak, the fitting functions were significantly larger than the data on the right side of the peak.

To obtain a better fit, interactions between 2D smectic lattices were required. Thus, they introduced exponentially decaying positional correlations between 2D smectic lattices in neighboring galleries. In addition, a cylindrical form factor was used to account for the finite radius of DNA. With the previous three fitting parameters and ξ_y, the correlation length in the y-direction, a reasonable fit was obtained. They found that $L \sim 1000$Å, and the domain size did not vary systematically with d. In addition, B_2 was in the range 10^{-1} to $10^{-2} T/\text{Å}^2$, decreased with increasing d, and obeyed the relation

$$B_2 \propto \pi T \frac{d}{l_B} \frac{1}{(d-\rho)^2}. \tag{1.8}$$

The $\mathcal{O}(1)$ proportionality factor is obtained by fitting to the X-ray scattering data. This expression for the compression modulus was derived previously in Ref. [28]

and includes both the electrostatic repulsion of the DNA rods and the pressure of condensed counterions. $\rho \approx 4.4$Å is an effective radius for the DNA strands, $l_B = e^2/\epsilon T \approx 7$Å is the Bjerrum length, and $\epsilon \approx 80$ is the dielectric constant of water. Thus, both the DNA bending and compression moduli can be obtained from X-ray scattering experiments on DNA-lipid complexes.

The correlation length perpendicular to lipid bilayers, ξ_y, increased with d in the range 10 to 60Å but was always less than the lamellar spacing $a = 65$Å. This implies that positional correlations between DNA molecules in neighboring galleries are extremely weak. Thus, a model with strong orientational and weak positional correlations between 2D smectic lattices in neighboring galleries may also yield a better fit compared to the one obtained using the decoupled model. A model with strong orientational and weak positional correlations will be discussed extensively in Ch. 3. Positional correlations between DNA molecules in neighboring galleries increase as the temperature decreases. At sufficiently low temperatures, a columnar phase forms in which there is a nonzero shear modulus that prevents one lattice of DNA molecules from shifting relative to neighboring lattices. In fact, a phase with centered rectangular symmetry in the yz plane was found in the low-temperature experiments on CL-DNA complexes performed by the Munich group, and these are described below.

1.3.2 Low-Temperature Regime

The Munich group studied mixtures of calf thymus DNA and cationic liposomes in pure water in the temperature range 15 to 55°C[3]. The cationic liposomes were composed of neutral DMPC and cationic DMTAP. The Munich group replaced the dioleoyl with dimyristoyl lipids; the dimyristoyl lipids undergo a chain order-disorder transition from the L_α^c to the $L_{\beta'}^c$ phase as temperature is increased[33]. They found that DNA and cationic liposomes self-assembled into liquid-crystalline aggregates throughout the temperature range. To investigate the internal structure of the complexes, they measured the small- and wide-angle X-ray scattering intensity at the isoelectric point of the complexes as a function of temperature and the mass ratio of neutral to cationic lipid. They obtained the spacing between DNA molecules from small-angle scattering. From the wide-angle scattering, they obtained the much smaller spacing between lipid molecules. Representative structure functions for the low- and high-temperature regimes are shown in Fig. 1.3. The structure function at 55°C reproduces the results from the UCSB experiments. Lamellar peaks occur at $q_{00n} = 2\pi n/a$ and a single, diffuse DNA peak occurs at $q_0 = 2\pi/d$. Thus, they confirmed that DNA strands are found in the galleries between lipid bilayers and within each gallery the DNA strands are situated on a one-dimensional lattice with spacing d. At high temperatures, neighboring lattices are positionally decoupled, and a model composed of weakly-coupled 2D smectics fits the scattering function.

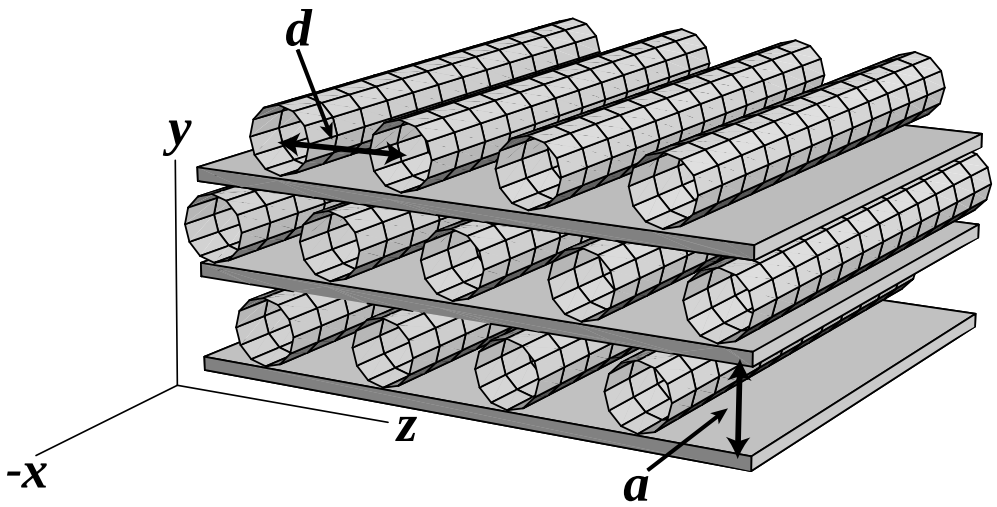

Figure 1.3: The small- and wide-angle X-ray scattering intensities from the CL-DNA complexes studied in Ref. [3]. The top and bottom curves show the X-ray scattering intensities at 15°C and 55°C respectively. The sharp quasi-Bragg peaks indicate the well-defined lamellar structure. The arrows highlight the much broader peaks from the intercalated DNA strands. The low-temperature scattering intensity possesses several DNA peaks while the high-temperature scattering intensity possesses a single, broad DNA peak. The wide-angle scattering shows that the $L^c_{\beta'}$ phase with strong positional correlations between lipid molecules in each layer forms at low-temperature, whereas the L^c_α phase with much weaker positional correlations forms at high-temperature.

The low-temperature (15°C) small-angle scattering intensity from the intercalated DNA strands differs from the high-temperature scattering intensity. Multiple DNA peaks occur, and they are not positioned at integer multiples of q_0. Instead, the peaks can be indexed to

$$q_{h,k} = 2\pi\sqrt{\left(\frac{h}{d}\right)^2 + \left(\frac{k}{2a}\right)^2}, \tag{1.9}$$

where h and k are integers and $h+k$ is even. In Fig. 1.3, the $q_{1,1}$, $q_{1,3}$, and $q_{1,5}$ peaks are present. These peaks imply that the DNA molecules are located on average on a centered rectangular lattice in the yz plane with lattice vectors $\mathbf{a}_1 = a\hat{y} + d/2\hat{z}$ and $\mathbf{a}_2 = -a\hat{y} + d/2\hat{z}$. (See Fig. 1.2.) The DNA spacing d changed with ν, while the lamellar spacing $a \approx 73$Å remained constant. The low-temperature wide-angle scan showed that short-range positional order in the lipid bilayers accompanied the formation of the phase with centered rectangular symmetry. The wide-angle peak yields $l \approx 4$Å for the average in-plane separation between lipid molecules.

The phase with centered rectangular symmetry can be distinguished from a phase with rectangular symmetry and lattice constants a and d in the y- and z-directions since the structure function from the latter would possess a (1,0) peak. Electrostatic interactions favor the centered rectangular arrangement since it maximizes the separation between DNA strands in adjacent galleries.

Relative displacement fluctuations between two DNA strands in neighboring galleries increase with temperature and cause the centered rectangular peaks to become

weak and diffuse. At high temperatures, it may be possible for the positions of strands in neighboring galleries to become completely uncorrelated. If the positions of strands in neighboring layers are uncorrelated, the centered rectangular peaks in the structure function are smeared in the q_y-direction, and instead maximum intensity occurs at $\mathbf{q} = hq_0\hat{z}$. However, at intermediate temperatures where there are nonvanishing positional correlations between strands in neighboring galleries, one would expect centered rectangular peaks in the structure function at $\mathbf{q}_{h,k}$ with $h + k$ even. More work must be done to determine whether the lowest order DNA reflection in the high-temperature X-ray scattering data[28, 29] is located at $q_{1,0}$ or $q_{1,1}$. At the largest DNA separations, the (1,0) and (1,1) peak positions differ by 10 per cent.

Only three DNA peaks ($q_{1,1}$, $q_{1,3}$, and $q_{1,5}$) are discernible in the low-temperature structure function in Fig. 1.3. However, in a true columnar phase, one expects many Bragg reflections. One possible cause for the small number of reflections is the DNA form factor which decays rapidly with $q_{h,k}r_{\mathrm{DNA}}$. Thus, peaks with $k > 5$ are suppressed. Also, visible peaks have $k > h$ because $2a \gg d$, and thus peaks with large h are extinguished before those with large k.

Short-ranged positional order in the yz plane also leads to the *broadening* of the low-temperature peaks. Thus, Artzner, *et al.* assumed that the correlation function

$$S(\mathbf{r}, y) = \langle \exp(iq_0[u_z(\mathbf{r}, y) - u_z(0)]) \rangle = \exp[-h^2(y/\xi_y + z/\xi_z)] \tag{1.10}$$

decayed exponentially in both the y- and z-directions. In the above expression, ξ_z

and ξ_y are the in-plane and out-of-plane correlation lengths, and $u_z(\mathbf{r}, y)$ is the continuum version of $u_z^{y/a}(\mathbf{r})$. They further assumed that the correlation function does not depend on the index k since the peak widths were independent of k. With these assumptions, the Fourier transform of the correlation function becomes a product of two Lorentzians. They then powder-averaged the single-crystal result and found that the structure function $I(q)$ is a sum of Lorentzians with widths that depend on h^2 and the correlation lengths. ξ_y, ξ_z, and a were then used as fitting parameters to fit $I(q)$ to the scattering data. They found that $\xi_y \approx 250$Å was an order of magnitude smaller than ξ_z, and thus positional correlations are stronger in the z-direction. Further analysis is required to determine whether the low-temperature X-ray scattering data is evidence for a nematic lamellar phase or the new sliding columnar phase discussed in Ch. 3. (See Sec. 3.5.2 for a calculation of the structure function from the sliding columnar phase.)

1.4 Phase Diagram

In this section, a possible phase diagram for CL-DNA complexes as a function of temperature is discussed. We will focus on lamellar phases where DNA molecules are located in galleries between lipid bilayers. We assume that fluctuations of the lipid bilayers are small, and thus the bilayers confine DNA molecules to well-defined, equally-spaced planes. The various lamellar phases are distinguished by the strength

of the correlations that exist between DNA strands in neighboring galleries. For instance, in a columnar phase DNA strands form a 2D lattice in the yz plane, and the positions of DNA in neighboring galleries are strongly correlated. As temperature increases, thermal fluctuations destroy the positional correlations between DNA in neighboring galleries, and the decoupled 2D smectic phase is the theoretical limit in which no correlations exist.

As discussed in Sec. 1.3.1, the high-temperature scattering intensity from CL-DNA complexes did not fit the decoupled 2D smectic model. In order to obtain a reasonable fit, weak correlations between DNA strands in neighboring galleries were required. In addition, the low-temperature scattering intensity in Fig. 1.3 did not display Bragg peaks that are expected for a true columnar phase. Instead, the $q_{1,1}$, $q_{1,3}$, and $q_{1,5}$ peaks were smeared in the q_y- and q_z-directions. This diffuse scattering indicates that DNA displacement fluctuations are large, and positional correlations between DNA strands in neighboring galleries are weak. The X-ray scattering data from both high- and low-temperature regimes suggest that there is an intermediate phase in CL-DNA complexes with weak positional correlations between neighboring 2D smectic lattices. One possibility is the sliding columnar phase with weak positional but strong orientational correlations between neighboring 2D smectic lattices. The weak positional correlations allow lattices to shift relative to each other without energy cost. The possible phases for CL-DNA complexes with 2D smectic order in the xz

plane are listed below.

1. Columnar Phase: In this low-temperature phase, the positions of DNA strands in neighboring 2D smectic lattices are strongly correlated, and DNA are situated on a 2D crystal lattice in the yz plane. This phase has a nonzero shear modulus, and thus DNA strands in adjacent galleries cannot shift relative to each other without an energy cost.

2. Sliding Columnar Phase: This intermediate phase is characterized by strong orientational but weak positional correlations between neighboring 2D smectic lattices. The orientational coupling is sufficiently strong that DNA in different galleries point on average in the same direction. This phase differs from the columnar phase in that it does not have long-range 2D crystalline order in the yz plane, and its shear modulus for sliding 2D smectic lattices relative to each other is zero.

3. Decoupled 2D Smectic Phase: In this phase there are no correlations between 2D smectic lattices in different galleries. In Sec. 2.3, we find that this phase does not exist at the longest lengthscales.

Less ordered phases occur when topological defects melt the 2D smectic lattices and destroy the in-plane positional order along z. After the 2D smectic lattices melt, DNA strands in each layer form a nematic phase with in-plane orientational order.

Even in the nematic phase, however, there are short-range positional correlations and diffuse peaks occur in the structure function at the reciprocal lattice vectors $\mathbf{q}_{h,k}$. If the nematic directions in neighboring layers are strongly correlated, a nematic lamellar phase forms with true long-range orientational order. In contrast, a sliding nematic lamellar phase forms when there are only weak orientational correlations between layers, and nematic directions vary from layer to layer. The properties of the various nematic phases are summarized below.

1. Nematic Lamellar Phase: In this phase, the nematic directions in each gallery are strongly correlated, and the system displays true three-dimensional long-range nematic order.

2. Sliding Nematic Lamellar Phase: Each layer has in-plane nematic order, however, the nematic directions in neighboring layers are only weakly correlated and can rotate relative to one another without energy cost.

3. Isotropic Lamellar Phase: In this phase, in-plane orientational order is destroyed, DNA strands within a gallery no longer point on average along a common direction, and each layer behaves as an isotropic fluid.

Note that the phase sequence nematic lamellar $\rightarrow$ sliding nematic lamellar is analogous to the phase sequence columnar $\rightarrow$ sliding columnar. The former sequence proceeds from coupled to decoupled in-plane orientations and the later proceeds from

coupled to decoupled in-plane positions. Properties of the sliding nematic lamellar phase, in particular the stability of the phase in the presence of vortex excitations, are discussed in Ref. [22].

1.5 Survey of Thesis

The bulk of the thesis will focus on deriving the elasticity theory and determining the structural properties of the new sliding columnar (SC) phase of matter. Ch. 2 begins by proposing a model for CL-DNA lipid complexes; the model is a stack of interacting 2D smectics. In Sec. 2.3, we couple the positions and orientations of nearest-neighbor 2D smectic lattices and show that the sliding columnar phase, not the decoupled 2D smectic phase, exists at the longest lengthscales. Then in Ch. 3, we determine the behavior of the sliding columnar phase in the presence of thermal fluctuations. For instance, in Sec. 3.2 we find that the mean-square displacements in the SC phase display unusual quasi-two-dimensional behavior and diverge as $\ln^2 L$, where L is the characteristic system size in the xz plane. The SC displacement fluctuations are not as large as 2D smectic displacement fluctuations that diverge as a power-law with system size, however, thermal fluctuations still destroy true long-range positional order. The behavior of the displacement fluctuations implies that the correlation function decays as $S(\mathbf{r}, 0) \sim \exp[-\ln^2 r]$, where r is the in-plane separation. In Sec. 3.3, we investigate the second-order transition from the columnar to the sliding

columnar phase. We show that there is a decoupling transition temperature, T_d, above which the positional coupling between 2D smectic lattices is irrelevant and the sliding columnar phase is stable and below which the positional coupling is relevant and the columnar phase is stable.

In Ch. 4, we derive the nonlinear elasticity for the sliding columnar phase. The rotationally invariant theory for the sliding columnar phase contains anharmonic terms that lead to renormalizations of the SC elastic constants similar to the Grinstein-Pelcovits renormalization of the elastic constants in smectic liquid-crystals[11]. We calculate these renormalizations at the critical dimension $d = 3$ and find that the elastic constants scale logarithmically with wavenumber q at long wavelengths. We use dimensional regularization rather than a hard-cutoff renormalization scheme because ambiguities arise in the one-loop integrals with a finite cutoff as shown in App. E.

Topological defects in the sliding columnar phase are discussed in Ch. 5. The energy of an isolated edge dislocation and pairs of dislocations in different layers in the sliding columnar phase scales logarithmically with system size as shown in Sec. 5.2. Thus, the sliding columnar phase will Kosterlitz-Thouless melt to a nematic lamellar phase above an in-plane dislocation unbinding temperature T_{KT}. Above T_{KT}, edge dislocations within each layer renormalize the compression modulus B to zero and destroy the smectic order in the xz plane. Hence, the necessary condition for the existence of a stable sliding columnar phase is $T_d < T_{KT}$. In Sec. 5.4, we show that

$T_d > T_{KT}$ for the sliding columnar model with orientational interactions between only nearest-neighbor lattices. Thus, the sliding columnar phase with nearest-neighbor interactions is unstable to the proliferation of edge dislocations, and the phase sequence proceeds from the columnar phase to the nematic lamellar phase as temperature is increased. However, we will show in a forthcoming publication [23] that if orientational interactions between further-neighbor lattices are included, T_d can be tuned below T_{KT}. When $T_{KT} > T_d$, there is a temperature window $T_d < T < T_{KT}$ in which the sliding columnar phase is the thermodynamically stable phase, and the phase sequence proceeds from the columnar phase to the sliding columnar phase and then to the nematic lamellar phase as temperature is increased.

We conclude in Ch. 6 by estimating several crossover lengths. The density-density correlation function $S(\mathbf{r})$ for a three-dimensional stack of 2D smectic lattices displays different functional forms depending on the magnitude of the in-plane separation $\mathbf{r}$. The crossover lengths delineate the different regions and determine where the crossovers from harmonic 2D smectic behavior to nonlinear 2D smectic behavior and 3D sliding columnar behavior occur. Knowing these characteristic lengthscales is important in determining whether sliding columnar behavior occurs in CL-DNA complexes.

Chapter 2

Theoretical Model of Cationic Lipid and DNA Complexes

2.1 Interacting 2D Smectics

The X-ray scattering experiments on CL-DNA complexes discussed in Ch. 1 showed that DNA and cationic liposomes form a stacked lamellar structure with alternating layers of DNA and lipid bilayers. We therefore first consider a model in which idealized DNA columns are confined to galleries between lipid bilayers in a perfect lamellar structure without dislocations or other defects. The lipid bilayers are parallel to the xz plane, and the DNA columns are aligned on average parallel to the x-axis as shown in Fig. 2.1. In addition, within each gallery the DNA strands form a 2D smectic lattice with spacing $d = 2\pi/q_0$. We assume initially that the lipid bilayers are perfectly flat and do not fluctuate. In this case, the long-wavelength properties of the DNA lattice in gallery n are described by the displacements $u_z^n(\mathbf{r})$ along the z-direction, where $\mathbf{r} = (x, z)$ is a position in the xz plane. The Hamiltonian for the complex is then a sum of independent elastic energies for each gallery and terms coupling the

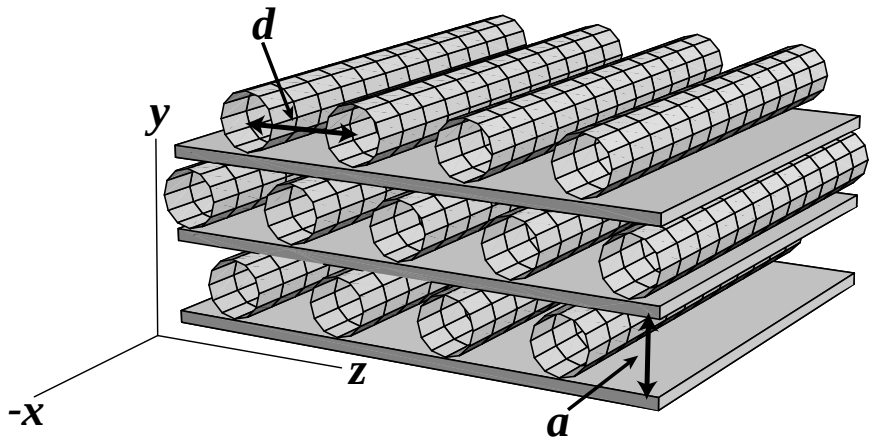

Figure 2.1: Picture of the idealized lamellar structure found in CL-DNA complexes. DNA columns are sandwiched between planar lipid bilayer sheets. The bilayer planes are stacked in the y-direction with spacing a. The DNA columns are oriented in the x direction, and, within each layer, the columns are separated by d.

displacements and angles in neighboring galleries: $\mathcal{H} = \mathcal{H}^{\rm el} + \sum_n (\mathcal{H}^u_n + \mathcal{H}^\theta_n)$ with

$$\begin{aligned} \mathcal{H}^{\rm el} &= \frac{1}{2}\sum_n \int d^2r \left[B_2 (u^n_{zz})^2 + K_2 (\partial_x^2 u^n_z)^2 \right], \qquad (2.1) \\ \mathcal{H}^\theta_n &= -V^\theta \int d^2r \cos[2(\theta^n - \theta^{n+1})], \\ \mathcal{H}^u_n &= -V^u \int d^2r \cos[q_0 (u^n_z - u^{n+1}_z)], \end{aligned}$$

where $\theta^n \approx \partial_x u^n_z$ and

$$u^n_{zz} = \partial_z u^n_z - [(\partial_x u^n_z)^2 + (\partial_z u^n_z)^2]/2 \qquad (2.2)$$

is the nonlinear strain for the 2D smectic lattice in gallery n. B_2 and K_2 are, respectively, the 2D compression and bending moduli. The coupling of displacements in nearest-neighbor galleries arises from electrostatic repulsions between DNA strands,

and thus the 2D shear modulus in the yz plane is proportional to λ^2/d, where λ is the linear charge density of DNA. In addition, electrostatic repulsions favor a centered rectangular lattice in the yz plane with strands in a given layer shifted by $d/2$ along z relative to those in neighboring layers. This arrangement is favored since it maximizes the separation between DNA strands in adjacent layers. The origin of the orientational coupling is steric interactions, i.e. strands can fluctuate more freely if they are aligned and $\theta^n \approx \theta^{n+1}$. Since the DNA strands are invariant under $\theta^n \rightarrow \theta^n + \pi$, the orientational interaction is a function of $2(\theta^n - \theta^{n+1})$.

The particular equilibrium phase that is favored depends on the relative values of B_2, K_2, V^u, and V^θ. At low temperatures, where thermal fluctuations and topological defects are suppressed, the positional coupling V_u and the compression modulus B_2 are large and DNA strands are situated on a 2D lattice in the yz plane. Note that long-range positional order in 2D insures that the DNA strands also possess long-range orientational order. As temperature is increased, both thermal fluctuations and topological defects increase positional disorder. For instance, thermal fluctuations can reduce the positional coupling V_u to zero above a critical decoupling temperature T_d while leaving B_2 and V^θ nonzero. This positionally decoupled phase is termed the sliding columnar phase because neighboring 2D smectic lattices can shift relative to one another without energy cost. However, since V^θ is finite, there is an energy cost for rotating one lattice of columns relative to neighboring lattices. Topological defects

also increase positional disorder. At temperatures above the in-plane dislocation unbinding temperature T_{KT}, edge dislocations cause $B_2 \to 0$, and melt the 2D smectic lattices. V^u is also zero since there is no periodic positional order along z. However, K_2 is nonzero and a nematic lamellar phase forms when the in-plane nematic order is strongly correlated from layer to layer.

We begin the investigation into the phase behavior of the Hamiltonian in Eq. 2.1 by assuming that V^θ and V^u are small. The expectation values of the positional and orientational energies with respect to the decoupled 2D smectic Hamiltonian are then calculated. The interaction energies are irrelevant and can be ignored if their expectation values scale to zero in the limit of infinite system size. The interaction energies are relevant and cannot be ignored if their expectation values scale to infinity in the limit of infinite system size. Before we determine whether the positional and orientational energies are relevant or irrelevant, the fluctuation behavior of 2D smectics should be reviewed.

2.2 Review of 2D Smectic Fluctuations

At lengthscales less than the nonlinear lengths

$$l_x = \frac{K_2^{3/2}}{T\sqrt{B_2}} \quad \text{and} \quad l_z = \frac{l_x^2}{\lambda}, \tag{2.3}$$

with $\lambda = \sqrt{K_2/B_2}$, 2D smectic fluctuations are described by the linearized elastic Hamiltonian with the nonlinear strain replaced by the linear strain $\partial_z u_z^n$[9]. At

lengthscales longer than l_x and l_z, the nonlinear terms in the rotationally invariant strain (Eq. 2.2) are comparable to the linear term and lead to renormalized bending and compression moduli $K_2(\mathbf{q})$ and $B_2(\mathbf{q})$ that respectively diverge and vanish at small wavenumber $\mathbf{q}$. Note that the nonlinear lengths l_x and l_z decrease with increasing temperature, and thus nonlinearities become important at high temperatures. In both the harmonic and nonlinear regimes, the Fourier transformed displacement correlation function in each gallery can be expressed as

$$G(\mathbf{q}) = \frac{T}{B_2(\mathbf{q})q_z^2 + K_2(\mathbf{q})q_x^4} = \frac{T}{B_2} l_z^2 \tilde{q}_x^{-\eta} Q(\tilde{q}_z/\tilde{q}_x^{\mu}), \tag{2.4}$$

where $\tilde{q}_{x,z} = q_{x,z} l_{x,z}$ and

$$\tilde{q}_x^{-\eta} Q(\tilde{q}_z/\tilde{q}_x^{\mu}) \sim \begin{cases} \tilde{q}_x^{-\eta}, & \tilde{q}_z = 0 \\ \\ \tilde{q}_z^{-\eta/\mu} & \tilde{q}_x = 0. \end{cases} \tag{2.5}$$

The scaling form of the correlation function implies that $K_2(q_x, q_z = 0) \sim q_x^{-4+\eta}$ and $B_2(q_x = 0, q_z) \sim q_z^{-2+\eta/\mu}$. In the harmonic regime where $q_{x,z} l_{x,z} > 1$, $K_2(\mathbf{q}) = K_2$ and $B_2(\mathbf{q}) = B_2$ are constants, and the scaling exponents are $\eta = 4$ and $\mu = 2$. In the anharmonic regime $q_{x,z} l_{x,z} < 1$, the scaling exponents η and μ can be calculated exactly by mapping the 2D smectic model with thermal fluctuations onto the KPZ model in $1+1$ dimensions [9]. The exponents in the anharmonic regime are $\eta = 7/2$ and $\mu = 3/2$.

The mean-square displacement fluctuations diverge in both regimes with lengths

L_x and L_z of the sample in the xz plane:

$$\langle u_z^2 \rangle = \int \frac{d^2q}{(2\pi)^2} G(\mathbf{q}) = \lambda^2 \tilde{L}_x^{2\alpha} f_u^{(1)}(\tilde{L}_z/\tilde{L}_x^{\mu}), \tag{2.6}$$

where $u_z \equiv u_z^n$, $2\alpha = \eta - 1 - \mu = 1$ in both regimes, $\tilde{L}_{x,z} = L_{x,z}/l_{x,z}$, $f_u^{(1)}(0) =$ const., and $f_u^{(1)}(w) \sim w^{2\alpha/\mu}$ as $w \to \infty$. This implies that the Debye-Waller factor $\langle \exp[iq_0 u_z] \rangle^2 = \exp[-q_0^2 \langle u_z^2 \rangle] = 0$ in the limit of infinite system size, and there is no long-range positional order at any finite temperature in a 2D smectic, even when there are no dislocations.

Since the mean-square displacement fluctuations diverge as a power-law with system size, the displacement correlation function

$$g_u^{2D}(\mathbf{r}) = \frac{1}{2}\langle [u_z(\mathbf{r}) - u_z(0)]^2 \rangle = \lambda^2 |\tilde{x}|^{2\alpha} f_u^{(2)}(|\tilde{z}|/|\tilde{x}|^{\mu}) \tag{2.7}$$

diverges algebraically with in-plane separation r. In Eq. 2.7, $\tilde{x} = x/l_x$, $\tilde{z} = z/l_z$, and the scaling behavior of $f_u^{(2)}(w)$ is similar to that of $f_u^{(1)}(w)$.

However, fluctuations in $\theta = \partial_x u_z$ are nondivergent due to an additional factor of q_x^2 in the numerator of Eq. 2.6:

$$\langle \theta^2 \rangle = \int \frac{d^2q}{(2\pi)^2} q_x^2 G(\mathbf{q}) = \left(\frac{\lambda}{l_x}\right)^2 f_\theta(\tilde{\Lambda}_z/\tilde{\Lambda}_x^{\mu}), \tag{2.8}$$

where $\Lambda_x = 2\pi/b$, $b \sim 4$Å is the spacing between DNA nucleotides, $\Lambda_z = 2\pi/d$, $\tilde{\Lambda}_{x,z} = \Lambda_{x,z} l_{x,z}$, and $f_\theta(0) =$ const. and $f_\theta(w) \sim w^{2\alpha/\mu}$ for large w. Finite angular fluctuations imply that $\langle \cos\theta \rangle = \exp[-\langle \theta^2 \rangle/2]$ is nonzero, and thus there is long-range orientational order in 2D smectics[31].

2.3 Relevance of the Translational and Orientational Couplings

The coupling energies $\mathcal{H}_n^\theta$ and $\mathcal{H}_n^u$ are irrelevant if they tend to zero at large L_x and L_z and relevant if they diverge with L_x and L_z. The expectation value of the positional coupling with respect to the decoupled state with $V^u = V^\theta = 0$ is

$$\langle \mathcal{H}_n^u \rangle = -V^u L_x L_z \langle \cos[q_0(u_z^n - u_z^{n+1})] \rangle = -V^u L_x L_z \exp[-q_0^2 \langle u_z^2 \rangle] \quad (2.9)$$

$$= -V^u L_x L_z \exp[-q_0^2 \lambda^2 \tilde{L}_x^{2\alpha} f_u^{(1)}(\tilde{L}_z/\tilde{L}_x^\mu)]. \quad (2.10)$$

The positional coupling tends to zero exponentially for both the harmonic and non-linear 2D smectic elasticities, and thus is irrelevant. However, the expectation value of the orientational coupling

$$\langle \mathcal{H}_n^\theta \rangle = -V^\theta L_x L_z \langle \cos[2(\theta^n - \theta^{n+1})] \rangle = -V^\theta L_x L_z \exp\left[-4\left(\frac{\lambda}{l_x}\right)^2 f_\theta(\tilde{\Lambda}_z/\tilde{\Lambda}_x^\mu)\right] \quad (2.11)$$

diverges with L_x and L_z since the angular fluctuations are finite. If edge dislocations are allowed in the 2D smectic lattices, $\langle \cos[2(\theta^n - \theta^{n+1})] \rangle$ decays algebraically at large L_x and L_z[31], and $\langle \mathcal{H}_n^\theta \rangle$ may be relevant or irrelevant. If we ignore dislocations for the moment, the angular coupling is relevant, and the decoupled 2D smectic Hamiltonian will flow to a new long-wavelength Hamiltonian with angular but not positional coupling between neighboring layers.

Chapter 3

Sliding Columnar Phase

In the previous chapter, we showed that the decoupled 2D smectic Hamiltonian flowed to a new Hamiltonian with relevant orientational but irrelevant translational couplings between neighboring 2D smectic lattices at the longest lengthscales. This Hamiltonian describes a new phase of matter called the sliding columnar (SC) phase in which neighboring 2D smectic lattices are able to shift relative to each other without energy cost. The goal of this chapter is to study the behavior of the sliding columnar phase in the presence of thermal fluctuations. We will determine whether the translational coupling between 2D smectic lattices is relevant or irrelevant with respect to the new sliding columnar Hamiltonian that includes strong orientational interactions between neighboring lattices. We show that when dislocations are ignored, there is a temperature range where the translational coupling is again irrelevant, and the sliding columnar phase is the stable equilibrium phase. We also find that the SC correlation function has unusual spatial dependence; it decays as $\exp[-\ln^2 r]$ for in-plane separa-

tions and as $\exp[-y/\xi_y]$ for out-of-plane separations[24]. Dislocations and the possibility of a melting transition from the sliding columnar phase to a high-temperature nematic lamellar phase will be examined in Ch. 5.

3.1 Hamiltonian

The SC phase is characterized by strong orientational but irrelevant positional correlations between nearest-neighbor 2D smectic lattices. The SC Hamiltonian is obtained from Eq. 2.1 by assuming that $V^u \ll V^\theta$ and then expanding $\cos[2(\theta^n - \theta^{n+1})]$ about $\theta^n = \theta^{n+1}$:

$$\mathcal{H}_{sc} = \frac{1}{2}\sum_n a \int d^2r \left[B(u^n_{zz})^2 + K(\partial_x^2 u^n_z)^2 + \frac{K_y}{a^2}[\partial_x(u^n_z - u^{n+1}_z)]^2 \right]. \tag{3.1}$$

The first two terms in Eq. 3.1 are the compression and bending energies for each 2D smectic lattice with $B = B_2/a$, $K = K_2/a$, and u_{zz} is the nonlinear strain defined in Eq. 2.2. The third term, with a rotation modulus $K_y = 4V^\theta a$, gives the energy cost for rotating a given 2D smectic lattice relative to nearest-neighbor lattices. Note that the self-consistent field solution $K_y = V^\theta a\langle\cos(2\theta^n)\rangle^2 = V^\theta a \exp[-4\langle(\theta^n)^2\rangle]$, where the angle fluctuations are given by Eq. 2.8, differs only by a multiplicative constant. The continuum version of this model is obtained by taking $y = na$ and $u^n_z - u^{n+1}_z = a\partial_y u_z$[20, 21].

The sliding columnar Hamiltonian is invariant under transformations of the form

$$u^n_z(\mathbf{r}) \to u^n_z(\mathbf{r}) + f_n, \tag{3.2}$$

where f_n is a function only of the layer index n. Since there are no terms in the SC Hamiltonian proportional to $(u_z^n - u_z^{n+1})^2$, shifting neighboring lattices relative to one another by an arbitrary amount does not cost energy. This symmetry permits additional terms in Eq. 3.1 proportional to $K_{zy}[\partial_z(u_z^n - u_z^{n+1})]^2$ and $K_{zx}(\partial_z\partial_x u_z^n)^2$. The K_{zy} term measures the energy cost associated with variation in the DNA lattice spacing from layer to layer, and the K_{zx} term measures the energy cost associated with the variation in the orientation with strand number of DNA strands within a layer. These terms are, however, subdominant to the compression energy $B(u_{zz}^n)^2$ and we will ignore them in what follows. (In other words, the K_{zy} and K_{zx} terms have two more z-derivatives than the compression energy.) Nevertheless, it is important to keep the K_{zy} and K_{zx} terms when discussing the Kosterlitz-Thouless transitions from the sliding columnar phase to the columnar phase and the nematic lamellar phase.

3.2 Displacement Fluctuations

Two important lengthscales can be obtained from Eq. 3.1 by comparing the orientational interaction energy with the 2D smectic compression and bending energies. The lengthscales

$$x^* = \frac{a}{\mu_y} \quad \text{and} \quad z^* = \frac{a^2}{\mu_y^2 \lambda}, \tag{3.3}$$

with $\mu_y = \sqrt{K_y/K}$ and $\lambda = \sqrt{K/B}$, separate two-dimensional from three-dimensional behavior. At lengthscales within a gallery less than x^* and z^*, the 2D compression

and bending energies are large compared to the orientational interaction, and the DNA lattices behave like independent 2D smectics with displacement fluctuations and correlation function given in Eqs. 2.6 and 2.7 respectively. On the other hand, at lengthscales greater than x^* and z^*, the orienational interaction is significant, and 3D sliding behavior occurs. Note that if $l_{x,z} < x^*, z^*$, the system proceeds from harmonic to nonlinear 2D smectic behavior and then to 3D sliding behavior as a function of increasing lengthscale. If on the other hand $l_{x,z} > x^*, z^*$, the system proceeds from harmonic 2D smectic to 3D sliding behavior as a function of increasing lengthscale, and nonlinear 2D smectic behavior is not seen.

In the SC harmonic regime, u_{zz} can be replaced by $\partial_z u_z$, and the Fourier transformed SC Hamiltonian takes the form

$$\mathcal{H}_{sc} = \frac{1}{2}\int_{-\pi/a}^{\pi/a}\frac{dq_y}{2\pi}\int\frac{d^2q_\perp}{(2\pi)^2}\left[Bq_z^2 + Kq_x^4 + K_y q_x^2 q_y^2 p(q_y a)\right]|u_z(\mathbf{q})|^2, \tag{3.4}$$

where $p(u) = 2(1-\cos[u])/u^2$,

$$u_z^n(\mathbf{r}) = \int_{-\pi/a}^{\pi/a}\frac{dq_y}{2\pi}\int\frac{d^2q_\perp}{(2\pi)^2}e^{i(\mathbf{q}_\perp\cdot\mathbf{r}+q_y n a)}u_z(\mathbf{q}), \tag{3.5}$$

and $\mathbf{q}_\perp = (q_x, q_z)$. The $q_\perp$-integrals have ultraviolet cutoffs $\Lambda_z = 2\pi/d$ and $\Lambda_x = 2\pi/b$, where b is the spacing between DNA nucleotides. The displacement fluctuations, correlation functions, and dislocation energies will in general depend on the ultraviolet cutoffs. In forthcoming calculations, we set $\Lambda_{x,z} \to \infty$ when the calculated quantities have well-defined limits. Otherwise, the dependence on $\Lambda_{x,z}$ is displayed.

The displacement fluctuations in the sliding columnar phase are obtained by integrating the SC propagator

$$G(\mathbf{q}) = \frac{T}{Bq_z^2 + Kq_x^4 + K_y q_y^2 q_x^2 p(q_y a)} \tag{3.6}$$

over all q-space. Since the SC phase has positional order in only one spatial dimension, the displacement fluctuations diverge with system size L. $\langle (u_z^n)^2 \rangle$ in the SC phase behaves quasi-two-dimensionally and diverges as $\ln^2 L$. Thus, SC fluctuations are less divergent than 2D smectic fluctuations that scale as a power-law with system size but more divergent than true 2D fluctuations that scale logarithmically with system size. We find that the displacement fluctuations

$$\langle (u_z^n)^2 \rangle = \frac{x^*}{l_x} \left(\frac{\lambda}{2\pi} \right)^2 \begin{cases} \frac{1}{2} \ln^2 \left[\alpha_z L_z / z^* \right] & \text{when } L_x \to \infty, L_y \sim L_z \\ \ln^2 \left[8 L_x / x^* \right] & \text{when } L_z \to \infty, L_x \sim L_y \end{cases} \tag{3.7}$$

are anisotropic and depend on the relative sizes of L_x and L_z. In the above expression, α_z is a number, $L_z \gg z^*$, $L_x \gg x^*$, and terms that do not diverge with system size have been dropped. The calculation of the fluctuations in the limit $L_z \to \infty$ and $L_x \sim L_y$ is detailed in Appendix A.

In contrast, the mean-square angular fluctuations $\langle (\theta^n)^2 \rangle$ are finite. This implies that the sliding columnar phase possesses three-dimensional long-range orientational order, and thus DNA strands in each layer point on average in the same direction.

3.3 Relevance of the Translational Coupling

In this section, we determine whether the translational coupling $\mathcal{H}^u$ is relevant or irrelevant with respect to the sliding columnar Hamiltonian. In Chap. 2, we found that the mean-square displacement $\langle (u_z^n - u_z^0)^2 \rangle = 2\langle u_z^2 \rangle$ taken with respect to the decoupled 2D smectic Hamiltonian diverged as a power-law with system size, and thus the translational coupling was irrelevant at all temperatures. However, in this section we show that the strong orientational couplings present in the sliding columnar phase mollify the divergent mean-square displacements $\langle (u_z^n - u_z^0)^2 \rangle$. Instead of diverging as a power-law, they diverge logarithmically with system size, and hence there is a temperature range in which the translational coupling is relevant.

To calculate the expectation value of the translational coupling, we must first evaluate the position correlation function

$$g_u(\mathbf{r}, na) = \frac{1}{2}\langle [u_z^n(\mathbf{r}) - u_z^0(0)]^2 \rangle = T \int \frac{dq_y}{2\pi} \int \frac{d^2q_\perp}{(2\pi)^2} \frac{1 - e^{i(\mathbf{q}_\perp \cdot \mathbf{r} + q_y na)}}{Bq_z^2 + Kq_x^4 + K_y q_x^2 q_y^2 p(q_y a)}. \quad (3.8)$$

The position correlation function can be decomposed into a term $g_u^{(1)}(0, na)$ that diverges with system size L_x and a term $g_u^{(2)}(\mathbf{r}, na)$ that does not diverge with system size:

$$g(\mathbf{r}, na) \equiv g_u^{(1)}(0, na) + g_u^{(2)}(\mathbf{r}, na). \quad (3.9)$$

The divergent term is isolated by adding and subtracting $\cos(q_y na)$ in the numerator

of Eq. 3.8. We find (with $\Lambda_z \to \infty$)

$$\begin{aligned} g_u^{(1)}(0,na) &= T\int \frac{d^3q}{(2\pi)^3}\frac{1-\cos(q_y na)}{Bq_z^2+Kq_x^4+K_y q_x^2 q_y^2 p(q_y a)} \\ &= \frac{T}{2\pi^2\sqrt{BK_y}} S_n(0)\ln\left[A_y(w)\frac{L_x}{x^*}\right], \end{aligned} \tag{3.10}$$

where A_y depends on $w \equiv \Lambda_x x^*$ with $A_y(\infty) = e^{\alpha+\beta}$, the constants α and β are given by

$$\alpha = \int_0^1 \frac{dt}{t}\left[\frac{S_n(t)}{S_n(0)} - 1\right], \tag{3.11}$$

$$\beta = \int_1^\infty \frac{dt}{t}\frac{S_n(t)}{S_n(0)}, \tag{3.12}$$

and

$$S_n(t) = \int_0^\pi du \frac{1-\cos(nu)}{\sqrt{t^2+u^2p(u)}}. \tag{3.13}$$

The nondivergent contribution to $g_u(\mathbf{r}, na)$,

$$g_u^{(2)}(\mathbf{r},na) = T\int \frac{d^3q}{(2\pi)^3}\cos(q_y na)\frac{1-\cos(q_x x)e^{iq_z z}}{Bq_z^2+Kq_x^4+K_y q_x^2 q_y^2 p(q_y a)}, \tag{3.14}$$

contains all of the $\mathbf{r}$ dependence. When only in-plane separations are considered, $n = 0$, $g_u^{(1)}(0,0)$ vanishes, and $g_u(\mathbf{r},0) = g_u^{(2)}(\mathbf{r},0)$. In summary, the position correlation function $g_u(\mathbf{r}, na)$ diverges logarithmically with system size L_x *unless* $n = 0$, i.e. unless the u_z's are in the same layer.

The weak $\ln L_x$ divergence of the position correlation function when $n \neq 0$ enables the translational coupling to become relevant below a critical decoupling temperature. This result is obtained by calculating the expectation value of the translation coupling

$$\langle \mathcal{H}^u \rangle = -V^u \int d^2r \langle \cos[q_0(u_z^n - u_z^{n+1})]\rangle = -V^u \int d^2r \exp[-q_0^2 g_u(0,a)] \tag{3.15}$$

with respect to the sliding columnar Hamiltonian in Eq. 3.1. Thus, the translational coupling scales as

$$\langle \mathcal{H}^u \rangle = -V^u L^{2-\eta(1)}, \tag{3.16}$$

where

$$\eta(1) = \frac{q_0^2 T}{2\pi^2 \sqrt{BK_y}} S_1(0) = \frac{4T}{d^2 \sqrt{BK_y}} \tag{3.17}$$

and $2 - \eta(1) = 0$ defines the critical decoupling temperature

$$T_d = \frac{d^2 \sqrt{BK_y}}{2}. \tag{3.18}$$

When $T < T_d$, the translational coupling scales as system size to a positive power and is relevant. In this case, the system becomes a columnar phase at the longest lengthscales with a nonzero shear modulus for shifting neighboring lattices relative to each other and long-range positional order in the yz plane. In contrast, the system flows to the sliding columnar phase at the longest lengthscales when $T > T_d$. In this temperature range, the translational coupling scales as system size to a negative power and is irrelevant. There is no energy cost for shifting neighboring lattices relative to each other, and thus the sliding columnar phase is positionally disordered in the yz plane.

3.4 Density-Density Correlation Function

In this section, we calculate the sliding columnar density-density correlation function

$$S(\mathbf{r}, na) = \langle \exp(iq_0[u_z^n(\mathbf{r}) - u_z^0(0)]) \rangle \tag{3.19}$$

between two DNA strands with in-plane separation $\mathbf{r}$ and out-of-plane separation $y = na$. This correlation function is relevant to recent experiments on CL-DNA complexes because its Fourier transform is proportional to the X-ray scattering intensity measured in Refs. [3, 26, 28, 29]. In the harmonic regime, Eq. 3.19 becomes $S(\mathbf{r}, na) = \exp[-q_0^2 g_u(\mathbf{r}, na)]$, and thus $g_u(\mathbf{r}, na)$ determines the spatial dependence of the density-density correlation function.

3.4.1 In-plane Separations

We now discuss the novel behavior of the in-plane position and density-density correlation functions, $g_u(\mathbf{r}, 0)$ and $S(\mathbf{r}, 0) \equiv S(\mathbf{r})$. $g_u(\mathbf{r}, 0)$ cannot be written in closed form for general in-plane separations $\mathbf{r}$, however, it has been calculated in the limits $z = 0$ and $x \gg x^*$ and $x = 0$ and $z \gg z^*$ in Appendix B. The results of the calculation are summarized below[10, 24]:

$$g_u(\mathbf{r}, 0) = \frac{x^*}{l_x} \left(\frac{\lambda}{2\pi}\right)^2 \begin{cases} \ln^2 [8e^\gamma x/x^*] + C_x & \text{if } z = 0 \\ \frac{1}{2} \ln^2 [32e^\gamma z/z^*] + C_z & \text{if } x = 0, \end{cases} \tag{3.20}$$

where $\gamma \approx 0.577$ is Euler's constant and C_x and C_z are constants that depend on Λ_x and Λ_z but have well-defined $\Lambda_{x,z} \to \infty$ limits. C_x and C_z are evaluated in Appendix B in the $\Lambda_{x,z} \to \infty$ limit. $S(\mathbf{r})$ along the special directions $(x, 0)$ and $(0, z)$ is obtained by exponentiating Eq. 3.20. Both $S(x, 0)$ and $S(0, z)$ display the exotic

$\exp[-\ln^2 r]$ behavior for large separations.

$$S(x,0) = \begin{cases} S_x e^{-a\ln^2[8e^\gamma x/x^*]}, & x \gg x^*; \\ \\ e^{-q_0^2 g_u^{2D}(x,0)}, & x \ll x^*, \end{cases} \tag{3.21}$$

where $S_x = e^{-aC_x}$ is a constant and

$$a = \frac{x^*}{l_x}\left(\frac{\lambda}{d}\right)^2 \tag{3.22}$$

is a dimensionless number. In the other direction,

$$S(0,z) = \begin{cases} S_z e^{-\frac{a}{2}\ln^2[32e^\gamma z/z^*]}, & z \gg z^*; \\ \\ e^{-q_0^2 g_u^{2D}(0,z)}, & z \ll z^*, \end{cases} \tag{3.23}$$

where $S_z = e^{-aC_z}$ is a constant. $g_u^{2D}(\mathbf{r})$ is the 2D smectic position correlation function defined in Eq. 2.7.

Thus, at the longest lengthscales, the sliding columnar density-density correlation function displays new spatial dependence. Table 3.1 lists the z-dependence of the correlation function $S(\mathbf{r})$ for three phases in the CL-DNA phase diagram: the nematic lamellar phase, sliding columnar phase, and columnar phase. The amount of positional order increases from the top to the bottom of the table. The nematic lamellar phase has only short-range positional order in the xz plane, and thus $S(0,z)$ decays exponentially. In contrast, the columnar phase possesses long-range positional order in the yz plane, and $S(0,z)$ is constant. $S(0,z)$ for the sliding columnar phase decays as $\exp[-\alpha\ln^2 z] = z^{-\alpha\ln z}$ where α is a constant, and thus it decays faster than any power-law. The sliding columnar phase possesses more positional order than the

Table 3.1: The scaling behavior of the density-density correlation function $S(0,z)$ for phases with varying degrees of positional order. Positional order increases from top to bottom.

Phase	$S(0,z)$
Nematic Lamellar	e^{-z}
Sliding Columnar	$e^{-\alpha \ln^2 z}$
Power-Law	$z^{-\alpha}$
Columnar	const.

nematic lamellar phase but less positional order than the columnar phase. Also, as pointed out in Table 3.1, the SC phase is more disordered than a quasi-long-range ordered 2D crystal in the xz plane which has correlations that decay as a power-law.

3.4.2 Out-of-plane Separations

We will now investigate the out-of-plane behavior of $S(\mathbf{r}, na)$. It was shown previously in Eq. 3.10 that $g_u(\mathbf{r}, na)$ diverges logarithmically with system size when V^u is irrelevant. The logarithmic divergence implies that

$$S(\mathbf{r}, na) = S(\mathbf{r})\delta_{n,0} \tag{3.24}$$

in the limit of infinite system size, and thus the positions of columns in neighboring lattices are completely decoupled. However, even though V^u is irrelevant, it is nonzero

for large but finite systems. When V^u is nonzero, we will show that there are short-range positional correlations between lattices. To study these short-range correlations, we add weak positional couplings between columns in nearest-neighbor lattices,

$$\mathcal{H}^u = -V^u \sum_n \int d^2r \cos[q_0(u_z^n - u_z^{n+1})], \tag{3.25}$$

to the sliding columnar Hamiltonian in Eq. 3.1. When $V^u/T \ll 1$, $\mathcal{H}^u$ is a small perturbation to $\mathcal{H}_{tot} = \mathcal{H}_{sc} + \mathcal{H}^u$, and

$$S(\mathbf{r}, na) = \frac{\prod_m \int \mathcal{D}u_z^m e^{-\mathcal{H}_{tot}/T} e^{iq_0[u_z^n(\mathbf{r}) - u_z^0(0)]}}{\prod_m \int \mathcal{D}u_z^m e^{-\mathcal{H}_{tot}/T}} = \frac{\langle e^{-\mathcal{H}^u/T} e^{iq_0[u_z^n(\mathbf{r}) - u_z^0(0)]} \rangle}{\langle e^{-\mathcal{H}^u/T} \rangle} \tag{3.26}$$

is calculated perturbatively in powers of V^u/T. In Eq. 3.26, $\mathcal{D}u_z^m$ is the functional integration measure for the displacement in layer m and the averages in the second equality are taken with respect to the sliding columnar Hamiltonian in Eq. 3.1. The normalization factor $\langle e^{-\mathcal{H}^u/T} \rangle$ has nonzero contributions even in the limit of infinite system size, but they are independent of n. Expanding $e^{-\mathcal{H}^u/T}$ in the numerator and neglecting the normalization factor yields

$$\begin{aligned} S(\mathbf{r}, na) \;=\; & \sum_p \frac{1}{p!} \left(\frac{V^u}{2T}\right)^p \int d^2r_1 \ldots d^2r_p \sum_{m_1} \cdots \sum_{m_p} \\ & \langle (\exp[iq_0 \Delta u_z(\mathbf{r}_1, m_1; \mathbf{r}_1, m_1 + 1)] + \exp[-iq_0 \Delta u_z(\mathbf{r}_1, m_1; \mathbf{r}_1, m_1 + 1)]) \times \\ & \ldots \times (\exp[iq_0 \Delta u_z(\mathbf{r}_p, m_p; \mathbf{r}_p, m_p + 1)] + \exp[-iq_0 \Delta u_z(\mathbf{r}_p, m_p; \mathbf{r}_p m_p + 1)]) \\ & \times \exp[iq_0 \Delta u_z(\mathbf{r}, n; 0, 0)] \rangle, \end{aligned} \tag{3.27}$$

where differences in displacements are defined by

$$\Delta u_z(\mathbf{r}_1, m; \mathbf{r}_2, p) = u_z^m(\mathbf{r}_1) - u_z^p(\mathbf{r}_2). \tag{3.28}$$

We must therefore calculate the expectation value of complex exponentials whose arguments are a series of displacement differences. Since $g_u(\mathbf{r}_1 - \mathbf{r}_2, m - p) = \frac{1}{2}\langle[\Delta u_z(\mathbf{r}_1, m; \mathbf{r}_2, p)]^2\rangle$ diverges logarithmically with system size unless $m = p$, all differences must be taken between two displacements in the same layer in order to obtain a nonzero $S(\mathbf{r}, na)$. This implies that at least one of the terms in the sums over $m_1, m_2, \ldots m_p$ must be proportional to $e^{-iq_0 u_z^n}$ and $e^{iq_0 u_z^0}$ to match the "external" factor of $e^{iq_0[u_z^n(\mathbf{r}) - u_z^0(0)]}$, while the remaining "internal" complex exponential factors must have as arguments differences between two displacements in the same layer. Only terms with $p \geq n$ in the expansion of $e^{-\mathcal{H}^u/T}$ satisfy this condition. We neglect the higher-order contributions and set $p = n$. There are $n!$ ways of generating terms proportional to $e^{-iq_0 u_z^n}$ and $e^{iq_0 u_z^0}$ with nonzero "internal" factors, and thus

$$S(\mathbf{r}, na) = \left(\frac{V^u}{2T}\right)^n \int d^2 r_1 \ldots d^2 r_n e^{-\Phi(\mathbf{r}_1, \ldots, \mathbf{r}_n, \mathbf{r})/2}, \tag{3.29}$$

where

$$\Phi(\mathbf{r}_1, \ldots, \mathbf{r}_n, \mathbf{r}) = q_0^2 \langle[\Delta u_z^0(0, \mathbf{r}_1) + \Delta u_z^1(\mathbf{r}_1, \mathbf{r}_2) + \cdots + \Delta u_z^n(\mathbf{r}_n, \mathbf{r})]^2\rangle \tag{3.30}$$

is the mean-square of sums of differences between displacements in the same layer and $\Delta u_z^m(\mathbf{r}_1, \mathbf{r}_2) \equiv \Delta u_z(\mathbf{r}_1, m; \mathbf{r}_2, m)$.

To determine the true n-dependence of $S(\mathbf{r}, na)$, we must also determine how the integral in Eq. 3.29 scales with n. When K_y is finite, the cross terms

$$\Phi_{m,n} = q_0^2 \langle \Delta u_z^m(\mathbf{r}_m, \mathbf{r}_{m+1}) \Delta u_z^n(\mathbf{r}_n, \mathbf{r}_{n+1})\rangle \tag{3.31}$$

in Eq. 3.30 are nonzero, and determining the scaling of the correlation function with n is difficult. The out-of-plane correlation function with nonzero K_y will be calculated in detail in a forthcoming publication[24]. However, when $K_y = 0$, all of the cross terms vanish, only the direct terms $\Phi_{m,m}$ contribute, and

$$S(\mathbf{r}, na) = \left(\frac{V^u}{2T}\right)^n \int d^2r_1 \dots d^2r_n S(-\mathbf{r}_1)S(\mathbf{r}_1 - \mathbf{r}_2)\dots S(\mathbf{r}_n - \mathbf{r}) \tag{3.32}$$

has a simple form. An algebraic expression for $\tilde{S}(\mathbf{q}_\perp, na)$ can be obtained by repeatedly applying the convolution theorem:

$$\tilde{S}(\mathbf{q}_\perp, na) = \int d^2r e^{-i\mathbf{q}_\perp\cdot\mathbf{r}} S(\mathbf{r}, na) = \left(\frac{V^u}{2T}\right)^n \tilde{S}^{n+1}(\mathbf{q}_\perp), \tag{3.33}$$

where $\tilde{S}(\mathbf{q}_\perp) \equiv \tilde{S}(\mathbf{q}_\perp, 0)$. We then Fourier transform Eq. 3.33 back into real space and find

$$S(\mathbf{r}, na) = \left(\frac{V^u}{2T}\right)^n \int \frac{d^2q_\perp}{(2\pi)^2} e^{i\mathbf{q}_\perp\cdot\mathbf{r}} e^{(n+1)\ln\tilde{S}(\mathbf{q}_\perp)}. \tag{3.34}$$

This integral can be evaluated in the limit of large n using the method of steepest descent.

$$S(0, na) \sim \frac{1}{na} e^{-na/\xi_y} \tag{3.35}$$

decays exponentially with a correlation length

$$\xi_y = a\left(\ln\left[\frac{2T}{V^u\tilde{S}(0)}\right]\right)^{-1}. \tag{3.36}$$

Thus, the out-of-plane correlation function in the limit $K_y = 0$ has short-range positional correlations. Note that correlation length is divergent for $T < V^u\tilde{S}(0)/2$. This

signals the onset of long-range positional order in the yz plane and the existence of the columnar phase. The out-of-plane correlation function with nonzero K_y and V^u also decays exponentially, but with a larger correlation length ξ_y due to the strong orientational correlations[24].

3.5 Structure Functions

We will now calculate the structure function $I(\mathbf{q})$ for CL-DNA complexes as a function of temperature. Below the critical decoupling temperature T_d, the positional coupling between lattices in neighboring galleries is relevant and diverges with system size. At the longest lengthscales and in the absence of dislocations, the system forms a columnar phase with DNA columns situated on a 2D crystal lattice in the yz plane. (Electrostatic interactions between DNA favor centered rectangular symmetry in the yz plane.) The columnar phase possesses a nonzero shear modulus for shifting lattices relative to each other which prevents positional fluctuations from diverging in the limit of infinite system size. As a result, the structure function for $T < T_d$ possesses Bragg peaks at reciprocal lattice vectors of a centered rectangular lattice.

Above the decoupling temperature, the positional coupling between lattices in neighboring galleries is irrelevant and scales to zero with increasing system size. At the longest lengthscales, the system forms a sliding columnar phase with weak positional but strong orientational correlations between lattices. The sliding columnar phase

has a vanishing shear modulus which allows positional fluctuations to diverge with system size. Thus, the Debye-Waller factor vanishes in the limit of infinite system size. Since the Debye-Waller factor is zero, the sliding columnar structure function does not possess Bragg peaks. However, as $T \to T_d$ and positional correlations between neighboring lattices increase, the structure function develops maxima at reciprocal lattice vectors corresponding to the centered rectangular lattice. These peaks are much weaker and broader than delta-function Bragg peaks. At high temperatures $T \gg T_d$, thermal fluctuations may extinguish the centered rectangular peaks, but leave diffuse maxima at $\mathbf{q} = nq_0\hat{z}$. The number of detectable reflections is limited by the DNA form factor. These maxima reflect the 2D smectic order within each gallery.

Scattering experiments measure the structure function

$$I(\mathbf{q}) = \int d^3x d^3x' e^{-i\mathbf{q}\cdot(\mathbf{x}-\mathbf{x}')} S(\mathbf{x}, \mathbf{x}'), \tag{3.37}$$

which is the Fourier transform of the density-density correlation function

$$S(\mathbf{x}, \mathbf{x}') = \langle \rho(\mathbf{x}) \rho(\mathbf{x}') \rangle. \tag{3.38}$$

$\rho(\mathbf{x})$ is the DNA density at position $\mathbf{x} = (\mathbf{r}, na)$. The structure factor $\mathcal{S}(\mathbf{q}) = V^{-1} I(\mathbf{q})$ is proportional to the structure function and can be decomposed into the sum of two terms:

$$\mathcal{S}(\mathbf{q}) = V^{-1} |\langle \rho(\mathbf{q}) \rangle|^2 + \mathcal{S}_{\rho\rho}(\mathbf{q}), \tag{3.39}$$

where

$$\mathcal{S}_{\rho\rho}(\mathbf{q}) = \frac{1}{V}\int d^3x d^3x' e^{-i\mathbf{q}\cdot(\mathbf{x}-\mathbf{x}')}\left[S(\mathbf{x},\mathbf{x}') - \langle\rho(\mathbf{x})\rangle\langle\rho(\mathbf{x}')\rangle\right]. \tag{3.40}$$

The first term in Eq. 3.39 scales with volume V and will produce Bragg peaks at reciprocal lattice vectors of the 2D columnar lattice if the positional fluctuations are finite. The second term, however, does not scale with volume since its integrand decays to zero for large $|\mathbf{x}-\mathbf{x}'|$. In the sliding columnar phase, the first term is nonzero only when $\mathbf{q} = 0$ since divergent position fluctuations remove the Bragg peaks at nonzero $\mathbf{q}$. The $\mathbf{q} \neq 0$ dependence in the sliding columnar structure factor is generated by the second term in Eq. 3.39.

In the columnar phase, DNA are situated on a centered rectangular lattice with positions

$$\mathbf{R}_{mn} = \left(nd + \frac{md}{2} + u_z^m(\mathbf{r})\right)\hat{z} + [ma + u_y^m(\mathbf{r})]\hat{y}, \tag{3.41}$$

where $\mathbf{u}^m = (u_y^m, u_z^m)$ are fluctuations in the y- and z-displacements in layer m. (See Fig. 2.1.) Note that equilibrium positions of columns in a given layer are shifted by $d/2$ in the z-direction with respect to the previous layer. We also assume that $\mathbf{R}_{mn}$ gives the positions of DNA columns in the sliding columnar phase for temperatures near T_d. The DNA density in both the columnar and sliding columnar phases can be written as a sum of density waves for each layer m:

$$\rho(\mathbf{x}) = \sum_m \rho^m(\mathbf{x}). \tag{3.42}$$

Since the density in each layer is periodic in z, each $\rho^m(\mathbf{x})$ can be expanded as a Fourier series

$$\rho^m(\mathbf{x}) = \sum_h e^{ihq_0 z} \rho_h^m(\mathbf{x}), \tag{3.43}$$

where h is an integer and

$$\rho_h^m(\mathbf{x}) = e^{-ihq_0[md/2 + u_z^m(\mathbf{r})]} \tilde{\rho}_h(y - ma - u_y^m(\mathbf{r})). \tag{3.44}$$

ρ_h^m includes phase factors for fluctuations in the z-displacement and for the staggered positions of DNA columns. Also, the Fourier coefficients

$$\tilde{\rho}_h(y) = \frac{\lambda}{d} \int \frac{dp}{2\pi} e^{ipy} f_{\mathrm{DNA}}(\sqrt{(hq_0)^2 + p^2}) \tag{3.45}$$

contain a form factor

$$f_{\mathrm{DNA}}(q) = \frac{2}{qr_{\mathrm{DNA}}} J_1(qr_{\mathrm{DNA}}), \tag{3.46}$$

which accounts for the finite thickness of DNA. λ is the mass per unit length of DNA and J_1 is a Bessel function.

3.5.1 Scattering from the Columnar Phase

To calculate the dominant contribution to the structure factor in the columnar phase, we only need to calculate the first term in Eq. 3.39. We obtain

$$\mathcal{S}(\mathbf{q}) = V \left(\frac{\lambda}{ad}\right)^2 \delta_{q_x,0} \sum_{h+k=\mathrm{even}} \delta_{q_z,hq_0} \delta_{q_y,\pi k/a} e^{-W_{\mathbf{G}}} \left| f_{\mathrm{DNA}}(\sqrt{(hq_0)^2 + q_y^2}) \right|^2, \tag{3.47}$$

where $W_{\mathbf{G}} = \langle (\mathbf{G} \cdot \mathbf{u}^m)^2 \rangle$ and $\mathbf{G} = hq_0\hat{z} + q_y\hat{y}$. The Debye-Waller factor $e^{-W_{\mathbf{G}}}$ for the columnar phase is a finite number that depends on h and k. Therefore, the structure

factor possesses delta-function peaks proportional to the volume of the sample. These Bragg peaks occur at the reciprocal lattice vectors

$$\mathbf{q}_{hk} = 2\pi \left(\frac{h}{d}\hat{z} + \frac{k}{2a}\hat{y} \right) \tag{3.48}$$

of a centered rectangular lattice with lattice constants $2a$ and d in the y- and z-directions. In the previous expression $h+k$ is constrained to be an even integer. The peak intensities decrease with increasing q_{hk} since both the Debye-Waller factor and form factor decay with increasing wavenumber.

3.5.2 Scattering from the Sliding Columnar Phase

The low-temperature structure functions shown in Fig. 1.3 possess several maxima at $q = q_{1,1}$, $q_{1,3}$, and $q_{1,5}$. However, these maxima are weak and diffuse which indicates that neighboring lattices are able to shift relative to each other. This suggests that the scattering data were taken at temperatures above T_d in the sliding columnar phase. Near T_d, DNA columns are located on average on a centered rectangular lattice with positions given in Eq. 3.41. When $T \gg T_d$, the positional couplings between columns in neighboring galleries vanish, and DNA are no longer situated on a centered rectangular lattice.

Position fluctuations in the sliding columnar phase diverge with system size, and thus the average density $\langle \rho(\mathbf{x}) \rangle$ vanishes when $\mathbf{G} \neq 0$. We must therefore calculate the Fourier transform of $S(\mathbf{x}, \mathbf{x}')$ to obtain the $\mathbf{q}$-dependence of the structure factor.

The structure factor in principle has many contributions

$$\mathcal{S}(\mathbf{q}) = \sum_h \mathcal{S}_h(\mathbf{q}). \tag{3.49}$$

However, terms with large h will be suppressed by the DNA form factor. Also, terms with $h = 0$ correspond to the lamellar peaks and do not arise from correlations between DNA. The lowest order DNA peaks have $h = \pm 1$. Therefore, the terms with $|h| > 1$ are dropped and we obtain in the limit $K_y = 0$

$$\mathcal{S}(\mathbf{q}) \approx \mathcal{S}_{h=\pm 1}(\mathbf{q}) = \frac{1}{a}\left(\frac{\lambda}{d}\right)^2 \widetilde{S}(\Delta\mathbf{q}_\perp)|f_{\rm DNA}(\sqrt{q_0^2+q_y^2})|^2 F(\mathbf{q}) + \ldots, \tag{3.50}$$

where

$$F(\mathbf{q}) = \frac{1-\left(\frac{V^u\widetilde{S}(\Delta\mathbf{q}_\perp)}{2T}\right)^2}{1-\frac{V^u\widetilde{S}(\Delta\mathbf{q}_\perp)}{T}\cos(q_y a \pm \pi)+\left(\frac{V^u\widetilde{S}(\Delta\mathbf{q}_\perp)}{2T}\right)^2} \tag{3.51}$$

and $\Delta\mathbf{q}_\perp = \mathbf{q}_\perp \mp q_0\hat{z}$. In the calculation of the sliding columnar structure factor, we have neglected fluctuations in the lipid bilayers. Neglecting these fluctuations is justified since the lamellar peaks in the X-ray scattering experiments of Refs. [3, 28] are not broadened. The sliding columnar structure factor does not possess Bragg peaks and is not proportional to the volume of the sample. When the positional coupling V^u is nonzero, maxima in $\mathcal{S}(\mathbf{q})$ occur at the centered rectangular positions $\mathbf{q} = \mathbf{q}_{\pm 1,k}$, where k is an odd integer. In contrast, when $T \gg T_d$, the positional coupling V^u is zero and the centered rectangular peaks vanish. When $V^u = 0$, only the form factor $f_{\rm DNA}$ determines the q_y dependence of the structure factor, and the maximum value of $|f_{\rm DNA}(\sqrt{q_0^2+q_y^2})|^2$ occurs at $q_y = 0$. In the high-temperature

regime, there is a maximum in $\mathcal{S}(q)$ at $q = q_0$. The shape of the high-temperature maximum will depend on the values of the characteristic lengthscales x^* and z^*.

Chapter 4

Nonlinear Elasticity of the Sliding Columnar (SC) Phase

4.1 Introduction

This chapter will investigate the nonlinear elasticity of the sliding columnar (SC) phase. Its principal purpose is to show that the nonlinear strains lead to a Grinstein-Pelcovits renormalization of the elastic constants [11] and not, as one could imagine, to the destruction of the sliding columnar phase itself. The lipid bilayers, which we take to be aligned on average parallel to the xz plane as shown in Fig. 2.1, fluctuate like bilayers in any lamellar phase. To understand correlations and fluctuations of the DNA smectic lattices, it is convenient to consider first a model in which the lipid bilayers are rigid planes with no fluctuations in the y-direction. In this case, displacements of the DNA lattices, which are aligned on average along the x-direction, are restricted to the z-direction.

The rotationally invariant Hamiltonian in units of k_BT for this system is

$$\mathcal{H} = \frac{1}{2}\int d^3x \left[B u_{zz}^2 + K_y(\partial_x \partial_y u_z)^2 + K(\partial_x^2 u_z)^2\right], \tag{4.1}$$

where B, K_y, and K are the compression, rotation, and bending moduli divided by k_BT, $u_z(\mathbf{x})$ with $\mathbf{x} = (\mathbf{r}, y)$ and $y = na$ is the continuum version of $u_z^n(\mathbf{r})$, and

$$u_{zz} = \partial_z u_z - \frac{1}{2}\left[(\partial_x u_z)^2 + (\partial_z u_z)^2\right] \tag{4.2}$$

is the nonlinear Eulerian strain appropriate for the sliding columnar phase. Note that $\mathcal{H}$ is invariant under

$$u_z'(\mathbf{x}) \to u_z(\mathbf{x}) + f(y). \tag{4.3}$$

It is this fact that ensures that nonlinearities do not destroy the sliding columnar phase.

The rotationally invariant strain u_{zz} introduces anharmonic terms into the Hamiltonian that lead to a Grinstein-Pelcovits renormalization of B, K_y, and K. The renormalized moduli scale logarithmically with q at long wavelengths:

$$K_y(q) \sim K^{1/2}(q) \sim B^{-1/3}(q) \sim \left[\ln\left(\frac{\mu}{q}\right)\right]^{1/4}, \tag{4.4}$$

where μ is a large momentum cutoff. A complete model for the sliding columnar phase allows both lipid bilayers and smectic lattices to fluctuate. This model also exhibits Grinstein-Pelcovits renormalization of the elastic constants. Table 4.1 lists the exponents describing singularities in the elastic constants for both the 3D smectic and sliding columnar phases.

The evaluation of the above renormalization presented some unexpected difficulties. The continuum Hamiltonian in (4.1) is formally invariant under arbitrary global

Table 4.1: Comparison of the logarithmic scaling exponents for the elastic moduli of the 3D smectic and sliding columnar phases. At long wavelengths the elastic moduli for both phases scale as $\ln^{\alpha}[1/q]$ with α given below.

Phase	B	K	K_y
3D smectic	$-4/5$	$2/5$	–
sliding columnar	$-3/4$	$1/2$	$1/4$

rotations. However, the introduction of a hard cutoff breaks this rotational invariance just as the introduction of a similar cutoff breaks gauge invariance in gauge Hamiltonians[16]. Nevertheless, hard-cutoff renormalization group (RG) procedures can with care be applied successfully to Hamiltonians with gauge [12] or rotation symmetries[18]. Indeed, the original Grinstein-Pelcovits calculation of the logarithmic renormalization of the smectic-A elastic constants used a hard-cutoff[11]. When we applied the popular momentum-shell hard-cutoff RG procedure [32] to the nonlinearities in the sliding columnar phase, we encountered ambiguities that we were unable to resolve. We found that the values of the one-loop diagrams depended on whether the external momentum was added to the top or the bottom part of the internal loop. Similar difficulties are not encountered in the Grinstein-Pelcovits calculation. To eliminate these ambiguities, we switched to the dimensional regularization procedure which explicitly preserves rotational invariance because the cutoffs

are infinite[2].

The remainder of this chapter will be organized as follows: we first rederive the results of Grinstein and Pelcovits in Sec. 4.2 using dimensional regularization. Then in Sec. 4.3, we calculate the renormalization of the sliding columnar elastic constants of the simplified theory using the same scheme. In Sec. 4.4 we relax the constraint of rigid membranes and show that the membrane fluctuations do not modify the scaling behavior of the elastic moduli of the rigid theory. In Appendices C and D, we evaluate the one-loop diagrams for the 3D smectic and simplified sliding columnar theories. In Appendix E we show that ambiguities arise when a finite cutoff is implemented to calculate the loop diagrams of the sliding columnar theory.

4.2 Renormalization Group (RG) Analysis of the 3D Smectic

The rotationally invariant elasticity theory for a smectic liquid crystal contains non-linear terms that renormalize the elastic constants of the harmonic theory for all dimensions below three. Grinstein and Pelcovits calculated the corrections to the elastic constants of a 3D smectic using an RG analysis with a finite wavenumber cutoff[11]. They found that the corrections to both the compression and bending moduli are logarithmic in the wavenumber q with the former scaling to zero and the latter scaling to infinity at long wavelengths. Application of a hard-cutoff RG procedure to the sliding columnar phase leads to ambiguities with no obvious resolution.

(See Appendix E.) We, therefore, employ a dimensional regularization procedure that sends the cutoff to infinity and thereby preserves rotational invariance. In this section we rederive the Grinstein-Pelcovits results for a 3D smectic using dimensional regularization. This establishes the language needed to calculate the renormalization in the sliding columnar phase.

4.2.1 Rotationally Invariant Theory

A smectic in d dimensions is characterized by a mass-density wave with period $P = 2\pi/q_0$ along one dimension and by fluid-like order in the other $d-1$ dimensions. The phase of the mass density wave at point $\mathbf{x} = (\mathbf{x}_\perp, z)$ is $q_0(z - u(\mathbf{x}))$. In units of k_BT, the elastic Hamiltonian for a smectic is

$$\mathcal{H} = \frac{1}{2}\int d^dx \left[B_{\rm sm} u_{zz}^2 + K_{\rm sm}(\boldsymbol{\nabla}_\perp^2 u)^2\right], \tag{4.5}$$

where $\boldsymbol{\nabla}_\perp$ is the gradient operator in the $d-1$ subspace spanned by $\mathbf{x}_\perp$ and $B_{\rm sm}$ and $K_{\rm sm}$ are, respectively, the compression and bending moduli divided by k_BT. The nonlinear Eulerian strain $u_{zz} = \partial_z u - (1/2)(\boldsymbol{\nabla} u)^2$ is invariant with respect to uniform, rigid rotations of the smectic layers. Below we will drop the $(\partial_z u)^2$ term in u_{zz} since its inclusion leads to nonlinear terms that are irrelevant in the RG sense with respect to the two quadratic terms in (4.5). Therefore, we will take

$$u_{zz} \approx \partial_z u - \frac{1}{2}(\boldsymbol{\nabla}_\perp u)^2. \tag{4.6}$$

Strictly speaking we should include a term linear in u_{zz} whose coefficient is chosen to make $\langle u_{zz} \rangle = 0$. The inclusion of and proper treatment of this term does not modify our RG equations, and we will ignore it here and in our treatment of the sliding columnar phase.

4.2.2 Engineering Dimensions

To implement our RG procedure it is convenient to rescale parameters so that $B_{\rm sm}$ is replaced by unity and the nonlinear form of u_{zz} is preserved. To this end, we scale u and $\mathbf{x}$ as follows:

$$u = L_u \tilde{u}, \quad z = L_z \tilde{z}, \text{ and } \mathbf{x}_\perp = \tilde{\mathbf{x}}_\perp. \tag{4.7}$$

Note that $\mathbf{x}_\perp$ does not rescale. Under these rescalings we obtain

$$u_{zz} = L_u L_z^{-1} \left(\partial_{\tilde{z}} \tilde{u} - \frac{1}{2} L_u L_z (\boldsymbol{\nabla}_{\tilde{\perp}} \tilde{u})^2 \right). \tag{4.8}$$

We require $u_{zz} = A \tilde{u}_{zz}$ where $\tilde{u}_{zz} = \partial_{\tilde{z}} \tilde{u} - (1/2)(\boldsymbol{\nabla}_{\tilde{\perp}} \tilde{u})^2$ is the rescaled nonlinear strain with the same form as (4.6). This yields $L_u = L_z^{-1}$ and $A = L_u^2$. The coefficient of $\tilde{u}_{zz}^2$ in the rescaled Hamiltonian is set to one with the choice

$$L_u = B_{\rm sm}^{-1/3}. \tag{4.9}$$

The rescaled theory then becomes

$$\mathcal{H} = \frac{1}{2} \int d^d \tilde{x} \left[\tilde{u}_{zz}^2 + \frac{1}{w} (\boldsymbol{\nabla}_{\tilde{\perp}}^2 \tilde{u})^2 \right] \tag{4.10}$$

with

$$w = \frac{B_{\rm sm}^{1/3}}{K_{\rm sm}}. \tag{4.11}$$

For the remainder of Sec. 4.2 we will use the Hamiltonian in (4.10) but drop the tilde on the scaled variables.

We determine the dimensions of the scaled variables using the engineering dimensions of $B_{\rm sm}$ and $K_{\rm sm}$. The dimension d_A determines how A scales with length L: $[A] = L^{d_A}$. From the respective dimensions $d_{B_{\rm sm}} = -d$ and $d_{K_{\rm sm}} = 2 - d$ of $B_{\rm sm}$ and $K_{\rm sm}$, we obtain $[L_u] = [L_z^{-1}] = L^{d/3}$. Using these we find the following for the dimensions of the scaled variables and the parameter w:

$$\begin{aligned} [u] &= \left[\frac{L}{L_u}\right] = L^{\epsilon/3}, \quad [z] = \left[\frac{L}{L_z}\right] = L^{1+d/3}, \\ [x_\perp] &= L, \text{ and } [w] = \left[\frac{L^{-d/3}}{L^{2-d}}\right] = L^{-2\epsilon/3}, \end{aligned} \tag{4.12}$$

where $\epsilon = 3 - d$. Using these definitions one can easily verify that both terms in (4.10) are dimensionless. $[w]$ scales as $\mu^{2\epsilon/3}$ where $[\mu] = L^{-1}$, and it is, therefore, a relevant variable below $d = 3$. The dimensions of the coefficients of the $(\partial_z u)^3$, $(\partial_z u)^2(\boldsymbol{\nabla}_\perp u)^2$, and $(\partial_z u)^4$ terms are $2d/3$, $2d/3$, and $4d/3$ respectively. These nonlinear terms are irrelevant and will be ignored in what follows.

The engineering dimensions in (4.12) imply that there is an invariance of $\mathcal{H}$ under the transformation $\mu \to \mu b$ and

$$u(\mathbf{x}_\perp, z) = b^{d_u} u'(\mathbf{x}'_\perp, z'), \tag{4.13}$$

where $\mathbf{x}'_\perp = b^{-1}\mathbf{x}_\perp$ and $z' = b^{-(1+d/3)}z$, *i.e.*

$$\mathcal{H}[u, w, \mu] = \mathcal{H}[u', wb^{2\epsilon/3}, \mu b]. \tag{4.14}$$

This in turn implies a scaling form for the position correlation function $G(\mathbf{x}_\perp, z) = \langle u(\mathbf{x}_\perp, z)u(0,0)\rangle$ and its Fourier transform $G(\mathbf{q})$. We find

$$G(\mathbf{x}_\perp, z, w) = b^{2(1-d/3)}G(\mathbf{x}'_\perp, z', wb^{2\epsilon/3}), \tag{4.15}$$

and from this we obtain the vertex function $\Gamma(\mathbf{q}) = G^{-1}(\mathbf{q})$,

$$\Gamma(\mathbf{q}_\perp, q_z, w) = b^{-2(1+d/3)}\Gamma(b\mathbf{q}_\perp, b^{1+d/3}q_z, wb^{2\epsilon/3}). \tag{4.16}$$

When $d = 3$ this reduces to the scaling form

$$\Gamma(\mathbf{q}_\perp, q_z, w) = q_\perp^4 \Gamma\left(1, \frac{q_z}{q_\perp^2}, w\right), \tag{4.17}$$

which the harmonic vertex function $\Gamma = q_z^2 + w^{-1}q_\perp^4$ satisfies.

4.2.3 RG Procedure

To calculate renormalized quantities, we seek a multiplicative procedure that yields a renormalized Hamiltonian with the same form as the original Hamiltonian, *i.e.*, a Hamiltonian that is a function of a renormalized nonlinear strain with the same form as (4.6). To preserve the form of the strains, it is necessary to rescale fields and lengths simultaneously. The rescaling that produced (4.10) shows that the form of u_{zz} is preserved if the rescaling coefficients of u and z are inverses of each other. We,

therefore, introduce a renormalization constant $\mathcal{Z}$ and a renormalized displacement u' such that

$$u(\mathbf{x}) = \mathcal{Z}^{1/3} u'(\mathbf{x}') = \mathcal{Z}^{1/3} u'(\mathbf{x}_\perp, \mathcal{Z}^{1/3} z). \tag{4.18}$$

This implies that $u_{zz}(\mathbf{x}) = \mathcal{Z}^{2/3} u'_{zz}(\mathbf{x}')$. We also introduce a unitless renormalized coupling constant g and renormalization constant $\mathcal{Z}_g$ via

$$w^{3/2} = g\mu^\epsilon \mathcal{Z}_g \mathcal{Z}^{1/2}, \tag{4.19}$$

where μ is an arbitrary wavenumber scale. The renormalized Hamiltonian then becomes

$$\mathcal{H}' = \frac{1}{2} \int d^d x' \ \left[\mathcal{Z} (u'_{zz})^2 + (g\mu^\epsilon \mathcal{Z}_g)^{-2/3} \left(\boldsymbol{\nabla}^2_{\perp'} u' \right)^2 \right]. \tag{4.20}$$

We now follow standard procedures to evaluate $\mathcal{Z}(g)$ and $\mathcal{Z}_g(g)$[2]. The renormalized Hamiltonian in (4.20) determines the vertex function

$$\begin{aligned} \Gamma(\mathbf{q}) &= q_z^2 + (g\mu^\epsilon)^{-2/3} q_\perp^4 + (\mathcal{Z} - 1) q_z^2 \\ &+ (g\mu^\epsilon)^{-2/3} \left(\mathcal{Z}_g{}^{-2/3} - 1 \right) q_\perp^4 + \Sigma(\mathbf{q}) \end{aligned} \tag{4.21}$$

to one-loop order, where $\Sigma(\mathbf{q})$ is the one-loop diagrammatic contribution to $\Gamma(\mathbf{q})$. We next impose the following conditions on the vertex function to enforce the correct scaling behavior:

$$\left. \frac{d\Gamma}{dq_z^2} \right|_{q_z = \mu^2, q_\perp = 0} = 1 \tag{4.22}$$

$$\left. \frac{d\Gamma}{dq_\perp^4} \right|_{q_z = \mu^2, q_\perp = 0} = (g\mu^\epsilon)^{-2/3}. \tag{4.23}$$

In Appendix C we show that the diagrammatic contributions are the following:

$$\left.\frac{d\Sigma(\mathbf{q})}{dq_z^2}\right|_{q_z=\mu^2,q_\perp=0} = -\frac{g}{16\pi\epsilon} \tag{4.24}$$

$$\left.\frac{d\Sigma(\mathbf{q})}{dq_\perp^4}\right|_{q_z=\mu^2,q_\perp=0} = (g\mu^\epsilon)^{-2/3}\frac{g}{32\pi\epsilon}. \tag{4.25}$$

Using the conditions on the vertex function we obtain the relations for the renormalization constants in terms of the one-loop diagrammatic corrections. The following relations are correct to lowest order in ϵ:

$$\mathcal{Z} = 1+\frac{g}{16\pi\epsilon} \tag{4.26}$$

$$\mathcal{Z}_g = 1+\frac{3g}{64\pi\epsilon}. \tag{4.27}$$

Callan-Symanzik Equation

The renormalized vertex function $\Gamma_r(\mathbf{q})$ satisfies a Callan-Symanzik (CS) equation under a change of length scale μ. We obtain the renormalized elastic moduli from the solution to this equation. The original theory in (4.10) did not depend on the length scale μ. We can therefore write the bare vertex function Γ in terms of the renormalized vertex function Γ_r and find the differential equation obeyed by Γ_r. Since the variables u and z scale as $u'(\mathbf{x}) = \mathcal{Z}^{1/3}u(\mathbf{x}')$ and $z' = \mathcal{Z}^{1/3}z$, the vertex function must scale as

$$\Gamma(\mathbf{q}_\perp, q_z, w) = \mathcal{Z}^{-1/3}\Gamma_r(\mathbf{q}_\perp, \mathcal{Z}^{-1/3}q_z, g, \mu). \tag{4.28}$$

The CS equation is determined by the condition $\mu d\Gamma/d\mu = 0$. Since the renormalized vertex function can have explicit as well as implicit μ dependence through the

functions $\mathcal{Z}$ and g, the CS equation for Γ_r has three terms:

$$\left[\mu\frac{\partial}{\partial\mu} - \frac{\eta(g)}{3}\left(1 + q_z\frac{\partial}{\partial q_z}\right) + \beta(g)\frac{\partial}{\partial g}\right]\Gamma_r = 0, \tag{4.29}$$

where

$$\beta(g) = \mu\frac{dg}{d\mu}, \tag{4.30}$$

$$\eta(g) = \beta(g)\frac{d\left(\ln\mathcal{Z}\right)}{dg}, \tag{4.31}$$

and $q_z\partial/\partial q_z = q_z'\partial/\partial q_z'$ with $q_z' = \mathcal{Z}^{-1/3}q_z$. This equation can be integrated to yield an equation for Γ_r as a function of the length scale μ.

$$\Gamma_r(\mathbf{q}_\perp, q_z, g, \mu) = \exp\left[\frac{1}{3}\int_0^l \eta dl'\right]\Gamma_r\left(\mathbf{q}_\perp, \exp\left[\frac{1}{3}\int_0^l \eta dl'\right]q_z, g(l), \mu_0\right), \tag{4.32}$$

where $\mu/\mu_0 = e^l$, $\mu d/d\mu = d/dl$, and $g(l)$ must satisfy

$$\frac{dg(l)}{dl} = -\beta(g). \tag{4.33}$$

At $l = 0$ we have set $\Gamma_r(l=0) = \Gamma_r(\mathbf{q}_\perp, q_z, g_0, \mu_0)$.

Now we must solve for β and η in terms of g in order to obtain the renormalized vertex function. To find $\beta(g)$, we note that

$$\frac{dw^{3/2}}{dl} = \frac{d}{dl}\left(g\mu_0^\epsilon e^{\epsilon l}\mathcal{Z}_g\mathcal{Z}^{1/2}\right) = 0. \tag{4.34}$$

From this relation we find $\beta(g) = -\epsilon/(d(\ln Q)/dg)$ where $Q = g\mathcal{Z}_g\mathcal{Z}^{1/2}$. We then insert the relations for $\mathcal{Z}$ and $\mathcal{Z}_g$ and determine β and η to be the following:

$$\beta(g) = \frac{5}{64\pi}g^2 - \epsilon g \tag{4.35}$$

$$\eta(g) = -\frac{1}{16\pi}g. \tag{4.36}$$

In three dimensions $\epsilon = 0$. In this case, integration of dg/dl yields

$$g(l) = \frac{g_0}{1 + 5g_0 l/(64\pi)}, \tag{4.37}$$

where $g_0 \equiv g(0) = w^{3/2}$. The remaining task is simple; we must evaluate the arguments of the exponentials in (4.32) to obtain the l dependence of Γ_r. Since $g \sim 1/l$, the integral of η will scale as $\ln l$ and the exponentials of the integral of η will give power-law dependence on l. We find that

$$\exp\left[\frac{1}{3}\int_0^l \eta(l')dl'\right] = \left[1 + \frac{5g_0}{64\pi}l\right]^{-4/15} \equiv [g/g_0]^{4/15}. \tag{4.38}$$

Renormalized Elastic Constants

The scaling relations in (4.16) and (4.32) imply that Γ_r satisfies

$$\Gamma_r(\mathbf{q}_\perp, q_z, g, \mu) = b^{-4}\,[g/g_0]^{4/15}\,\Gamma_r(b\mathbf{q}_\perp, b^2\,[g/g_0]^{4/15}\,q_z, g, \mu_0 b). \tag{4.39}$$

We now choose the reference length scale $b = \mu_0^{-1} = (q_z^2 + w^{-1}q_\perp^4)^{-1/4} \equiv [h(\mathbf{q})]^{-1}$. This implies that

$$l = \ln\left[\frac{\mu}{h(\mathbf{q})}\right] \tag{4.40}$$

since $\mu/\mu_0 = e^l$. We find the scaling form of the renormalized vertex function,

$$\begin{aligned}\Gamma_r &= [h(\mathbf{q})]^4\,[g/g_0]^{4/15}\,\Gamma_r\left(\frac{q_\perp}{h(\mathbf{q})}, \frac{q_z\,[g/g_0]^{4/15}}{[h(\mathbf{q})]^2}, g, 1\right) \\ &= g^{-2/3}\,[g/g_0]^{4/15}\,q_\perp^4 + [g/g_0]^{4/5}\,q_z^2,\end{aligned} \tag{4.41}$$

by squaring the term in the second slot of the renormalized vertex function and adding it to $g^{-2/3}$ times the fourth power of the term in the first slot. We then insert (4.37)

for g and transform back to variables with dimension to find the following expression for the renormalized vertex function:

$$\Gamma_r(\mathbf{q}) = B_{\rm sm}\left(1+\frac{5g_0}{64\pi}\ln\left[\frac{\overline{\mu}}{\overline{h}(\mathbf{q})}\right]\right)^{-4/5} q_z^2 + K_{\rm sm}\left(1+\frac{5g_0}{64\pi}\ln\left[\frac{\overline{\mu}}{\overline{h}(\mathbf{q})}\right]\right)^{2/5} q_\perp^4, \quad (4.42)$$

where $g_0 = B_{\rm sm}^{1/2}K_{\rm sm}^{-3/2}$, $\overline{\mu} = \mu/B_{\rm sm}^{1/6}$, and $\overline{h}(\mathbf{q}) = (q_z^2+\lambda^2 q_\perp^4)^{1/4}$ with $\lambda^2 = K_{\rm sm}/B_{\rm sm}$. $\overline{\mu}^2$ is a wavenumber $\Lambda \sim 1/a$ associated with the short distance scale a. We identify the renormalized compression and bending moduli $B_{\rm sm}(\mathbf{q})$ and $K_{\rm sm}(\mathbf{q})$ as the coefficients of the q_z^2 and $q_\perp^4$ terms respectively. The renormalized elastic constants scale as powers of logarithms at long wavelengths:

$$K_{\rm sm}(\mathbf{q}) \sim B_{\rm sm}^{-1/2}(\mathbf{q}) \sim \left[\ln\left(\frac{\overline{\mu}}{\overline{h}(\mathbf{q})}\right)\right]^{2/5}, \quad (4.43)$$

where the long wavelength regime is defined by wavenumbers q that satisfy $\overline{h}(\mathbf{q}) \ll \Lambda^{1/2}\exp\left[64\pi/(5g_0)\right]$. We see that $K_{\rm sm}(\mathbf{q})$ scales to infinity and $B_{\rm sm}(\mathbf{q})$ scales to zero as $q \to 0$.

4.3 RG Analysis of the Sliding Columnar Phase with Rigid Layers

In this section we calculate the logarithmic corrections to the elastic constants for the sliding columnar phase using the dimensional regularization scheme employed in the previous section. The steps we follow for the dimensional regularization of the SC phase closely resemble those followed for the dimensional regularization of the 3D smectic phase since the two Hamiltonians have similar forms. In this section we

assume that each 2D lattice of columns is flat and only allowed to fluctuate in the z-direction. We relax this assumption in Sec. 4.4 and find that the renormalized elastic constants are identical to those of the flat theory to lowest order in the coupling between strains in the y- and z-directions.

4.3.1 Rotationally Invariant Theory

The rotationally invariant continuum elasticity theory describing the sliding columnar phase was derived previously in Ref. [10, 20]. We found that a phase with weak positional correlations but strong orientational correlations between neighboring 2D smectic lattices was possible for sufficiently low temperatures. The strong orientational correlations require a rotation modulus in the Hamiltonian that assesses an energy cost for relative rotations of the lattices in addition to the compression and bending energy costs for a single lattice of columns. The continuum Hamiltonian for the idealized sliding columnar phase in three dimensions and in units of k_BT is

$$\mathcal{H} = \frac{1}{2}\int d^3x \left[B u_{zz}^2 + K(\partial_x^2 u_z)^2 + K_y(\partial_y \partial_x u_z)^2 \right], \tag{4.44}$$

where B, K_y, and K are the compression, rotation, and bending moduli divided by k_BT. The nonlinear strain u_{zz} is identical to the nonlinear strain for one layer of columns $u_{zz} = \partial_z u_z - (1/2)[(\partial_x u_z)^2 + (\partial_z u_z)^2]$. Below we will drop the $(\partial_z u_z)^2$ term from the nonlinear strain since it leads to terms in the nonlinear theory that are also irrelevant with respect to the three harmonic terms in (4.44). Therefore, we use the

approximate expression,

$$u_{zz} \approx \partial_z u_z - \frac{1}{2} \left(\partial_x u_z\right)^2 . \tag{4.45}$$

We note that u_{zz} and $\mathcal{H}$ do not possess a shear strain term $(\partial_y u_z)^2$ because neighboring layers of columns can slide relative to one another without energy cost. The absence of the shear energy cost is a unique feature of the sliding columnar elasticity theory. Because the Hamiltonian lacks terms with y-derivatives alone, it is invariant with respect to shifts in u_z that are only a function of y. Hence, $\mathcal{H}[u_z'] = \mathcal{H}[u_z]$ with

$$u_z' = u_z + f(y). \tag{4.46}$$

This invariance restates that there is no energy cost for sliding neighboring layers of columns relative to one another by an arbitrary amount.

4.3.2 Engineering Dimensions

We simplify the sliding columnar theory in (4.44) by rescaling the lengths so that B and K_y are replaced by unity and the nonlinear form of u_{zz} is preserved. We accomplish this by scaling u_z, y, and z but not x. To implement a dimensional regularization scheme it is necessary to let x become a $d-2$ dimensional displacement in the space perpendicular to y and z. Rescaled variables are defined via

$$\begin{aligned} u_z &= L_u \widetilde{u}_z, x = \widetilde{x}, \\ y &= L_y \widetilde{y}, \text{ and } z = L_z \widetilde{z}. \end{aligned} \tag{4.47}$$

We first set $L_u = L_z^{-1}$ to preserve the form of u_{zz} under (4.47). We then set the coefficients of $\tilde{u}_{zz}^2$ and $(\partial_{\tilde{y}}\partial_{\tilde{x}}\tilde{u}_z)^2$ to unity by choosing

$$L_y = \left(\frac{K_y^3}{B}\right)^{1/4} \text{ and } L_z = (K_y B)^{1/4}. \tag{4.48}$$

The rescaled Hamiltonian becomes

$$\mathcal{H} = \frac{1}{2}\int d^d\tilde{x}\left[\tilde{u}_{zz}^2 + (\partial_{\tilde{x}}\partial_{\tilde{y}}\tilde{u}_z)^2 + w^{-1}(\partial_{\tilde{x}}^2\tilde{u}_z)^2\right] \tag{4.49}$$

with

$$w = \frac{B^{1/2}}{KK_y^{1/2}} \tag{4.50}$$

and $d = 3 - \epsilon$. In the rest of this section we use (4.49) and drop the tildes.

We determine the dimension of the scaled variables from the dimensions of the elastic constants in (4.44). The dimensions $[B] = L^{-d}$ and $[K_y] = [K] = L^{2-d}$ dictate

$$\begin{aligned} [u_z] &= L^{(3-d)/2}, [x] = L, \\ [y] &= L^{(d-1)/2}, [z] = L^{(d+1)/2}, \text{ and } [w] = L^{d-3}. \end{aligned} \tag{4.51}$$

Note that $[w]$ scales as μ^ϵ with $[\mu] = L^{-1}$ and is relevant below $d = 3$.

The engineering dimensions in (4.51) imply that the Hamiltonian is invariant under the transformations $\mu \to \mu b$ and

$$u_z(\mathbf{x}) = b^{d_{u_z}} u_z'(\mathbf{x}') \tag{4.52}$$

with $x' = b^{-1}x$, $y' = b^{-(d-1)/2}y$, and $z' = b^{-(d+1)/2}z$, *i.e.* the Hamiltonian obeys

$$\mathcal{H}\left[u_z, w, \mu\right] = \mathcal{H}\left[u_z', wb^\epsilon, \mu b\right]. \tag{4.53}$$

This implies that there is a scaling form for the position correlation function $G(\mathbf{x}) = \langle u_z(\mathbf{x}) u_z(0) \rangle$ and the vertex function $\Gamma = G^{-1}$. We find that $\Gamma(\mathbf{q})$ obeys the following scaling relation:

$$\Gamma(\mathbf{q}, w) = b^{-(d+1)} \Gamma \left(b q_x, b^{(d-1)/2} q_y, b^{(d+1)/2} q_z, w b^{\epsilon} \right). \tag{4.54}$$

When $d = 3$ this reduces to

$$\Gamma(\mathbf{q}, w) = q_x^4 \Gamma \left(1, q_y/q_x, q_z/q_x^2 \right), \tag{4.55}$$

which is satisfied by the SC harmonic vertex function $\Gamma = q_z^2 + q_x^2 q_y^2 + w^{-1} q_x^4$.

4.3.3 RG Procedure

We now follow closely the RG procedure in Sec. 4.2.3. We rescale the lengths and fields, ensure that the SC Hamiltonian has the same form as the unscaled SC Hamiltonian, impose boundary conditions on the vertex function, and determine the renormalization constants in terms of the one-loop diagrammatic corrections. The first step in the process is to rescale lengths such that the renormalized SC Hamiltonian has the same form as (4.49). To preserve the form of the nonlinear strain, the z and u rescalings must be inverses of one another and the y rescaling is arbitrary. We, therefore, introduce two renormalization constants $\mathcal{Z}$ and $\mathcal{Z}_y$ such that

$$u_z(\mathbf{x}) = \mathcal{Z}^{1/3} u_z'(\mathbf{x}') = \mathcal{Z}^{1/3} u_z'(x, \mathcal{Z}_y y, \mathcal{Z}^{1/3} z). \tag{4.56}$$

This implies that $u_{zz}(\mathbf{x}) = \mathcal{Z}^{2/3} u'_{zz}(\mathbf{x}')$ and $\partial_x \partial_y u_z(\mathbf{x}) = \mathcal{Z}^{1/3} \mathcal{Z}_y \partial_{x'} \partial_{y'} u'_z(\mathbf{x}')$. We also define a unitless coupling constant g and renormalization constant $\mathcal{Z}_g$ by setting

$$w = g\mu^\epsilon \mathcal{Z}^{1/3} \mathcal{Z}_g \mathcal{Z}_y^{-1}. \tag{4.57}$$

The renormalized Hamiltonian then becomes

$$\mathcal{H}' = \frac{1}{2} \int d^d x' \left[\mathcal{Z} \mathcal{Z}_y^{-1} (u'_{zz})^2 + \mathcal{Z}^{1/3} \mathcal{Z}_y (\partial_{x'} \partial_{y'} u'_z)^2 + (g\mu^\epsilon \mathcal{Z}_g)^{-1} (\partial_{x'}^2 u'_z)^2 \right]. \tag{4.58}$$

We again employ standard RG procedures to calculate $\mathcal{Z}$, $\mathcal{Z}_y$, and $\mathcal{Z}_g$. The renormalization constants are fixed once we impose the following three conditions on the vertex function:

$$\begin{aligned} \left. \frac{d\Gamma}{dq_z^2} \right|_{q_z = \mu^2, q_{x,y} = 0} &= 1 \\ \left. \frac{d\Gamma}{d(q_x^2 q_y^2)} \right|_{q_z = \mu^2, q_{x,y} = 0} &= 1 \\ \left. \frac{d\Gamma}{dq_x^4} \right|_{q_z = \mu^2, q_{x,y} = 0} &= (g\mu^\epsilon)^{-1}. \end{aligned} \tag{4.59}$$

(Note that we have dropped the primes on the rescaled Hamiltonian.) The vertex function to one-loop order,

$$\begin{aligned} \Gamma &= q_z^2 + q_x^2 q_y^2 + (g\mu^\epsilon)^{-1} q_x^4 + \left(\mathcal{Z} \mathcal{Z}_y^{-1} - 1 \right) q_z^2 \\ &+ \left(\mathcal{Z}^{1/3} \mathcal{Z}_y - 1 \right) q_x^2 q_y^2 + (g\mu^\epsilon)^{-1} \left(\mathcal{Z}_g^{-1} - 1 \right) q_x^4 + \Sigma(\mathbf{q}), \end{aligned} \tag{4.60}$$

is obtained from (4.58) by adding and subtracting $q_z^2 + q_x^2 q_y^2 + (g\mu^\epsilon)^{-1} q_x^4$ and including the one-loop diagrammatic contributions to the vertex function, $\Sigma(\mathbf{q})$. In Appendix

D we calculate the diagrammatic contributions,

$$\left.\frac{d\Sigma}{dq_z^2}\right|_{q_z=\mu^2,q_{x,y}=0} = -\frac{g}{8\pi^2\epsilon} \tag{4.61}$$

$$\left.\frac{d\Sigma}{d(q_x^2q_y^2)}\right|_{q_z=\mu^2,q_{x,y}=0} = \frac{g}{24\pi^2\epsilon} \tag{4.62}$$

$$\left.\frac{d\Sigma}{dq_x^4}\right|_{q_z=\mu^2,q_{x,y}=0} = (g\mu^\epsilon)^{-1}\frac{g}{12\pi^2\epsilon}, \tag{4.63}$$

to lowest order in ϵ. From these we determine the renormalization constants to be

$$\mathcal{Z} = 1+\frac{g}{16\pi^2\epsilon} \tag{4.64}$$

$$\mathcal{Z}_y = 1-\frac{g}{16\pi^2\epsilon} \tag{4.65}$$

$$\mathcal{Z}_g = 1+\frac{g}{12\pi^2\epsilon}. \tag{4.66}$$

Callan-Symanzik Equation

The Callan-Symanzik equation is obtained by requiring that the original theory in (4.49) be independent of the length scale μ. To ensure this, we set $\mu d\Gamma/d\mu = 0$. This can be converted into a differential equation in the renormalized vertex function Γ_r using the following scaling relation:

$$\Gamma(\mathbf{q},w) = \mathcal{Z}^{-1/3}\mathcal{Z}_y\Gamma_r\left(q_x,\mathcal{Z}_y^{-1}q_y,\mathcal{Z}^{-1/3}q_z,g,\mu\right). \tag{4.67}$$

From the scaling relation we determine that the CS equation has the following four terms:

$$\left[\mu\frac{\partial}{\partial\mu}-\frac{\eta(g)}{3}\left(1+q_z\frac{\partial}{\partial q_z}\right)+\eta_y(g)\left(1-q_y\frac{\partial}{\partial q_y}\right)+\beta(g)\frac{\partial}{\partial g}\right]\Gamma_r = 0, \tag{4.68}$$

where $\eta(g)$ and $\beta(g)$ were defined previously in Sec. 4.2.3 and $\eta_y(g) = \beta(g) d \ln \mathcal{Z}_y/dg$. The solution to (4.68) is

$$\begin{aligned} \Gamma_r(\mathbf{q}, g, \mu) &= \exp\left[\int_0^l \left(\frac{\eta}{3} - \eta_y\right) dl'\right] \times \\ &\quad \Gamma_r\left(q_x, \exp\left[\int_0^l \eta_y dl'\right] q_y, \exp\left[\frac{1}{3}\int_0^l \eta dl'\right] q_z, g, \mu_0\right), \end{aligned} \tag{4.69}$$

with $\Gamma_r(l=0) = \Gamma_r(\mathbf{q}, g_0, \mu_0)$ and $\mu/\mu_0 = e^l$.

The coupling constant w must be independent of the length scale l. This condition yields a differential equation for the dimensionless constant g whose solution is

$$g(l) = \frac{g_0}{1 + g_0 l/(6\pi^2)}. \tag{4.70}$$

This equation in turn determines the l dependence of η and η_y since they are both proportional to g. We find

$$\eta(g) = -\eta_y(g) = \frac{g}{16\pi^2}, \tag{4.71}$$

and thus these scale as $1/l$ at long wavelengths.

Renormalized Elastic Constants

Using (4.70) for $g(l)$ and the relations for $\eta(g)$ and $\eta_y(g)$ in (4.71), we obtain the scaling form of the renormalized vertex function:

$$\Gamma_r(\mathbf{q}, g, \mu) = b^{-4} \left[g/g_0\right]^{1/2} \Gamma_r\left(bq_x, bq_y \left[g/g_0\right]^{-3/8}, b^2 q_z \left[g/g_0\right]^{1/8}, g, \mu_0 b\right). \tag{4.72}$$

To set the length scale, we choose

$$b = \mu_0^{-1} = (q_z^2 + q_x^2 q_y^2 + w^{-1} q_x^4)^{-1/4} \equiv [h(\mathbf{q})]^{-1} . \tag{4.73}$$

It follows that

$$l = \ln \left[\frac{\mu}{h(\mathbf{q})} \right] \tag{4.74}$$

since μ and l are related via $\mu/\mu_0 = e^l$. We then substitute (4.70) for g and transform back to variables with dimension to obtain the following expression for $\Gamma_r(\mathbf{q})$:

$$\begin{aligned} \Gamma_r(\mathbf{q}) &= B \left(1 + \frac{g_0}{6\pi^2} \ln \left[\frac{\overline{\mu}}{\overline{h}(\mathbf{q})} \right] \right)^{-3/4} q_z^2 \\ &+ K_y \left(1 + \frac{g_0}{6\pi^2} \ln \left[\frac{\overline{\mu}}{\overline{h}(\mathbf{q})} \right] \right)^{1/4} q_x^2 q_y^2 \\ &+ K \left(1 + \frac{g_0}{6\pi^2} \ln \left[\frac{\overline{\mu}}{\overline{h}(\mathbf{q})} \right] \right)^{1/2} q_x^4, \end{aligned} \tag{4.75}$$

where $g_0 = B^{1/2}/(K K_y^{1/2})$, $\overline{\mu} = \mu/(K_y B)^{1/8}$, and $\overline{h}(\mathbf{q}) = (q_z^2 + \lambda_y^2 q_x^2 q_y^2 + \lambda^2 q_x^4)^{1/4}$ with $\lambda_y^2 = K_y/B$ and $\lambda^2 = K/B$. $\overline{\mu}^2$ is an upper momentum cutoff $\Lambda \sim 1/a$ associated with the short distance scale a. We can now identify the q dependent elastic constants and determine their scaling as q tends to zero. At long wavelengths such that $\overline{h}(\mathbf{q}) \ll \Lambda^{1/2} \exp[6\pi^2/g_0]$ the ln term dominates, and we find

$$K_y(\mathbf{q}) \sim K^{1/2}(\mathbf{q}) \sim B^{-1/3}(\mathbf{q}) \sim \left[\ln \left(\frac{\overline{\mu}}{\overline{h}(\mathbf{q})} \right) \right]^{1/4} . \tag{4.76}$$

We see that $B(\mathbf{q})$ scales to zero and $K(\mathbf{q})$ and $K_y(\mathbf{q})$ scale to infinity as $q \to 0$. Also note in Table 4.1 that the exponents of the logarithmic power-laws of $B(\mathbf{q})$ and $K(\mathbf{q})$ are different from those of $B_{\rm sm}(\mathbf{q})$ and $K_{\rm sm}(\mathbf{q})$, but the signs of the respective exponents are the same.

4.4 Sliding Columnar Phase with Fluctuating Lipid Bilayers

In the preceeding section, we considered a model for lamellar DNA-lipid complexes in which lipid bilayers were treated as rigid planes and no displacements of DNA lattices in the y-direction were allowed. In physically realized complexes, lipid bilayers can undergo shape fluctuations and DNA lattices can undergo y-displacements. We can parameterize the shape of the nth bilayer by a height function $h_n(x,z)$, which in the continuum limit becomes $h(\mathbf{x}) = h_{y/a}(x,z)$. The y-displacement of the DNA lattices in the continuum limit is $u_y(\mathbf{x})$. At long wavelengths the displacements $h(\mathbf{x})$ and $u_y(\mathbf{x})$ are locked together. The lock-in occurs because there is an energy cost for translating each lattice of columns and the lipid bilayers by different constant amounts in the y-direction. (See Fig.2.1.) We can, therefore, describe long wavelength elastic distortions and fluctuations of the sliding columnar phase in terms of an elastic Hamiltonian expressed in terms of displacements u_z and u_y:

$$\begin{aligned} \mathcal{H}_b\,[u_y,u_z] &= \frac{1}{2}\int d^3x\,\Big[B^z u_{zz}^2 + K_{xx}^z(\partial_x^2 u_z)^2 + K_{xy}^z(\partial_x\partial_y u_z)^2 + B^y u_{yy}^2 \\ &+ K_{xx}^y(\partial_x^2 u_y)^2 + K_{xz}^y(\partial_x\partial_z u_y)^2 + K_{zz}^y(\partial_z^2 u_y)^2 + 2B^{yz}u_{yy}u_{zz}\Big], \end{aligned} \tag{4.77}$$

where u_{yy} and u_{zz} are nonlinear strains. We define $\mathcal{H}_b$ to have units of k_BT, and therefore the constants appearing in this equation are the compression and bending moduli divided by k_BT. The first three terms in (4.77) were discussed previously in Sec. 4.3 as the u_z theory for the sliding columnar phase without fluctuations of the

lipid bilayers. The next four terms are the compression and bending energies for an anisotropic 3D smectic with layers parallel to the xz plane. The bending energy is anisotropic due to the presence of the DNA columns. The final term is a coupling of the nonlinear strains u_{yy} and u_{zz}.

The form of the nonlinear strains depends on whether Eulerian or Lagrangian coordinates are used[6]. We find it convenient to use a mixed parameterization in which x and z are Eulerian coordinates specifying a position in space and $y = na$ is a Lagrangian coordinate specifying the layer number. The nonlinear strains u_{zz} and u_{yy} for this mixed parameterization were derived previously in Ref. [21]. To quadratic order in gradients of u_y and u_z, we find

$$u_{yy} = \partial_y u_y - \frac{1}{2}\left[(\partial_x u_y)^2 + (\partial_z u_y)^2 - (\partial_y u_y)^2\right] \tag{4.78}$$

$$u_{zz} = \partial_z u_z - \frac{1}{2}\Big[(\partial_x u_z)^2 + (\partial_z u_z)^2 - (\partial_z u_y)^2\Big]. \tag{4.79}$$

Note that the nonlinear strain u_{zz} does not contain the shear strain term proportional to $(\partial_y u_z)^2$. Thus, layer fluctuations do not modify the essential invariance $u_z' \to u_z + f(y)$ of the sliding columnar phase to the order considered here. In what follows, we will truncate the nonlinear strains to

$$u_{yy} \approx \partial_y u_y \tag{4.80}$$

$$u_{zz} \approx \partial_z u_z - \frac{1}{2}(\partial_x u_z)^2 \tag{4.81}$$

since the other nonlinear terms are irrelevant with respect to the sliding columnar

harmonic terms in (4.77).

The goal of this section is to calculate the Grinstein-Pelcovits renormalization of the eight elastic constants found in the theory of the sliding columnar phase with lipid bilayer fluctuations. Since the nonlinear strains do not introduce a $(\partial_y u_z)^2$ term, we do not expect the bilayer fluctuations to alter the renormalization of the SC elastic constants in the simplified theory of the previous section to lowest order in B^{yz}. We will again use dimensional regularization to calculate the renormalization. The format will closely parallel the previous SC calculation. We first determine which of the harmonic terms in (4.77) are relevant and drop irrelevant terms. We then rescale lengths and fields, ensure that the Hamiltonian retains its unscaled form, impose boundary boundary conditions on the vertex function, and calculate the renormalization constants. The renormalization constants then determine the scaling form of the vertex function.

4.4.1 Engineering Dimensions

We begin by rescaling the lengths and the fields in $\mathcal{H}_b$. In addition to the rescalings in Sec. 4.3.2, we also rescale u_y according to

$$u_y = L_{u_y} \tilde{u}_y. \tag{4.82}$$

We first impose the conditions of the previous section, *i.e.* we set the coefficients of $\tilde{u}_{zz}^2$ and $(\partial_{\tilde{x}}\partial_{\tilde{y}} u_z)^2$ to unity and ensure that both terms in the nonlinear strain u_{zz}

scale the same way. As an added constraint, we set the coefficient of $\tilde{u}_{yy}^2$ to unity. These conditions fix

$$\begin{aligned} L_{u_y} &= \left(\frac{K_{xy}^z}{B^z}\right)^{1/4} \frac{1}{(B^y)^{1/2}} \\ L_y &= \left(\frac{(K_{xy}^z)^3}{B^z}\right)^{1/4} \\ L_z &= L_{u_z}^{-1} = (K_{xy}^z B^z)^{1/4}. \end{aligned} \tag{4.83}$$

Once we plug in these scaling lengths, the rescaled Hamiltonian becomes

$$\begin{aligned} \widetilde{\mathcal{H}}_b &= \frac{1}{2}\int d^d\tilde{x}\Big[\tilde{u}_{zz}^2 + (\partial_{\tilde{x}}\partial_{\tilde{y}}u_z)^2 + w^{-1}(\partial_{\tilde{x}}^2\tilde{u}_z)^2 + (\partial_{\tilde{y}}\tilde{u}_y)^2 + 2v(\partial_{\tilde{y}}\tilde{u}_y)\tilde{u}_{zz} \\ &+ v_1(\partial_{\tilde{x}}^2\tilde{u}_y)^2 + v_2(\partial_{\tilde{x}}\partial_{\tilde{z}}\tilde{u}_y)^2 + v_3(\partial_{\tilde{z}}^2\tilde{u}_y)^2\Big] \end{aligned} \tag{4.84}$$

with

$$\begin{aligned} w &= \frac{(B^z)^{1/2}}{K_{xx}^z(K_{xy}^z)^{1/2}}, \quad v = \frac{B^{yz}}{(B^yB^z)^{1/2}}, \quad v_1 = \frac{K_{xx}^y(K_{xy}^z)^{3/2}}{B^y(B^z)^{1/2}}, \\ v_2 &= \frac{K_{xz}^yK_{xy}^z}{B^yB^z}, \text{ and } v_3 = \frac{K_{zz}^y(K_{xy}^z)^{1/2}}{(B^z)^{3/2}B^y}. \end{aligned} \tag{4.85}$$

(It is again necessary to let x represent a $d-2$ displacement with $d = 3-\epsilon$.) The dimensions of the scaled variables and the w and v coefficients are determined using (4.83) and the dimensions of the compression and bending moduli, $[B] = L^{-d}$ and $[K] = L^{2-d}$. (Note we have dropped the tildes on the scaled variables in the following discussion.) We find

$$\begin{aligned} [u_y] &= L^{(1-d)/2}, \quad [v] = L^0, \quad [v_1] = L^{5-d}, \\ [v_2] &= L^4, \text{ and } [v_3] = L^{d+3}, \end{aligned} \tag{4.86}$$

while the dimensions of u_z, y, z, and w were given previously in (4.51). Note that v does not scale with length. Also note that the coefficients v_1, v_2, and v_3 are irrelevant when $d = 3$. We drop the irrelevant terms and arrive at the following simplified Hamiltonian:

$$\mathcal{H}_b = \frac{1}{2}\int d^dx \left[u_{zz}^2 + (\partial_x\partial_y u_z)^2 + w^{-1}(\partial_x^2 u_z)^2 + (\partial_y u_y)^2 + 2v(\partial_y u_y)u_{zz}\right]. \quad (4.87)$$

4.4.2 RG Procedure

The present RG procedure will be similar to those employed in sections 4.2.3 and 4.3.3, except we now have two coupling constants, w and v, instead of one. We will show that the inclusion of v does not alter the renormalization of the sliding columnar elastic constants to lowest order in v. As before, we rescale the fields and lengths and seek a renormalized Hamiltonian with the same form as (4.87). We scale y, z, and u_z as we did previously in (4.56) and u_y by $\tilde{\mathcal{Z}}^{1/2}$ as follows:

$$u_y(\mathbf{x}) = \tilde{\mathcal{Z}}^{1/2}u_y'(\mathbf{x}') = \tilde{\mathcal{Z}}^{1/2}u_y'(x, \mathcal{Z}_y y, \mathcal{Z}^{1/3}z). \quad (4.88)$$

The rescaled Hamiltonian $\mathcal{H}_b'$ looks similar to (4.58) with two additional terms due to fluctuations of the bilayers. We drop the primes on the variables and find

$$\begin{aligned}\mathcal{H}_b &= \frac{1}{2}\int d^dx\Big[\mathcal{Z}\mathcal{Z}_y^{-1}u_{zz}^2 + \mathcal{Z}^{1/3}\mathcal{Z}_y(\partial_x\partial_y u_z)^2 + (g\mu^\epsilon\mathcal{Z}_g)^{-1}(\partial_x^2 u_z)^2 \quad (4.89)\\ &+ \mathcal{Z}^{-1/3}\mathcal{Z}_y\tilde{\mathcal{Z}}(\partial_y u_y)^2 + 2\overline{v}\mathcal{Z}_v(\partial_y u_y)u_{zz}\Big],\end{aligned}$$

where

$$\overline{v}\mathcal{Z}_v = v\tilde{\mathcal{Z}}^{1/2}\mathcal{Z}^{1/3} \quad (4.90)$$

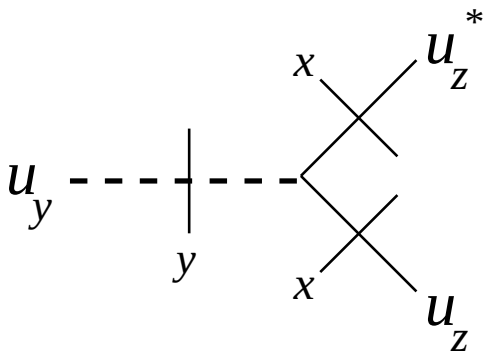

Figure 4.1: Schematic diagram of the relevant nonlinear term $\partial_y u_y (\partial_x u_z)^2$ generated by the sliding columnar theory with lipid bilayer fluctuations. The symbols x and y written adjacent to the dividing lines represent x and y derivatives of the respective fields. The u_y field is denoted by a dashed line while u_z is denoted by an unbroken line.

and $\mathcal{Z}_g$ was defined previously.

Boundary conditions imposed on the vertex functions $\Gamma_{ij}(\mathbf{q})$ with $i, j = y, z$ ensure that the Hamiltonian retains its original form in (4.87) after rescaling. The vertex function is defined by $\Gamma_{ij}(\mathbf{q}) = G_{ij}^{-1}(\mathbf{q})$ with $G_{ij}(\mathbf{x}) = \langle u_i(\mathbf{x}) u_j(0) \rangle$. The conditions imposed on Γ_{zz} are identical to those given in (4.59); these are augmented by two conditions on Γ_{yz} and Γ_{yy}.

$$\begin{aligned} \left. \frac{d\Gamma_{yz}}{d(q_y q_z)} \right|_{q_z = \mu^2, q_{x,y} = 0} &= 2\overline{v} \\ \left. \frac{d\Gamma_{yy}}{dq_y^2} \right|_{q_z = \mu^2, q_{x,y} = 0} &= 1. \end{aligned} \tag{4.91}$$

Once we impose these conditions on the vertex functions, we solve for the $\mathcal{Z}$'s in terms of the one-loop diagrammatic contributions Σ_{ij}, where, for instance, Σ_{zz} is the one-loop correction to the vertex function Γ_{zz}. The diagrammatic corrections arise from the quadratic term in u_{zz}. u_{zz}^2 generates $\partial_z u_z (\partial_x u_z)^2$, which was already present

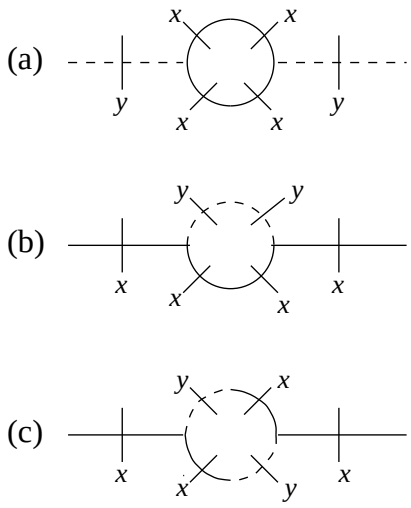

Figure 4.2: The three diagrams that can be formed by contracting $\partial_y u_y (\partial_x u_z)^2$ with itself. The only diagram that contributes to the renormalization of B^y is pictured in (a). The diagrams in (b) and (c) contribute to the renormalization of both K^z_{xx} and K^z_{xy}.

in the theory with $u_y = 0$. The coupling of u_{yy} to u_{zz} generates a new nonlinear term, $\partial_y u_y (\partial_x u_z)^2$. This term is shown schematically in Fig. 4.1. There are six new one-loop diagrams in addition to the three diagrams of the rigid sliding columnar theory; these are shown in Figs. 4.2 and 4.3. The diagrams in Fig. 4.2 arise from contractions of $\partial_y u_y (\partial_x u_z)^2$ with itself and the diagrams in Fig. 4.3 arise from contractions of $\partial_y u_y (\partial_x u_z)^2$ with $\partial_z u_z (\partial_x u_z)^2$. The one-loop diagrammatic corrections Σ_{zz} are easy to calculate since the form of the propagator G_{zz} is unchanged from its form in the rigid sliding columnar theory. The form is not changed, but the compression modulus B is renormalized by a factor of $1 - \overline{v}^2$. The one-loop diagrammatic corrections to

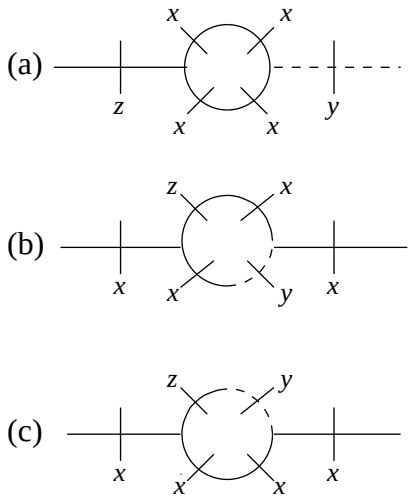

Figure 4.3: The three diagrams that can be formed by contracting $\partial_z u_z (\partial_x u_z)^2$ with $\partial_y u_y (\partial_x u_z)^2$. The only diagram that contributes to the renormalization of B^{yz} is pictured in (a). The diagrams pictured in (b) and (c) contribute to the renormalization of both K^z_{xx} and K^z_{xy}.

Γ_{zz} are shown below to lowest order in ϵ:

$$\begin{aligned}
\left.\frac{d\Sigma_{zz}}{dq_z^2}\right|_{q_z=\mu^2, q_{x,y}=0} &= -\frac{g}{8\pi^2\epsilon}\frac{1}{\sqrt{1-\overline{v}^2}} \\
\left.\frac{d\Sigma_{zz}}{d(q_x^2 q_y^2)}\right|_{q_z=\mu^2, q_{x,y}=0} &= \frac{g}{24\pi^2\epsilon}\sqrt{1-\overline{v}^2} \\
\left.\frac{d\Sigma_{zz}}{dq_x^4}\right|_{q_z=\mu^2, q_{x,y}=0} &= (g\mu^\epsilon)^{-1}\frac{g}{12\pi^2\epsilon}\sqrt{1-\overline{v}^2}.
\end{aligned} \tag{4.92}$$

These expressions reduce to those found for the rigid theory when $\overline{v} = 0$.

The calculation of one-loop diagrammatic corrections to Γ_{yz} and Γ_{yy} is similarly straightforward. Σ_{yz} is given by the diagram in Fig. 4.3(a). This amplitude is proportional to $\overline{v}$ since it is formed by contracting $\partial_y u_y (\partial_x u_z)^2$ with $\partial_z u_z (\partial_x u_z)^2$. Σ_{yy} is given by the diagram in Fig. 4.2(a); it must be proportional to $\overline{v}^2$ since it is formed by contracting $\partial_y u_y (\partial_x u_z)^2$ with itself. The one-loop corrections to Γ_{yz} and Γ_{yy} are

given below to lowest order in ϵ:

$$\begin{aligned} \left.\frac{d\Sigma_{yz}}{d(q_y q_z)}\right|_{q_z=\mu^2, q_{x,y}=0} &= -\frac{g\overline{v}}{8\pi^2\epsilon}\frac{1}{\sqrt{1-\overline{v}^2}} \\ \left.\frac{d\Sigma_{yy}}{dq_y^2}\right|_{q_z=\mu^2, q_{x,y}=0} &= -\frac{g\overline{v}^2}{8\pi^2\epsilon}\frac{1}{\sqrt{1-\overline{v}^2}}. \end{aligned} \tag{4.93}$$

We then use the conditions imposed on the vertex functions in (4.59) and (4.91) and the one-loop diagrammatic corrections in (4.92) and (4.93) to find the renormalization constants (the $\mathcal{Z}$'s) in terms of g and $\overline{v}$. We find that the relations for $\mathcal{Z}$, $\mathcal{Z}_y$, and $\mathcal{Z}_g$ are unchanged to zeroth order in $\overline{v}$. $\tilde{\mathcal{Z}}$ and $\mathcal{Z}_v$ also have terms that are independent of $\overline{v}$ as shown below to lowest order in ϵ:

$$\begin{aligned} \tilde{\mathcal{Z}} &\approx 1 + \frac{g}{12\pi^2\epsilon} \\ \mathcal{Z}_v &\approx 1 + \frac{g}{8\pi^2\epsilon}. \end{aligned} \tag{4.94}$$

The variation of g and $\overline{v}$ with the length scale μ is obtained by enforcing that both bare coupling constants do not depend on μ, *i.e.*, we set $\mu dw/d\mu = \mu dv/d\mu = 0$. These two requirements determine the recursion relations for g and $\overline{v}$; we find that dg/dl is unchanged to lowest order in $\overline{v}$ and

$$\frac{d\overline{v}}{dl} = -\frac{g\overline{v}}{16\pi^2}. \tag{4.95}$$

The zeroth order solution for g was found previously in (4.70); we plug this solution into (4.95) and find

$$\overline{v}(l) = \frac{\overline{v}_0}{\left[1 + g_0 l/(6\pi^2)\right]^{3/8}}, \tag{4.96}$$

where $\overline{v}_0 = B^{yz}/\sqrt{B^y B^z}$ and $g_0 = \sqrt{B^z/K^z_{xy}}/K^z_{xx}$.

4.4.3 Renormalized Elastic Constants

We found in the previous two sections that the renormalized elastic constants are obtained by solving the Callan-Symanzik equation for the renormalized vertex function. We find the CS equations for Γ^r_{ij} using the following scaling equations which relate the bare and renormalized vertex functions:

$$\Gamma_{zz}(\mathbf{q}, w, v) = \mathcal{Z}^{-1/3}\mathcal{Z}_y\Gamma^r_{zz}(\mathbf{q}', g, \overline{v}, \mu) \tag{4.97}$$

$$\Gamma_{yy}(\mathbf{q}, w, v) = \widetilde{\mathcal{Z}}^{-1}\mathcal{Z}_y^{-1}\mathcal{Z}^{1/3}\Gamma^r_{yy}(\mathbf{q}', g, \overline{v}, \mu) \tag{4.98}$$

$$\Gamma_{yz}(\mathbf{q}, w, v) = \widetilde{\mathcal{Z}}^{-1/2}\mathcal{Z}_y\Gamma^r_{yz}(\mathbf{q}', g, \overline{v}, \mu). \tag{4.99}$$

Eq. (4.97) yields a CS equation identical to (4.68) to lowest order in $\overline{v}$, and thus the renormalized elastic constants $B^z(\mathbf{q})$, $K^z_{xx}(\mathbf{q})$, and $K^z_{xy}(\mathbf{q})$ are identical to those obtained in (4.75) using the $u_y = 0$ theory. The fact that the elastic constants are identical to zeroth order in $\overline{v}$ is a consequence of the fact that the nonlinear term proportional to $\overline{v}$ does not introduce any harmonic terms that were not already present in the theory without u_y fluctuations. We also find that the coefficient of $\Gamma^r_{yy}(\mathbf{q}')$ is unity to lowest order $\overline{v}$, and hence the vertex function Γ_{yy} does not rescale. As a result, $B^y = B^y(l = 0)$ plus higher order terms in $\overline{v}$.

We do, however, find a nontrivial renormalization of B^{yz}. The scaling relation in (4.99) leads to a CS equation for Γ^r_{yz} with a similar form to the one found in (4.68).

We find

$$\left[\mu\frac{\partial}{\partial\mu} - \frac{\widetilde{\eta}(g)}{2} - \frac{\eta(g)}{3}\left(q_z\frac{\partial}{\partial q_z}\right) + \eta_y(g)\left(1 - q_y\frac{\partial}{\partial q_y}\right) + \beta(g)\frac{\partial}{\partial g}\right]\Gamma_r = 0 \quad (4.100)$$

to zeroth order in $\overline{v}$, where

$$\widetilde{\eta}(g) = \beta(g)\frac{d(\ln\widetilde{\mathcal{Z}})}{dg} = \frac{g}{12\pi^2} \quad (4.101)$$

and η and η_y were defined previously. The solution to (4.100) can be transcribed from (4.69) and is displayed below:

$$\Gamma^r_{yz}(\mathbf{q}, g, \overline{v}(g), \mu) = \exp\left[\int_0^l \left(\frac{\widetilde{\eta}}{2} - \eta_y\right) dl'\right] \times \quad (4.102)$$
$$\Gamma^r_{yz}\left(q_x, \exp\left[\int_0^l \eta_y dl'\right] q_y, \exp\left[\frac{1}{3}\int_0^l \eta dl'\right] q_z, g, \mu_0\right).$$

Since η, η_y, and $\widetilde{\eta}$ scale as $1/l$, the integrals in the arguments of the exponentials scale logarithmically with l. Thus, the exponentials yield power-laws in g, and we find, for example,

$$\exp\left[\int_0^l \left(\frac{\widetilde{\eta}}{2} - \eta_y\right) dl'\right] = \left[\frac{g(l)}{g_0}\right]^{5/8}. \quad (4.103)$$

The renormalized vertex function in (4.102) obeys a scaling form analogous to the one obeyed by the renormalized sliding columnar vertex function in (4.72). We find

$$\Gamma^r_{yz}(\mathbf{q}, g, \mu) = b^{-3}\left[g/g_0\right]^{5/8}\Gamma^r_{yz}\left(bq_x, bq_y\left[g/g_0\right]^{-3/8}, b^2 q_z\left[g/g_0\right]^{1/8}, g, \mu_0 b\right), \quad (4.104)$$

where the b^{-3} prefactor is present because y scales as b and z scales as b^2. We then choose $b = \mu_0^{-1} = [q_z^2 + q_x^2 q_y^2 + w^{-1}q_x^4]^{-1/4} \equiv [h(\mathbf{q})]^{-1}$ to match the conventions of the

previous section, substitute (4.70) for g/g_0, and return to variables with dimension. The renormalized vertex function becomes

$$\Gamma^r_{yz}(\mathbf{q}) = 2B^{yz}\left[1 + \frac{g_0}{6\pi^2}\ln\left[\frac{\overline{\mu}}{\overline{h}(\mathbf{q})}\right]\right]^{-3/4} q_y q_z, \tag{4.105}$$

where $\overline{\mu}$ and $\overline{h}(\mathbf{q})$ were defined previously. The renormalized elastic constant $B^{yz}(\mathbf{q})$ is the coefficient of $q_y q_z$ in the above expression. Therefore, we find that both B^z and B^{yz} scale to zero logarithmically with $\mathbf{q}$ at long wavelengths defined by $\overline{h}(\mathbf{q}) \ll \Lambda^{1/2}\exp[6\pi^2/g_0]$.

4.5 Conclusion

We have calculated the Grinstein-Pelcovits renormalization of the elastic constants for the sliding columnar phase. We used a simplified model of the sliding columnar phase in which the DNA columns were prevented from fluctuating perpendicular to the lipid layers. We found that the elastic constants scaled as powers of $\ln[1/q]$ at long wavelengths. In particular, we found that the compression modulus B scales to zero and the rotation and bending moduli K_y and K scale to infinity as q tends to zero. We employed dimensional regularization in our RG analysis of the sliding columnar phase to ensure rotational invariance. RG schemes that break rotational invariance, such as the momentum-shell technique, did not yield correct results.

Chapter 5

Transition to the Nematic Lamellar Phase

In the preceding chapters, we studied the effects of thermal fluctuations on CL-DNA complexes and found that they induce a second-order phase transition from a columnar phase with strong positional correlations between neighboring lattices to the sliding columnar phase with weak positional correlations between neighboring lattices. In this chapter, we focus instead on the disordering effects of dislocations. Edge dislocations in 2D smectic systems have a finite core energy and thus exist at all temperatures. As a result, they destroy the positional order and convert the 2D smectic phase to a nematic phase at the longest lengthscales[31]. We show below that, in contrast to true two-dimensional smectic systems, edge dislocations in the sliding columnar phase have a core energy that scales logarithmically with system size, and therefore there is a transition temperature T_{KT} below which the defect-free sliding columnar phase is favored and above which edge dislocations unbind, melt the 2D smectic lattices in each gallery, and convert the sliding columnar phase into a

nematic lamellar phase.

5.1 Edge Dislocations

The DNA mass density is only defined within each two-dimensional layer, and thus point dislocations with cores parallel to the y-axis are the only allowed defects. These edge dislocations signal the removal or insertion of DNA columns in a given layer n which causes the phase of the DNA mass density wave $q_0(z - u_z^n(\mathbf{r}))$ to jump by integer multiple multiples of 2π. If we define $\mathbf{v}^n(\mathbf{r}) = \boldsymbol{\nabla}_\perp u_z^n(\mathbf{r})$, the dislocation is characterized by

$$\oint_\Gamma \mathbf{v}^n \cdot d\boldsymbol{\ell} = k_n d, \tag{5.1}$$

where k_n is its integer strength and Γ is some contour in the nth gallery enclosing the dislocation. Eq. 5.1 indicates that $\mathbf{v}^n(\mathbf{r})$ has a singular part satisfying $\boldsymbol{\nabla}_\perp \times \mathbf{v}^n(\mathbf{r}) = b_y(\mathbf{x})\hat{y}$, where

$$b_y(\mathbf{x}) = da \sum_n m_n(\mathbf{r})\delta(y - na) \tag{5.2}$$

and

$$m_n(\mathbf{r}) = \sum_l k_{n,l}\delta^2(\mathbf{r} - \mathbf{r}_{n,l}) \tag{5.3}$$

is the dislocation density in gallery n with l labeling each dislocation.

We will now calculate the energy cost for edge dislocations in the sliding columnar phase. Since the DNA columns bend to fill the void caused by edge dislocations, we include energy costs associated with nonuniform changes in the DNA director in

addition to the sliding columnar elastic energy in Eq. 3.1. We therefore consider the Hamiltonian

$$\begin{aligned}\mathcal{H}_g[\mathbf{v}^n,\theta^n] &= \frac{1}{2}\sum_n a\int d^2r\Big[B(v_z^n)^2+D(v_x^n-\theta^n)^2+K(\partial_x\theta^n)^2 \\ &\quad +\frac{K_y}{a^2}(\theta^n-\theta^{n+1})^2+K_{zx}(\partial_z\theta^n)^2\Big]\end{aligned} \tag{5.4}$$

that couples displacements and angles in a rotationally invariant way. This energy reduces to the sliding columnar elastic energy in Eq. 3.1 when θ^n is integrated out. Our strategy is to minimize this Hamiltonian subject to a nonzero dislocation density $b_y(\mathbf{x})$. The algebra is simpler in Fourier space. To transform from real space to Fourier space, we use

$$\mathbf{v}(\mathbf{q})=\sum_n a\int d^2r e^{-i(\mathbf{q}_\perp\cdot\mathbf{r}+q_yna)}\mathbf{v}^n(\mathbf{r}) \tag{5.5}$$

and a similar expression for $\theta(\mathbf{q})$. The Euler-Lagrange equations yield expressions for $\theta(\mathbf{q})$ and $v_z(\mathbf{q})$:

$$\theta(\mathbf{q}) = \frac{Dv_x(\mathbf{q})}{D+K(\mathbf{q})q^2} \tag{5.6}$$

$$v_z(\mathbf{q}) = -\frac{D}{B}\frac{q_x}{q_z}\frac{K(\mathbf{q})q^2}{D+K(\mathbf{q})q^2}v_x(\mathbf{q}), \tag{5.7}$$

where

$$K(\mathbf{q})q^2=Kq_x^2+K_yq_y^2p(q_ya)+K_{zx}q_z^2 \tag{5.8}$$

and $p(u)=2(1-\cos[u])/u^2$. We then employ the constraint equation

$$i\mathbf{q}_\perp\times\mathbf{v}(\mathbf{q})=b_y(\mathbf{q})\hat{y} \tag{5.9}$$

which relates $v_x(\mathbf{q})$ to $v_z(\mathbf{q})$ and the specified dislocation density $b_y(\mathbf{q})$ to completely determine $\theta(\mathbf{q})$ and $\mathbf{v}(\mathbf{q})$. In the final step, we insert the expressions for $\theta(\mathbf{q})$ and $\mathbf{v}(\mathbf{q})$ into the Fourier transformed version of Eq. 5.4 and find

$$E = \frac{B}{2}\int_{-\pi/a}^{\pi/a}\frac{dq_y}{2\pi}\int\frac{d^2q_\perp}{(2\pi)^2}\frac{K(\mathbf{q})q^2|b_y(\mathbf{q})|^2}{Bq_z^2 + K(\mathbf{q})q^2[q_x^2 + (B/D)q_z^2]} \tag{5.10}$$

for the energy of edge dislocations in the sliding columnar phase. In the calculations of the self energy and interaction energy below, we take the $D \to \infty$ limit and assume $K(\mathbf{q})q^2 \approx Kq_x^2 + K_y q_y^2 p(q_y a)$. The terms that are neglected in these approximations are subdominant to the Bq_z^2 term at long lengthscales, i.e. these terms have at least two more factors of q_z. If we set $K_y = 0$, Eq. 5.10 reduces to expression for the energy cost for edge dislocations in a 2D smectic[31].

5.2 Self and Interaction Energies

We now calculate the energy of an individual dislocation and the interaction energy of a pair of dislocations using Eq. 5.10. We find that both the energy of an isolated dislocation and the energy of two dislocations in different layers diverges logarithmically with system size. In contrast, the energy of two dislocations in the same layer with equal and opposite signs diverges only with their separation. Since the energy of an isolated dislocation or pairs of dislocations in different layers diverges logarithmically with system size, the sliding columnar phase will Kosterlitz-Thouless melt to a nematic lamellar phase when the temperature is greater than a dislocation unbinding

temperature T_{KT} which will be calculated below.

The self energy of an isolated ± 1 dislocation is obtained by inserting $b_y(\mathbf{q}) = \pm ad$ into Eq. 5.10. We find that

$$E_{\pm} = \frac{d^2\sqrt{BK_y}}{\pi^2} \ln\left[e^{D(w)} w L_x/x^*\right] \tag{5.11}$$

diverges logarithmically with system size. In the above expression, $w = \Lambda_x x^*$,

$$D(w) = \int_0^w \frac{dt}{t}\left[\frac{J(t)}{J(0)} - 1\right] = \begin{cases} \pi w/4 & \text{when } w \to \infty \\ 0 & \text{when } w \to 0, \end{cases} \tag{5.12}$$

$$J(t) = \int_0^\pi du\sqrt{f(u) + t^2}, \tag{5.13}$$

$f(u) \equiv u^2 p(u)$, and $J(0) = 4$.

The interaction energy of two dislocations with strengths k_1 and k_2 separated by $\mathbf{x} = (\mathbf{r}, na)$ is obtained using

$$b_y(\mathbf{q}) = ad\left(k_1 + k_2 e^{-i\mathbf{q}\cdot\mathbf{x}}\right). \tag{5.14}$$

We find that the interaction energy of the pair of dislocations can be decomposed as

$$E_2(\mathbf{r}, na) \equiv E_2^{\text{div}} + E_2^{\text{int}}. \tag{5.15}$$

The first term E_2^{div} diverges logarithmically with system size, and the second term E_2^{int} does not diverge with system size. The divergent contribution is given by

$$E_2^{\text{div}} = C_2(n, k_1, k_2) \ln\left[e^{F_n(w,k_1,k_2)} w L_x/x^*\right], \tag{5.16}$$

where

$$F_n(w,k_1,k_2) = \int_0^w \frac{dt}{t} \frac{(k_1+k_2)^2\left[J(t)-J(0)\right] - 2k_1k_2\left[L_n(t)-L_n(0)\right]}{J(0)[k_1+k_2]^2 - 2k_1k_2L_n(0)} \tag{5.17}$$

depends on n, the upper wavenumber cutoff w, and the strengths of the dislocations. In the expression for $F_n(w,k_1,k_2)$,

$$L_n(t) = \int_0^\pi du(1-\cos[nu])\sqrt{f(u)+t^2}, \tag{5.18}$$

$$L_n(0) = \frac{16n^2}{4n^2-1}, \tag{5.19}$$

and $F_0(w,k_1,k_2) = D(w)$. The coefficient of the $\ln L_x$ term is given by

$$C_2(n,k_1,k_2) = \frac{d^2\sqrt{BK_y}}{\pi^2}\left([k_1+k_2]^2 - \frac{8n^2}{4n^2-1}k_1k_2\right). \tag{5.20}$$

It is apparent from this expression that when $k_1 = -k_2$ and $n = 0$ (i.e. the two dislocations are located in the same layer), $C_2(0,k_1,-k_1) = 0$ and the energy does not diverge with system size.

However, when $n \neq 0$, $C_2(n,k_1,k_2) > 0$ and the dislocation energy diverges logarithmically with system size. To see this, consider the two cases: $k_1/k_2 < 0$ and $k_1/k_2 > 0$. When the two dislocations have opposite signs, both terms in Eq. 5.20 are positive and $C_2(n,|k_1|,-|k_2|) > 0$. In this case, the configuration with the lowest energy is $k_1 = -k_2 = 1$ with $n \to \infty$, and thus opposite-signed dislocations in different layers repel each other. The energy of this configuration is $E_{+-} = 2E_+$. When the two dislocations have the same sign, the two terms in Eq. 5.20 have opposite signs,

but $C_2(n,|k_1|,|k_2|) > 0$. In this case, the minimum value of C_2 occurs at $n = 1$ and

$$C_2(1,|k_1|,|k_2|) = \frac{d^2 k_2^2 \sqrt{BK_y}}{\pi^2}\left[\left(\frac{k_1}{k_2}\right)^2 - \frac{2}{3}\frac{k_1}{k_2} + 1\right] > 0 \tag{5.21}$$

for all values of $k_1/k_2 > 0$. Since $n = 1$ corresponds to the minimum energy, like-signed dislocations in different layers attract each other. The configuration $k_1 = k_2 = 1$ and $n = 1$ has energy $E_{++} = 4E_+/3$ and thus $E_{+-} > E_{++} > E_+$. The energy of an arbitrary configuration of dislocations can also be calculated; we find that the energy of an individual dislocation yields the lowest energy[23].

The nondivergent contribution to $E_2(\mathbf{r}, na)$ is given by

$$E_2^{\text{int}} = -k_1 k_2 \frac{d^2\sqrt{BK_y}}{2\pi^2} K_2(\mathbf{r}, na). \tag{5.22}$$

If the system overcomes the $\ln L_x$ energy barrier, the two dislocations interact via $K_2(\mathbf{r}, na)$ which is defined by

$$K_2(\mathbf{r}, na) = \int_0^w \frac{dt}{t}\int_0^\pi du\sqrt{f(u)+t^2}\cos[nu]\left(1 - \cos\left[t\frac{x}{x^*}\right]\exp\left[-\frac{z}{z^*}t\sqrt{f(u)+t^2}\right]\right).$$

$K_2(\mathbf{r}, na)$ is difficult to calculate for arbitrary separations $\mathbf{x}$, however, it can be calculated in the limits $x \gg x^*$, $z = 0$ and $z \gg z^*$, $x = 0$. We find that K_2 scales as

$$K_2(\mathbf{r}, na) = \frac{4}{1-4n^2}\begin{cases} \ln[e^{\gamma + D_n(w)} w|x|/x^*] & \text{if } x \gg x^* \text{ and } z = 0 \\ \ln[e^{D_n^z + D_n(w)} w|z|/z^*] & \text{if } z \gg z^* \text{ and } x = 0, \end{cases} \tag{5.23}$$

where $D_n(w)$ is defined by

$$D_n(w) = \int_0^w \frac{dt}{t}\left[\frac{J_n(t)}{J_n(0)} - 1\right] \tag{5.24}$$

with

$$J_n(t) = \int_0^\pi du\sqrt{f(u)+t^2}\cos[nu] \tag{5.25}$$

and $J_n(0) = 4/(1-4n^2)$.

$$D_n^z = \int_0^1 dy\left[\frac{1-F_n(y)}{y}\right] - \int_1^\infty dy\frac{F_n(y)}{y} \tag{5.26}$$

is a finite number that depends on n with

$$F_n(y) = \frac{1}{J_n(0)}\int_0^\pi du\cos(nu)\sqrt{f(u)}\exp\left[-y\sqrt{f(u)}\right]. \tag{5.27}$$

Thus, $E_2^{\rm int} \sim -Ak_1k_2/(1-4n^2)\ln r$ for large r, with $A > 0$. If $k_1/k_2 > 0$, the coefficient of $\ln r$ is positive for all $n > 0$ and negative for $n = 0$. As a result, like-signed dislocations in different layers *attract* each other, whereas like-signed dislocations in the same layer *repel* each other.

5.3 Dislocation Unbinding Temperature

In the previous section, we showed that the energies of unmatched dislocations (i.e. two +1 dislocations) in the same gallery and pairs of dislocations in different galleries scale logarithmically with system size. Thus, we can borrow the Kosterlitz-Thouless (KT) argument which balances the energy cost for creating dislocations with the entropy gain of placing dislocations anywhere in each two-dimensional layer to predict the dislocation unbinding temperature[15]. Each configuration of dislocations will have a different unbinding temperature, however, the lowest unbinding temperature

is the most relevant. Above this temperature, dislocations (either composite or individual) unbind, renormalize the compression modulus B to zero, and destroy the in-plane 2D smectic order of the sliding columnar phase. The lowest unbinding temperature corresponds to the configuration of dislocations with the lowest energy. We showed in Sec. 5.2 that an individual dislocation has the lowest energy. This result, however, depends on the form of the orientational interactions between smectic lattices. If further-neighbor orientational couplings are included, composite dislocations can have lower energy than an individual dislocation.

The difference in free energy between the defect-free state and the state with a single dislocation is

$$\Delta F = (E_+ - 2T) \ln L, \tag{5.28}$$

The dislocation unbinding temperature

$$T_{KT} = \frac{d^2 \sqrt{BK_y}}{2\pi^2} \tag{5.29}$$

is obtained by setting $\Delta F = 0$. When $T < T_{KT}$, the energy term dominates and the defect-free sliding columnar phase has lower energy. When $T > T_{KT}$, the entropy term dominates, dislocations are favored, and each layer becomes a nematic phase.

5.4 Thermodynamic Stability

To determine the thermodynamic stability of the sliding columnar phase, we must compare the critical temperatures T_d and T_{KT}. If $T_{KT} > T_d$, there is a temperature

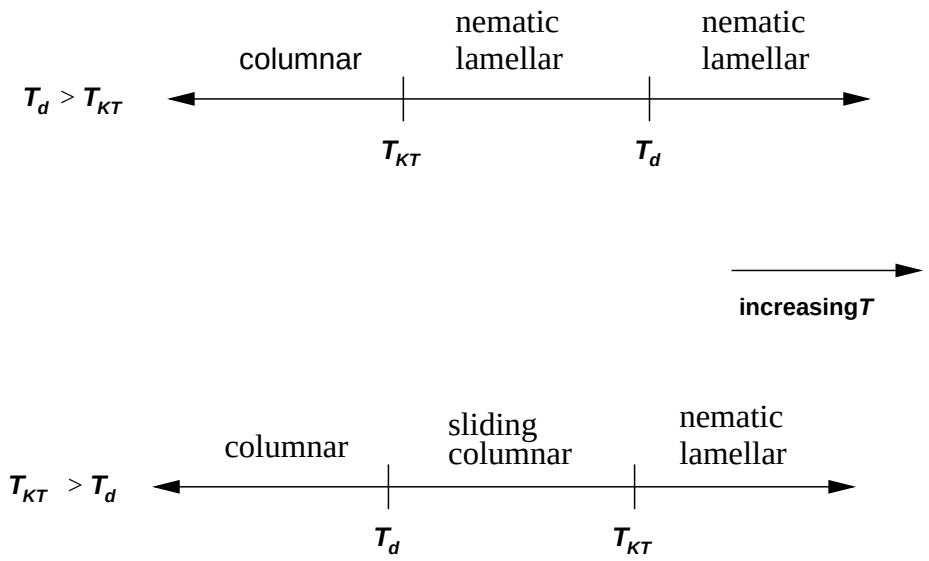

Figure 5.1: Two possibilities for the relative magnitudes of T_d and T_{KT}. If $T_{KT} > T_d$, there is a temperature window where the sliding columnar phase is the stable phase. If on the other hand $T_{KT} < T_d$, the sliding columnar phase is bypassed, and the system proceeds from the columnar phase to the nematic lamellar phase as temperature is increased.

window $T_d < T < T_{KT}$ where the positional coupling between lattices in neighboring layers is irrelevant, dislocations are energetically unfavorable, and the sliding columnar phase is thermodynamically stable. The system proceeds from the columnar phase to the sliding columnar phase to the nematic lamellar phase as temperature is increased as shown in Fig. 5.1.

However, if $T_{KT} < T_d$ there is no temperature window where the sliding columnar phase is thermodynamically stable, and the system proceeds from the columnar phase directly to the nematic lamellar phase as temperature is increased. In this scenario, the positional coupling is *irrelevant* only in the temperature regime where dislocations

are energetically favorable. Using Eqs. 3.18 and 5.29, we find

$$\beta \equiv \frac{T_{KT}}{T_d} = \frac{1}{\pi^2} \tag{5.30}$$

is less than one, and there is no temperature window where the sliding columnar phase is stable.

However, further-neighbor orientational interactions of the form

$$\mathcal{H}^{\theta} = -\sum_{n,m} a \int d^2r \; K_y^m [\theta_n(\mathbf{r}) - \theta_{n+m}(\mathbf{r})]^2 \tag{5.31}$$

can also be included in the SC Hamiltonian in Eq. 3.1. We will show in a forthcoming paper [23] that the K_y^m can be tuned so that there is a temperature window where the sliding columnar phase is stable.

Chapter 6

Conclusion

In this thesis, we have introduced the new sliding columnar (SC) phase of matter which may exist in layered systems composed of weakly-coupled 2D smectic lattices. The sliding columnar phase is characterized by weak positional but strong orientational correlations between neighboring 2D smectic lattices. The SC harmonic free energy contains an orientational rigidity that aligns neighboring 2D smectic lattices in addition to in-plane compression and bending moduli. The presence of the orientational rigidity fundamentally alters the energy spectrum. In light of this, we have calculated the structural properties of the sliding columnar phase, for example, the SC displacement correlation function, scattering intensity, and dislocation energy. We found that thermal fluctuations give rise to the sliding columnar phase by reducing the positional coupling between neighboring 2D smectic lattices to zero. However, at the longest lengthscales edge dislocations melt 2D smectic lattices and convert the sliding columnar phase into a nematic lamellar phase. We are able to fine-tune

further-neighbor interactions so that they stabilize the sliding columnar phase[23], however, these interactions do not yet have a physical origin.

6.1 Characteristic Lengthscales

A current topic of research is determining whether sliding columnar behavior is present in recent X-ray scattering experiments on CL-DNA complexes[3, 28]. Even though we found that the sliding columnar phase is converted into a nematic lamellar phase at the longest lengthscales, the SC phase may exist on shorter lengthscales determined by the density of edge dislocations. Thus, CL-DNA complexes studied in recent experiments with domain sizes $L \approx 0.1\mu$m may exhibit sliding columnar behavior. However, in the next round of experiments it will be important to prepare aligned CL-DNA samples because powder-averaging complicates the functional form of the scattering intensity and makes it difficult to identify sliding columnar behavior.

We showed in Sec. 3.4 that the density-density correlation function $S(\mathbf{r})$ displays different functional forms depending on the magnitude of the in-plane separation $\mathbf{r}$. The crossover lengthscales for the correlation function are l_x, l_z, ξ_d, x^*, and z^*. The harmonic 2D smectic regime is defined by $x, z < l_{x,z}$ and the nonlinear 2D smectic regime is defined by $x, z > l_{x,z}$, where the nonlinear lengths $l_{x,z}$ are given in Eq. 2.3. In the nonlinear regime, the anharmonic terms in the rotationally invariant strain u_{zz} are significant and cause the in-plane compression and bending moduli to depend on

Table 6.1: The nonlinear lengths, l_x and l_z, calculated as a function of the DNA spacing d using the experimental values of the in-plane correlation length ξ_z in Ref. [28].

Nonlinear length	$d = 28$Å	$d = 55$Å
l_x	0.35μm	0.24μm
l_z	9μm	6μm

the wavenumber $\mathbf{q}$. Using

$$B_2 = (32)^{1/3}\pi^2 T \frac{\xi_z^{2/3}}{d^{7/3}\xi_p^{1/3}} \tag{6.1}$$

and $K_2 = T\xi_p/2d$, we can write $l_{x,z}$ in terms of the in-plane correlation length ξ_z and the DNA spacing d. (Note that the nonlinear length l_x includes an extra factor of 8π relative to the definition in Eq. 2.3.) Both ξ_z and d were measured in the high-temperature X-ray scattering experiments[26, 28]. In Table 6.1, we have calculated the nonlinear lengths for small and large DNA spacings. Note that $L < l_{x,z}$, and thus significant departure from harmonic 2D smectic behavior was not found in the high-temperature CL-DNA experiments[26, 28].

The finite length of the DNA molecules $l_{\rm DNA} \approx 16\mu$m introduces another crossover lengthscale. The density of DNA molecules within a given layer is $\rho = 1/dl_{\rm DNA}$, and thus edge dislocations occur on lengthscales $x, z > \xi_d$, where

$$\xi_d = \sqrt{dl_{\rm DNA}} \tag{6.2}$$

is the dislocation length due to finite-sized DNA. We find $\xi_d \approx 0.21\mu$m and 0.30μm when $d = 28$Å and 55Å respectively. Note that $L < \xi_d$, and thus the subdomains are small enough to possess 2D smectic ordering. We can also estimate the core energy cost for creating hairpin edge dislocations within the 2D smectic lattices. Hairpins cause the DNA director to change by $\Delta\theta \approx \pi$ over a lattice spacing d. The energy cost for a hairpin can be estimated from the 2D bending energy. We obtain

$$\frac{E_{hp}}{2T} = \frac{\pi}{4}\frac{\xi_p}{d}, \tag{6.3}$$

which implies that hairpins are favored on lengthscales greater than

$$\xi_{hp} = d \exp\left(\frac{E_{hp}}{2T}\right). \tag{6.4}$$

Since $\xi_{hp} \gg \xi_d > L$ throughout the experimental range in d, hairpins do not affect the analysis of the shape of $I(q)$ in Ref. [28]. We do not yet have accurate estimates of x^* and z^* since the value of the orientational rigidity K_y is unknown. Scattering experiments will see sliding columnar behavior on lengthscales less than ξ_d if $x^*, z^* < \xi_d$.

6.2 Future Projects

The ideas presented here can also be applied to a three-dimensional stack of XY-models. We have found a sliding XY phase which behaves essentially like decoupled, independent 2D XY-models with zero free energy cost associated with rotating spins

in one layer relative to those in neighboring layers[22]. As a result, the two-point spin-correlation function for the sliding XY phase decays algebraically with in-plane separation. We propose that this sliding XY phase may exist between the low-temperature 3D orientationally ordered phase and the high-temperature disordered phase. Since the XY order parameter is analogous to the nematic order parameter, the phase sequence columnar $\rightarrow$ sliding columnar $\rightarrow$ nematic lamellar $\rightarrow$ sliding nematic lamellar $\rightarrow$ disordered layers is possible in CL-DNA complexes.

Appendix A

Calculation of the Sliding Columnar Displacement Fluctuations

In this Appendix, the expression for the sliding columnar displacement fluctuations given in Eq. 3.7 will be derived. To do this, we evaluate the integral of the the Fourier transformed SC correlator $G(\mathbf{q})$ over all q-space:

$$\langle (u_z^n)^2 \rangle = \int \frac{d^3q}{(2\pi)^3} G(\mathbf{q}) = \int \frac{d^3q}{(2\pi)^3} \frac{T}{Bq_z^2 + Kq_x^4 + K_y q_x^2 q_y^2 p(q_y a)}, \tag{A.1}$$

where $p(u) = 2[1-\cos(u)]/u^2$. The fluctuations diverge at small wavenumbers $\mathbf{q} \sim 1/L$, where L is the system size. To calculate how the fluctuations scale with L_x, we set $L_z \to \infty$ and $L_y \sim L_x$. Note that the SC form for $G(\mathbf{q})$ is valid only when $L_x \gg x^*$, where $x^* = a/\mu_y$ and $\mu_y = \sqrt{K_y/K}$. The first step in the calculation is to perform the integration over q_z with $\Lambda_z \to \infty$ and then use the fact that $G(\mathbf{q})$ is an even function of $\mathbf{q}$ so that the remaining integrals run over only positive q_x and q_y. Note that taking the $\Lambda_z \to \infty$ limit does not alter $q_{x,y} \to 0$ divergences. The resulting expression

$$\langle (u_z^n)^2 \rangle = \frac{T}{2\pi^2\sqrt{BK}} \int_{L_x^{-1}}^{\Lambda_x} \frac{dq_x}{q_x} \int_{L_y^{-1}}^{\Lambda_y} dq_y \frac{1}{\sqrt{q_x^2 + \mu_y^2 q_y^2 p(q_y a)}}, \tag{A.2}$$

where $\Lambda_y = \pi/a$, is made dimensionless by changing variables to $v = q_x x^*$ and $w = q_y a$. The $\ln^2 L_x$ divergence of the displacement fluctuations can be seen immediately by looking at the $q_{x,y} \to 0$ limit of Eq. A.2.

The SC displacement fluctuations can be written as the sum of a continuum term I_c that does not depend on $p(w)$ and discrete term I_d that does depend on $p(w)$.

$$\langle (u_z^n)^2 \rangle \equiv \frac{T}{2\pi^2 \sqrt{B K_y}} \left[I_c + I_d \right], \tag{A.3}$$

where I_c and I_d are defined by

$$\begin{aligned} I_c &= \int_{x^* L_x^{-1}}^{\Lambda_x x^*} \frac{dv}{v} \int_{a L_y^{-1}}^{a\Lambda_y} \frac{dw}{\sqrt{v^2 + w^2}} \\ I_d &= \int_{x^* L_x^{-1}}^{\Lambda_x x^*} \frac{dv}{v} \int_{a L_y^{-1}}^{a\Lambda_y} dw \left[\frac{1}{\sqrt{v^2 + w^2 p(w)}} - \frac{1}{\sqrt{v^2 + w^2}} \right]. \end{aligned} \tag{A.4}$$

We first focus on the continuum contribution I_c. The integral over w is straightforward;

$$I_c = \int_{x^* L_x^{-1}}^{\Lambda_x x^*} \frac{dv}{v} \left[f(\Lambda_y a, v) - f(L_y^{-1} a, v) \right] \equiv I_c^{(1)} - I_c^{(2)}, \tag{A.5}$$

where

$$f(x, v) = \ln \left[x + \sqrt{x^2 + v^2} \right]. \tag{A.6}$$

The integral over v in $I_c^{(1)}$ can be evaluated by separating the function

$$f(\Lambda_y a, v) = \ln[2\Lambda_y a] + \ln \left[\frac{1}{2} + \frac{1}{2} \sqrt{1 + (v/\Lambda_y a)^2} \right], \tag{A.7}$$

into a constant term and a term that is well-behaved at small v. We then insert this

expression into Eq. A.5 and find that

$$I_c^{(1)} = \ln[2\Lambda_y a]\ln[\Lambda_x L_x] + \int_{x^* L_x^{-1}}^{\Lambda_x x^*} \frac{dv}{v} \ln\left[\frac{1}{2} + \frac{1}{2}\sqrt{1+(v/\Lambda_y a)^2}\right]. \tag{A.8}$$

The first term diverges with system size L_x, and the second term is nondivergent. $f(aL_y^{-1}, v)$ can also be separated into a constant term and a term that depends on v. We then integrate $f(aL_y^{-1}, v)$ over v to find

$$I_c^{(2)} = \ln[2aL_y^{-1}]\ln[\Lambda_x L_x] + \int_{x^* L_x^{-1}}^{\Lambda_x x^*} \frac{dv}{v} \ln\left[\frac{1}{2} + \frac{1}{2}\sqrt{1+\left(\frac{L_y v}{a}\right)^2}\right]. \tag{A.9}$$

The L_y dependence in the integrand of the second term can be moved to limits of the integral by changing variables to $s = L_y v/a$. In contrast to the previous expression for $I_c^{(1)}$ in Eq. A.8, the large s part of the integral in Eq. A.9 diverges with system size. The divergence can be isolated by adding and subtracting $\ln[s/2]/s$. The resulting expression,

$$\begin{aligned} I_c^{(2)} &= \ln[2aL_y^{-1}]\ln[\Lambda_x L_x] + \frac{1}{2}\ln^2\left[\frac{\Lambda_x L_y}{2\mu_y}\right] - \frac{1}{2}\ln^2\left[\frac{L_y}{2\mu_y L_x}\right] \\ &+ \int_{L_y/L_x\mu_y}^{\Lambda_x L_y/\mu_y} \frac{ds}{s}\left(\ln\left[\frac{1}{2} + \frac{1}{2}\sqrt{1+s^2}\right] - \ln[s/2]\right), \end{aligned} \tag{A.10}$$

has two terms that diverge and two terms that do not diverge with system size. Note that $L_y/L_x\mu_y$ is $\mathcal{O}(1)$ since $L_x \sim L_y$. We then subtract $I_c^{(2)}$ from $I_c^{(1)}$, drop the nondivergent terms, and set $L_y = L_x$ to obtain

$$I_c = \ln[\Lambda_x L_x]\ln[\Lambda_y L_y] - \frac{1}{2}\ln^2\left[\frac{\Lambda_x L_y}{2\mu_y}\right] = \frac{1}{2}\ln^2[2\mu_y \Lambda_y L_x] \tag{A.11}$$

for the continuum contribution to the displacement fluctuations.

The discrete contribution is obtained by evaluating

$$I_d = \int_{x^* L_x^{-1}}^{\Lambda_x x^*} \frac{dv}{v} F(v), \tag{A.12}$$

where

$$F(v) = \int_0^\pi dw \left[\frac{1}{\sqrt{v^2 + w^2 p(w)}} - \frac{1}{\sqrt{v^2 + w^2}} \right] \tag{A.13}$$

In the definition of $F(v)$, the lower limit $a/L_y = 0$ since the small w part of integral is well-behaved. In contrast to the continuum term, the discrete term diverges logarithmically with system size. To see this, we expand $F(v)$ around $v = 0$ and find $F(v) \approx F(0) + av^2 + \mathcal{O}(v^4)$, where $F(0) = \ln[4/\pi]$ and a is a constant. Thus, $I_d = \ln[4/\pi] \ln[\Lambda_x L_x]$ plus terms that do not diverge with system size. To make the argument of the ln term in I_d match the $\ln^2$ term in I_c, we add and subtract the constant $\ln[4/\pi] \ln[2\mu_y \Lambda_y / \Lambda_x]$ to find

$$I_d = \ln[4/\pi] \ln[2\mu_y \Lambda_y L_x]. \tag{A.14}$$

We then add I_c and I_d and rewrite Eq. A.3 as

$$\langle (u_z^n)^2 \rangle = \frac{T}{2\pi^2 \sqrt{B K_y}} \left(\frac{1}{2} \ln^2[2\mu_y \Lambda_y L_x] + \ln[4/\pi] \ln[2\mu_y \Lambda_y L_x] \right). \tag{A.15}$$

In the final step, we factor out a 1/2, combine the $\ln L_x$ and $\ln^2 L_x$ terms, and drop a nondivergent term to yield the following expression for the displacement fluctuations in the limit $L_z \to \infty$ and $L_x \sim L_y$:

$$\langle (u_z^n)^2 \rangle = \frac{x^*}{l_x} \left(\frac{\lambda}{2\pi} \right)^2 \ln^2 \left[8 \frac{L_x}{x^*} \right]. \tag{A.16}$$

Appendix B

Calculation of the Sliding Columnar Position Correlation Function

In this Appendix, we evaluate the SC position correlation function

$$g_u(\mathbf{r},0) = \frac{1}{2}\langle[u_z^0(\mathbf{r}) - u_z^0(0)]^2\rangle \tag{B.1}$$

between two DNA strands located in layer $n = 0$ and separated by $\mathbf{r}$ in the xz plane. For general separations, $g_u(\mathbf{r},0)$ cannot be expressed in closed form. The aim of this Appendix is to calculate $g_u(\mathbf{r},0)$ along the special directions $z = 0$, $x \gg x^*$ and $x = 0$, $z \gg z^*$.

B.1 Large x, Small z Limit

The following expression for $g_u(x,0)$ is obtained by setting z and n to zero in Eq. 3.14:

$$g_u(x,0) = T\int \frac{d^3q}{(2\pi)^2}\frac{1-\cos(q_x x)}{Bq_z^2 + Kq_x^4 + K_y q_x^2 q_y^2 p(q_y a)}. \tag{B.2}$$

The first step in the derivation of $g_u(x,0)$ is to perform the integration over q_z with $\Lambda_z \to \infty$. The q_z integration yields

$$g_u(x,0) = \frac{T}{2\pi^2\sqrt{BK_y}} I(x,\Lambda_x), \tag{B.3}$$

where

$$I(x,\Lambda_x) = \int_0^{\Lambda_x} dq_x \frac{1-\cos(q_x x)}{q_x} \int_0^{\pi/x^*} \frac{dq_y}{\sqrt{q_x^2 + q_y^2 p(q_y x^*)}}. \tag{B.4}$$

We then decompose $I(x,\Lambda_x) \equiv I_c(x,\Lambda_x) + I_d(x,\Lambda_x)$ into continuum and discrete contributions as we did previously in Appendix A, where

$$I_c(x,\Lambda_x) = \int_0^{\Lambda_x} dq_x \frac{1-\cos(q_x x)}{q_x} \int_0^{\pi/x^*} \frac{dq_y}{\sqrt{q_x^2+q_y^2}} \tag{B.5}$$

$$I_d(x,\Lambda_x) = \int_0^{\Lambda_x} dq_x \frac{1-\cos(q_x x)}{q_x} \int_0^{\pi/x^*} dq_y \left[\frac{1}{\sqrt{q_x^2 + q_y^2 p(q_y x^*)}} - \frac{1}{\sqrt{q_x^2+q_y^2}} \right].$$

Since the $\Lambda_x \to \infty$ limit is well-defined, we calculate $I_c(x) \equiv I_c(x,\infty)$ and $I_d(x) \equiv I_d(x,\infty)$ and drop terms that depend on the finite ultraviolet cutoff.

To calculate the continuum contribution, we first set $q_x = uq_y$ and then $v = q_y x$. These changes of variables yield

$$I_c(x) = \int_0^{\pi x/x^*} \frac{dv}{v} K(v), \tag{B.6}$$

where

$$K(v) = \int_0^\infty du \frac{1-\cos(uv)}{u\sqrt{1+u^2}}. \tag{B.7}$$

The strategy for calculating the $\ln^2 x$ term in $I_c(x)$ is to isolate the part of $K(v)$ that scales as $\ln v$ for large v. To this end, we write

$$\begin{aligned} K(v) &= \int_0^1 \frac{du}{u}[1-\cos(uv)] + \int_0^1 \frac{du}{u}\,[1-\cos(uv)]\left[\frac{1}{\sqrt{1+u^2}}-1\right] \\ &+ \int_1^\infty \frac{du}{u}\frac{1-\cos(uv)}{\sqrt{1+u^2}}. \end{aligned} \tag{B.8}$$

It is obvious that only the first term has the correct scaling; the remaining terms in $K(v)$ are then separated into constants and functions of v that are well-behaved either as $v \to 0$ or $v \to \infty$. This partitioning leads to

$$K(v) = \ln(Bv) + \widetilde{K}(v), \tag{B.9}$$

where $B = 2e^\gamma$, γ is Euler's constant, and

$$\widetilde{K}(v) = \int_v^\infty du\frac{\cos u}{u} - \int_0^1 du\frac{\cos(uv)}{u}\left[\frac{1}{\sqrt{1+u^2}}-1\right] - \int_1^\infty \frac{du}{u}\frac{\cos(uv)}{\sqrt{1+u^2}} \tag{B.10}$$

scales as $1/v^2$ for large v.

We then plug $K(v)$ into Eq. B.6 and break the integral over v into small- and large-v parts to obtain

$$I_c(x) = \int_0^1 \frac{dv}{v}K(v) + \int_1^{\pi x/x^*} \frac{dv}{v}\ln[Bv] + \int_1^{\pi x/x^*} \frac{dv}{v}\widetilde{K}(v). \tag{B.11}$$

Next, we evaluate the integral over v in the second term, collect constants, and find

$$I_c(x) = \frac{1}{2}\ln^2[2e^\gamma \pi x/x^*] + A_x, \tag{B.12}$$

where

$$A_x = -\frac{1}{2}\ln^2[2e^\gamma] + \int_0^1 \frac{dv}{v}K(v) + \int_1^\infty \frac{dv}{v}\widetilde{K}(v). \tag{B.13}$$

The second and third terms in A_x are finite since $K(v)$ scales as v^2 for small v in the former and there is phase cancellation from the $\cos(uv)$ factor at large v in the later.

We will now calculate the discrete contribution to $g_u(x,0)$. The first step is to rewrite $I_d(x)$ in dimensionless form:

$$I_d(x) = \int_0^{\Lambda_x x^*} \frac{dv}{v}[1-\cos(vx/x^*)]F(v), \tag{B.14}$$

where $F(v)$ was defined previously in Eq. A.13. We next break the integral over v into small- and large-v parts and take the $x \gg x^*$ and $\Lambda_x \to \infty$ limits to obtain

$$I_d(x) = F(0)\int_0^1 \frac{dv}{v}[1-\cos(vx/x^*)] + \int_0^1 \frac{dv}{v}[F(v)-F(0)] + \int_0^\infty \frac{dv}{v}F(v). \tag{B.15}$$

Note that taking the $x \gg x^*$ limit removed the $\cos(vx/x^*)$ terms from the last two terms in Eq. B.15 due to phase cancellations. It is again obvious that the first term in Eq. B.15 scales logarithmically with x/x^*, and thus

$$I_d(x) = \ln[4/\pi]\ln\left[e^\gamma \frac{x}{x^*}\right] + B_x, \tag{B.16}$$

where

$$B_x = \int_0^1 \frac{dv}{v}[F(v)-F(0)] + \int_1^\infty \frac{dv}{v}F(v) \tag{B.17}$$

is a constant. The last step in the calculation of $g(x,0)$ is to add the continuum and discrete terms, $I_c(x)$ and $I_d(x)$. The final result is

$$g_u(x,0) = \frac{x^*}{l_x}\left(\frac{\lambda}{2\pi}\right)^2\left(\ln^2\left[8e^\gamma\frac{x}{x^*}\right] + C_x\right), \tag{B.18}$$

where $C_x = 2(A_x + B_x) - \ln^2[4/\pi] - 2\ln[4/\pi]\ln[2\pi]$. Both the x-dependent term and the constant term in $g_u(x,0)$ agree with a recent calculation in Ref. [10]. Numerical calculation of the constant yields $|C_x| < 0.002$.

B.2 Large z, Small x Limit

The calculation of $g_u(z,0)$ is similar to the calculation of $g_u(x,0)$ given previously given in Sec. B.1. The expression for $g_u(z,0)$ is obtained by setting x and n to zero in Eq. 3.14. The first step in the calculation is to perform the integration over q_z with $\Lambda_z \to \infty$ which yields

$$g_u(z,0) = \frac{T}{2\pi^2\sqrt{BK_y}} I(z,\Lambda_x), \tag{B.19}$$

where

$$I(z,\Lambda_x) = \int_0^{\Lambda_x} \frac{dq_x}{q_x} \int_0^{\pi/x^*} dq_y \frac{1 - e^{-z\lambda q_x\sqrt{q_x^2 + q_y^2 p(q_y x^*)}}}{\sqrt{q_x^2 + q_y^2 p(q_y x^*)}}. \tag{B.20}$$

In what follows, we set $\Lambda_x \to \infty$, drop terms that depend on the finite ultraviolet cutoff, and define $I(z) \equiv I(z,\infty)$. The second step is to change variables to $u = q_x/q_y$ and $v = \lambda z q_y^2$ and decompose $I(z) \equiv I_c(z) + I_d(z)$ into continuum and discrete terms, where

$$\begin{aligned} I_c(z) &= \frac{1}{2}\int_0^{\eta} \frac{dv}{v} \int_0^{\infty} du \frac{1 - e^{-vu\sqrt{1+u^2}}}{u\sqrt{1+u^2}} \\ I_d(z) &= \int_0^{\infty} \frac{dv}{v} \left[F(v,0) - F(v, vz/z^*)\right], \end{aligned} \tag{B.21}$$

where $\eta = \pi^2 z/z^*$, $z^* = a^2/\mu_y^2\lambda$,

$$F(v,\eta) = \int_0^\pi du \left[\frac{e^{-\eta\sqrt{v^2+u^2p(u)}}}{\sqrt{v^2+u^2p(u)}} - \frac{e^{-\eta\sqrt{v^2+u^2}}}{\sqrt{v^2+u^2}} \right], \tag{B.22}$$

and $F(v,0)$ is equivalent to $F(v)$ defined in Eq. A.13.

We first focus on the continuum contribution to $g_u(z,0)$. The integral over v in $I_c(z)$ can be broken into small- and large-v parts,

$$I_c(z) = \frac{1}{2}\int_0^1 \frac{dv}{v} J(v) + \frac{1}{2}\int_1^\eta \frac{dv}{v} J(v), \tag{B.23}$$

where

$$J(v) = \int_0^\infty du \frac{1 - e^{-vu\sqrt{1+u^2}}}{u\sqrt{1+u^2}}. \tag{B.24}$$

The strategy is to extract the part of $J(v)$ that scales as $\ln v$ for large v. If $J(v) \sim \ln v$ for large v, $I_c(z)$ will scale as $\ln^2[z/z^*]$ as expected. Note that $J(v)$ scales as v^2 for small v, and thus the first term in Eq. B.23 is a finite constant. After some algebra, we find

$$J(v) = \ln[Dv] + \tilde{J}(v), \tag{B.25}$$

where $D = 2e^\gamma$,

$$\tilde{J}(v) = \int_{\sqrt{2}v}^\infty du \frac{e^{-u}}{u} - \int_0^1 du \frac{1-\Phi(u)}{u\sqrt{1+u^2}} e^{-vu\sqrt{1+u^2}} - \int_1^\infty du \frac{e^{-vu\sqrt{1+u^2}}}{u\sqrt{1+u^2}}, \tag{B.26}$$

and

$$\Phi(u) = \frac{1+2u^2}{\sqrt{1+u^2}}. \tag{B.27}$$

We can now plug the expression for $J(v)$ in Eq. B.25 into Eq. B.23 and obtain the continuum contribution

$$I_c(z) = \frac{1}{4}\ln^2\left[2e^\gamma\pi^2\frac{z}{z^*}\right] + A_z, \tag{B.28}$$

where

$$A_z = -\frac{1}{4}\ln^2\left[2e^\gamma\right] + \frac{1}{2}\int_0^1 \frac{dv}{v}J(v) + \frac{1}{2}\int_1^\infty \frac{dv}{v}\tilde{J}(v) \tag{B.29}$$

is a constant. Note that $\tilde{J}(v)$ decays exponentially for large v, and thus the third term in A_z is finite.

We now concentrate on the discrete contribution to $g_u(z,0)$. The integral over v in $I_d(z) \equiv I_d^{(1)} + I_d^{(2)}$ can also be broken into small- and large-v parts, where

$$I_d^{(1)} = \int_0^1 \frac{dv}{v}\left[F(v,0) - F(v,vz/z^*)\right] \tag{B.30}$$

and $I_d^{(2)}$ is an identical expression except the limits on the integral over v run from one to infinity. To isolate the $\ln z$ term in $I_d^{(1)}$, we change variables to $t = vz/z^*$ and take the $z \gg z^*$ limit. In the large z limit, Eq. B.30 becomes

$$I_d^{(1)} = F(0,0)\ln\left[\frac{z}{z^*}\right] + \overline{B}_z, \tag{B.31}$$

where $F(0,0) = \ln[4/\pi]$ and

$$\overline{B}_z = \int_0^1 \frac{dt}{t}\left[F(0,0) - F(0,t)\right] - \int_1^\infty \frac{dt}{t}F(0,t) \tag{B.32}$$

is a constant. The large-v contribution to I_d,

$$I_d^{(2)} = \int_1^\infty \frac{dv}{v}F(v,0), \tag{B.33}$$

is simply a constant when $z \gg z^*$. We then collect the discrete contributions and find

$$I_d(z) = \ln\left[\frac{4}{\pi}\right] \ln\left[\frac{z}{z^*}\right] + B_z, \tag{B.34}$$

where $B_z = \overline{B}_z + I_d^{(2)}$.

The last step in the calculation of $g_u(z)$ is to add $I_c(z)$ and $I_d(z)$. The final result is

$$g_u(z) = \frac{x^*}{l_x}\left(\frac{\lambda}{2\pi}\right)^2 \left(\frac{1}{2}\ln^2\left[32e^{\gamma}\frac{z}{z^*}\right] + C_z\right), \tag{B.35}$$

where $C_z = 2(A_z + B_z) - 2\ln^2[4/\pi] - 2\ln[4/\pi]\ln[2e^{\gamma}\pi^2] \approx 1.35$ was evaluated numerically. Ref. [10] obtained the same z-dependence for $g_u(z,0)$ but obtained a different constant with $C_z = \pi^2/8 \approx 1.23$.

Appendix C

Evaluation of the 3D Smectic One-Loop Diagrams

Our task in this Appendix is to calculate $\Sigma(\mathbf{q})$ defined in Sec. 4.2.3 as the one-loop diagrammatic corrections to $\Gamma(\mathbf{q})$, the vertex function for the 3D smectic. These corrections arise from the nonlinear terms in the Hamiltonian in (4.10). The two nonlinear terms are $\partial_z u_z(\boldsymbol{\nabla}_\perp u)^2/2$ and $(\boldsymbol{\nabla}_\perp u)^4/8$ (shown schematically in Fig. C.1), and only contractions of the former contribute to the renormalization to one-loop order. The three possible contractions are shown in Fig. C.2. The diagrammatic corrections $\Sigma(\mathbf{q})$ can be expressed as

$$\Sigma(\mathbf{q}) = \Pi_1(\mathbf{q})q_z^2 + \Pi_2(\mathbf{q})q_\perp^4 \equiv \Sigma_1(\mathbf{q}) + \Sigma_2(\mathbf{q}). \tag{C.1}$$

Note that we have separated the q_z^2 and $q_\perp^4$ dependence of $\Sigma(\mathbf{q})$ so that to lowest order in $\mathbf{q}$

$$\left.\frac{d\Sigma}{dq_z^2}\right|_{q_z=\mu^2,q_\perp=0} = \left.\frac{d\Sigma_1}{dq_z^2}\right|_{q_z=\mu^2,q_\perp=0} \tag{C.2}$$

and

$$\left.\frac{d\Sigma}{dq_\perp^4}\right|_{q_z=\mu^2,q_\perp=0} = \left.\frac{d\Sigma_2}{dq_\perp^4}\right|_{q_z=\mu^2,q_\perp=0}. \tag{C.3}$$

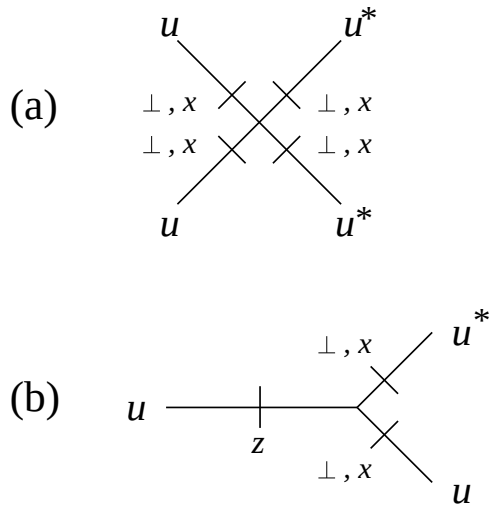

Figure C.1: Schematic representation of the two relevant nonlinear terms in both the 3D smectic and sliding columnar elasticity theories. The perpendicular derivatives ($\perp$) correspond to the 3D smectic theory and the x derivatives to the sliding columnar theory. The term $(\partial_{\perp,x}u)^4$ is pictured in (a) and the term $(\partial_z u)(\partial_{\perp,x}u)^2$ is pictured in (b). The symbols $\perp$, x, and z represent $\perp$, x, and z derivatives of the u field. The diagram with four u fields in (a) does not contribute to the renormalization to one-loop order; only contractions of (b) with itself contribute.

The contributions of $d\Sigma_2/dq_z^2$ to $d\Sigma/dq_z^2$ and of $d\Sigma_1/dq_\perp^4$ to $d\Sigma/dq_\perp^4$ at the special point $q_z = \mu^2$ and $q_\perp = 0$ are higher order in ϵ than the contributions in (C.2) and (C.3). We begin by calculating $\Sigma_1(\mathbf{q})$.

The diagram in Fig. C.2(a) alone contributes to $\Sigma_1(\mathbf{q})$ since it is the only one with q_z^2 on the external legs. To evaluate the integrals in the perturbation theory, we use dimensional regularization, *i.e* we take $d = 3 - \epsilon$, set the cutoff to infinity, and look for the $1/\epsilon$ terms. $\Sigma_1(\mathbf{q})$ is obtained by calculating the q_z^2 contribution from the following integral:

$$\Sigma_1(\mathbf{q}) = -\frac{q_z^2}{2}\int_{-\infty}^{\infty}\frac{d^{3-\epsilon}k}{(2\pi)^{3-\epsilon}}\Big[(q_\perp + k_\perp)_i(q_\perp + k_\perp)_j k_{\perp i}k_{\perp j}G(\mathbf{k}+\mathbf{q})G(-\mathbf{k})\Big], \qquad \text{(C.4)}$$

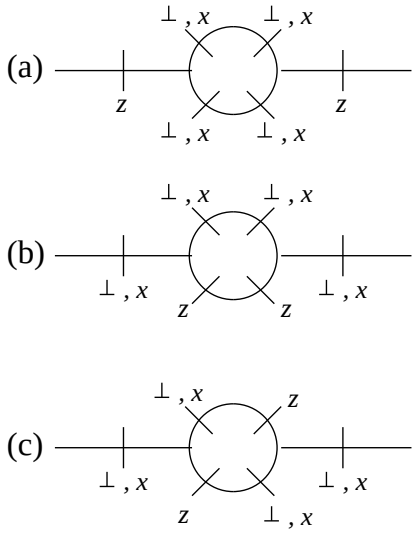

Figure C.2: The three one-loop diagrams that contribute to the renormalization of the 3D smectic and sliding columnar elastic constants. These diagrams are formed by contracting $\partial_z u(\partial_{\perp,x} u)^2$ with itself. The diagram in (a) contributes terms proportional to q_z^2 since a factor of q_z is on each external leg. The diagrams in (b) and (c) contribute terms proportional to $q_\perp^4$ in the 3D smectic theory and terms proportional to $q_x^2 q_y^2$ and q_x^4 in the sliding columnar theory since these diagrams have $q_\perp^2$ or q_x^2 on the external legs.

where $i, j = x, y$ and

$$G(\mathbf{q}) = \frac{1}{q_z^2 + w^{-1} q_\perp^4}. \tag{C.5}$$

The coefficient of the q_z^2 term in (C.4) is $\Pi_1(\mathbf{q})$. We can then approximate $\Sigma_1(\mathbf{q})$ by writing $\Sigma_1(\mathbf{q}) = q_z^2 \Pi_1(q_\perp = 0, q_z)$ plus higher order terms in $q_\perp$ that vanish when we apply the boundary condition in Eq. (4.22). We obtain $\Pi_1(q_z)$ by setting $q_\perp = 0$ in the integral on the right hand side of (C.4).

To evaluate the integral, we first combine the denominators of $G(\mathbf{k}+\mathbf{q})$ and $G(-\mathbf{k})$

employing the following identity:

$$\frac{1}{(k_z+q_z)^2+w^{-1}k_\perp^4}\,\frac{1}{\left[k_z^2+w^{-1}k_\perp^4\right]}=\int_0^1\frac{dx}{\left[(k_z+xq_z)^2+x(1-x)q_z^2+w^{-1}k_\perp^4\right]^2}. \quad \text{(C.6)}$$

We then change variables to $k_z'=k_z+xq_z$ and perform the integration over k_z'. We find that $\Sigma_1(\mathbf{q})$ can be written in terms of the integral $J(4,3,x,q_z)$ with $J(s,v,x,q_z)$ defined by

$$\begin{aligned} J(s,v,x,q_z) &= \int_0^\infty dk_\perp k_\perp^{1-\epsilon}\frac{k_\perp^s}{[x(1-x)q_z^2+w^{-1}k_\perp^4]^{v/2}} \\ &= \frac{w^{v/2}}{4\Gamma(v/2)}\Gamma\left(\frac{1}{4}(2v-s-2+\epsilon)\right)\Gamma\left(\frac{1}{4}(s+2-\epsilon)\right) \\ &\quad\times\left[x(1-x)wq_z^2\right]^{(s-2v+2-\epsilon)/4}, \end{aligned} \quad \text{(C.7)}$$

where $\Gamma(x)$ is the gamma function evaluated at x. The expression for $\Sigma_1(\mathbf{q})$ is simple when expressed in terms of the integral $J(4,3,x,q_z)$; we find

$$\Sigma_1(\mathbf{q})=-\frac{q_z^2}{16\pi}\int_0^1 dx\ J(4,3,x,q_z). \quad \text{(C.8)}$$

From (C.7) we know that the most dominant term in $J(4,3,x,q_z)$ scales as $1/\epsilon$ and thus

$$\Sigma_1(\mathbf{q})=-\frac{w^{3/2}}{16\pi\epsilon}q_z^2\left(wq_z^2\right)^{-\epsilon/4} \quad \text{(C.9)}$$

plus higher order terms in ϵ. We can also write $\Sigma_1(\mathbf{q})$ as

$$\left.\frac{d\Sigma_1(\mathbf{q})}{dq_z^2}\right|_{q_z=\mu^2,q_\perp=0}=-\frac{g}{16\pi\epsilon} \quad \text{(C.10)}$$

when we replace w by $(g\mu^\epsilon)^{2/3}$.

$\Sigma_2(\mathbf{q})$ is determined by calculating the $q_\perp^4$ contributions from the diagrams in Figs. C.2 (b) and (c). $\Sigma_2(\mathbf{q})$ is the $q_\perp^4$ part of the the following integral:

$$\begin{aligned}\Sigma_2(\mathbf{q}) &= -q_{\perp i}q_{\perp j}\int \frac{d^{3-\epsilon}k}{(2\pi)^{3-\epsilon}}\left[(k_z+q_z)^2 k_{\perp i}k_{\perp j}+(k_z+q_z)(k_\perp+q_\perp)_j k_{\perp i}k_z\right] \\ &\quad \times G(\mathbf{k}+\mathbf{q})G(-\mathbf{k}). \qquad \text{(C.11)}\end{aligned}$$

The $q_\perp^4$ contributions come from expanding $G(\mathbf{k}+\mathbf{q})$ to second order in $q_\perp$; we see from (C.11) that we need both the first and second order terms in the expansion. The coefficient of the $q_\perp^4$ term in the above expansion is $\Pi_2(q_\perp = 0, q_z)$, and thus $\Sigma_2(\mathbf{q}) = q_\perp^4 \Pi_2(q_z)$ plus higher order terms in $q_\perp$ that vanish when we apply the boundary condition in (4.23).

The first and second terms in the integrand of (C.11) correspond to the diagrams in Figs. C.2 (b) and (c), respectively. We break up the integral so that $\Sigma_2(\mathbf{q}) = \Sigma_2^b(\mathbf{q}) + \Sigma_2^c(\mathbf{q})$, and we first calculate $\Sigma_2^b(\mathbf{q})$.

$$\begin{aligned}\Sigma_2^b(\mathbf{q}) &= -\frac{1}{2}q_{\perp i}q_{\perp j}q_{\perp l}q_{\perp m}\int_{-\infty}^{\infty}\frac{dk_z}{2\pi}\int\frac{d\Omega}{(2\pi)^{2-\epsilon}}dk_\perp k_\perp^{1-\epsilon} \\ &\quad \times\left[(k_z+q_z)^2 k_{\perp i}k_{\perp j}G(-\mathbf{k})\left.\frac{d^2G(\mathbf{k}+\mathbf{q})}{dq_{\perp l}dq_{\perp m}}\right|_{q_\perp=0}\right],\end{aligned}$$

where Ω is the solid angle in $2-\epsilon$ dimensions and the second derivative of G gives the coefficient of the quadratic term in the expansion of $G(\mathbf{k}+\mathbf{q})$. We then remove the angular dependence by integrating over Ω and using the following two identities:

$$\int\frac{d\Omega}{(2\pi)^{2-\epsilon}}\,k_{\perp i}k_{\perp j} = \frac{S_{2-\epsilon}}{2-\epsilon}k_\perp^2\delta_{ij} \qquad \text{(C.12)}$$

and

$$\int \frac{d\Omega}{(2\pi)^{2-\epsilon}}\, k_{\perp i}k_{\perp j}k_{\perp l}k_{\perp m} = \frac{S_{2-\epsilon}}{(2-\epsilon)^3}k_\perp^4(\delta_{ij}\delta_{lm}+\delta_{il}\delta_{jm}+\delta_{im}\delta_{jl}), \tag{C.13}$$

where δ_{ij} is the Kronecker delta and $S_d = \Omega/(2\pi)^d = 2\pi^{d/2}/((2\pi)^d\Gamma(d/2))$ with $d = 2-\epsilon$. We are interested in the lowest order terms in ϵ and hence will use $S_{2-\epsilon} \approx (2\pi)^{-1}$ below. We then change variables to $k_z' = k_z + q_z$ and combine the denominators of $G(-\mathbf{k})$ and $G(\mathbf{k}+\mathbf{q})$ using an identity similar to (C.6).

$$\frac{1}{(k_z-q_z)^2+w^{-1}k_\perp^4} \times \frac{1}{\left[k_z^2+w^{-1}k_\perp^4\right]^n} = \tag{C.14}$$
$$\Gamma(n+1)\int_0^1 dx \frac{f_n(x)}{\left[(k_z-xq_z)^2+x(1-x)q_z^2+w^{-1}k_\perp^4\right]^{n+1}},$$

where $n = 2, 3$ and

$$f_n(x) = \begin{cases} 1-x, & n=2 \\ (1-x)^2/2, & n=3. \end{cases} \tag{C.15}$$

We change variables again to $k_z'' = k_z + xq_z$ and integrate over k_z''; we find that $\Sigma_2^b(\mathbf{q})$ can be written in terms of the integrals $J(s,v,x,q_z)$ defined previously in (C.7):

$$\Sigma_2^b(\mathbf{q}) = -\frac{w^{-1}}{32\pi}q_\perp^4\int_0^1 dx\, \Big[-5(1-x)J(4,3,x,q_z) - 15x^2(1-x)q_z^2J(4,5,x,q_z)$$
$$+9w^{-1}(1-x)^2J(8,5,x,q_z) + 45w^{-1}x^2(1-x)^2q_z^2J(8,7,x,q_z)\Big].$$

$J(4,3,x,q_z)$ and $J(8,5,x,q_z)$ have terms proportional to $1/\epsilon$ but $J(4,5,x,q_z)$ and $J(8,7,x,q_z)$ do not. We keep the terms that are proportional to $1/\epsilon$ and drop the others. In the last step we perform the x integration and find

$$\Sigma_2^b(\mathbf{q}) = -\frac{w^{1/2}}{64\pi\epsilon}q_\perp^4(wq_z^2)^{-\epsilon/4} \tag{C.16}$$

plus higher order terms in ϵ.

We next obtain $\Sigma_2^c(\mathbf{q})$ by calculating the $q_\perp^4$ contributions from the diagram in Fig. C.2(c). $\Sigma_2^c(\mathbf{q})$ can be written in terms of the following integral:

$$\Sigma_2^c(\mathbf{q}) = -q_{\perp i}q_{\perp j}\int \frac{d\Omega}{(2\pi)^{2-\epsilon}} dk_\perp k_\perp^{1-\epsilon}\int_{-\infty}^{\infty}\frac{dk_z}{2\pi}$$
$$\Big[k_z(k_z+q_z)G(-\mathbf{k})\Big[k_{\perp i}q_{\perp j}q_{\perp l}\left.\frac{dG(\mathbf{k}+\mathbf{q})}{dq_{\perp l}}\right|_{q_\perp=0}$$
$$+k_{\perp i}k_{\perp j}\frac{q_{\perp l}q_{\perp m}}{2}\left.\frac{d^2G(\mathbf{k}+\mathbf{q})}{dq_{\perp l}dq_{\perp m}}\right|_{q_\perp=0}\Big]\Big]. \qquad \text{(C.17)}$$

The first and second derivatives of G give the coefficients of the linear and quadratic terms in $q_\perp$ in the expansion of $G(\mathbf{k}+\mathbf{q})$. We then follow a procedure similar to the one employed to find $\Sigma_2^b(\mathbf{q})$, *i.e.*, we change variables to $k_z' = k_z + q_z$, combine the denominators of $G(\mathbf{k}+\mathbf{q})$ and $G(-\mathbf{k})$, and integrate over Ω. The remaining integrals in (C.17) are over $k_\perp$ and x. We then integrate over $k_\perp$ and write $\Sigma_2^c(\mathbf{q})$ in terms of $J(s,v,x,q_z)$; we find

$$\Sigma_2^c(\mathbf{q}) = -\frac{w^{-1}}{32\pi}q_\perp^4\int_0^1 dx\,\Big[-9(1-x)J(4,3,x,q_z)+27x(1-x)^2q_z^2J(4,5,x,q_z)$$
$$+9w^{-1}(1-x)^2J(8,5,x,q_z)-45w^{-1}x(1-x)^2q_z^2J(8,7,x,q_z)\Big]. \qquad \text{(C.18)}$$

Only $J(4,3,x,q_z)$ and $J(8,5,x,q_z)$ have terms proportional to $1/\epsilon$. We keep these terms and perform the integration over x to find

$$\Sigma_2^c(\mathbf{q}) = \frac{3w^{1/2}}{64\pi\epsilon}q_\perp^4(wq_z^2)^{-\epsilon/4}. \qquad \text{(C.19)}$$

We obtain $\Sigma_2(\mathbf{q})$ by adding $\Sigma_2^b(\mathbf{q})$ and $\Sigma_2^c(\mathbf{q})$ in (C.16) and (C.19) to yield

$$\left.\frac{d\Sigma_2(\mathbf{q})}{dq_\perp^4}\right|_{q_z=\mu^2,q_\perp=0} = (g\mu^\epsilon)^{-2/3}\frac{g}{32\pi\epsilon}, \tag{C.20}$$

once we set $w = (g\mu^\epsilon)^{2/3}$ and ignore higher order terms in ϵ.

Appendix D

Evaluation of the Sliding Columnar One-Loop Diagrams

The aim of this Appendix is to calculate $\Sigma(\mathbf{q})$, the one-loop diagrammatic corrections to the vertex function for the sliding columnar phase. The rotationally invariant theory given in (4.49) contains two relevant nonlinear terms, $\partial_z u_z(\partial_x u_z)^2$ and $(\partial_x u_z)^4$. These terms are pictured schematically in Fig. C.1. From this figure we see that only contractions of $\partial_z u_z(\partial_x u_z)^2$ renormalize the elastic constants to one-loop order. The three possible contractions are shown in Fig. C.2. $\Sigma(\mathbf{q})$ has q_z^2, $q_x^2 q_y^2$, and q_x^4 contributions, and we will calculate each separately below. To do this, we express $\Sigma(\mathbf{q})$ as

$$\begin{aligned} \Sigma(\mathbf{q}) &= \Pi_1(\mathbf{q}) q_z^2 + \Pi_2(\mathbf{q}) q_x^2 q_y^2 + \Pi_3(\mathbf{q}) q_x^4 \\ &\equiv \Sigma_1(\mathbf{q}) + \Sigma_2(\mathbf{q}) + \Sigma_3(\mathbf{q}). \end{aligned} \tag{D.1}$$

We have separated the q_z^2, $q_x^2 q_y^2$, and q_x^4 dependences so that, for instance,

$$\left.\frac{d\Sigma}{dq_x^4}\right|_{q_z=\mu^2, q_\perp=0} = \left.\frac{d\Sigma_3}{dq_x^4}\right|_{q_z=\mu^2, q_\perp=0}. \tag{D.2}$$

As in Appendix C, we use dimensional regularization to calculate the integrals.

The q_z^2 contribution to $\Sigma(\mathbf{q})$ results from squaring the diagram in Fig. C.1(b) and contracting both pairs of x derivatives. This leaves q_z on each external leg as shown in Fig. C.2(a). $\Sigma_1(\mathbf{q})$ is the q_z^2 part of the following integral:

$$\Sigma_1(\mathbf{q}) = -\frac{q_z^2}{2}\int \frac{d^{3-\epsilon}k}{(2\pi)^{3-\epsilon}}\Big[(q_x+k_x)^2 k_x^2 G(\mathbf{q}+\mathbf{k})G(-\mathbf{k})\Big], \tag{D.3}$$

where

$$G(\mathbf{q}) = \frac{1}{q_z^2 + q_x^2 q_y^2 + w^{-1}q_x^4}. \tag{D.4}$$

The coefficient of the q_z^2 in the above integral is $\Pi_1(\mathbf{q})$ and thus $\Sigma_1(\mathbf{q}) = q_z^2\Pi_1(q_{x,y} = 0, q_z)$ plus higher order terms in q_x and q_y that vanish when we apply the boundary condition in (4.59). Thus, $\Sigma_1(\mathbf{q})$ is obtained by setting $q_x = q_y = 0$ in (D.3). We find

$$\Sigma_1(\mathbf{q}) = -\frac{w^{-1/2}}{2}\frac{q_z^2}{(2\pi)^{3-\epsilon}}\int dk_x dk_z d^{1-\epsilon}k_y \frac{k_x^4}{\left[k_z^2 + w^{-1}k_x^2k_\perp^2\right]\left[(q_z+k_z)^2 + w^{-1}k_x^2k_\perp^2\right]}, \tag{D.5}$$

where we have changed variables to $k_y = w^{-1/2}k_y'$ and dropped the prime. The first step in evaluating this integral is to combine the two denominators in (D.5) using the identity in (C.6) with $k_\perp^4$ replaced by $k_x^2k_\perp^2$. We then perform the integration over k_z and find that $\Sigma_1(\mathbf{q})$ can be written in terms of the integral $I(4,0,3,x,q_z)$, where

$$\begin{aligned} I(s,t,v,x,q_z) &= \int_0^\infty dk_x dk_y \, \frac{k_x^s k_y^{t-\epsilon}}{\left[x(1-x)q_z^2 + w^{-1}k_x^2k_\perp^2\right]^{v/2}} \\ &= \frac{w^{v/2}}{8\Gamma(v/2)}\Gamma\left(\frac{1}{2}(t+1-\epsilon)\right)\Gamma\left(\frac{1}{4}(s-t+\epsilon)\right) \\ &\quad \times\Gamma\left(\frac{1}{4}(2v-t-s-2+\epsilon)\right) \\ &\quad \times\Big[x(1-x)wq_z^2\Big]^{(s+t-2v+2-\epsilon)/4}. \end{aligned} \tag{D.6}$$

We give the most general form for the integrals over k_x and k_y since we will need these integrals later when we calculate $\Sigma_2(\mathbf{q})$ and $\Sigma_3(\mathbf{q})$. We find

$$\Sigma_1(\mathbf{q}) = \frac{-w^{-1/2}}{8\pi^2} q_z^2 \int_0^1 dx\ I(4,0,3,x,q_z). \tag{D.7}$$

and

$$\Sigma_1(\mathbf{q}) = -\frac{w}{8\pi^2\epsilon} q_z^2 (w q_z^2)^{-\epsilon/4} \tag{D.8}$$

since $I(4,0,3,x,q_z) \propto 1/\epsilon$. We then set $w = g\mu^\epsilon$ to find $\Sigma_1(\mathbf{q})$ as a function of g,

$$\left.\frac{d\Sigma_1(\mathbf{q})}{dq_z^2}\right|_{q_z=\mu^2, q_{x,y}=0} = -\frac{g}{8\pi^2\epsilon}. \tag{D.9}$$

Both the $q_x^2 q_y^2$ and q_x^4 contributions to $\Sigma(\mathbf{q})$ come from the diagrams with x derivatives on the external legs. The two contributing diagrams are shown in Figs. C.2 (b) and (c). Their sum is given by

$$S = -q_x^2 \int \frac{d^{3-\epsilon}k}{(2\pi)^3} \Big[(k_z+q_z)^2 k_x^2 + (q_z+k_z)(q_x+k_x) k_z k_x \Big] G(\mathbf{k}+\mathbf{q}) G(-\mathbf{k}). \tag{D.10}$$

We find the $q_x^2 q_y^2$ terms by expanding $G(\mathbf{k}+\mathbf{q})$ to second order in q_y. We see that only the quadratic term in the expansion contributes. Higher order terms will vanish when we apply the second boundary condition in (4.59). We then follow a procedure similar to the one employed to calculate the $q_\perp^4$ contribution to the 3D smectic vertex function in Appendix C. We find that $\Sigma_2(\mathbf{q})$ can be written in terms of the integrals $I(s,t,v,x,q_z)$ as shown below:

$$\begin{aligned}\Sigma_2(\mathbf{q}) &= -\frac{w^{-1/2}}{8\pi^2} q_x^2 q_y^2 \int_0^1 dx \Big[-2(1-x) I(4,0,3,x,q_z) + 6w^{-1}(1-x)^2 I(6,2,5,x,q_z) \\ &- 3x q_z^2 (2x-1)(1-x) I(4,0,5,x,q_z) + 15 w^{-1} x q_z^2 (2x-1)(1-x)^2 I(6,2,7,x,q_z) \Big].\end{aligned}$$

We then look for the leading order terms in ϵ; $I(4,0,3,x,q_z)$ and $I(6,2,5,x,q_z)$ have leading order terms proportional to $1/\epsilon$ while $I(4,0,5,x,q_z)$ and $I(6,2,7,x,q_z)$ do not and are dropped. After integrating over x we obtain

$$\Sigma_2(\mathbf{q}) = \frac{w}{24\pi^2\epsilon} q_x^2 q_y^2 (w q_z^2)^{-\epsilon/4} \tag{D.11}$$

and

$$\left.\frac{d\Sigma_2}{d(q_x^2 q_y^2)}\right|_{q_z=\mu^2, q_{x,y}=0} = \frac{g}{24\pi^2\epsilon}. \tag{D.12}$$

$\Sigma_3(\mathbf{q})$ is obtained by calculating the terms proportional to q_x^4 in (D.10). We obtain these terms by expanding $G(\mathbf{k}+\mathbf{q})$ to second order in q_x and noting that both first and second order terms in the expansion contribute. Note that higher order terms in the expansion will vanish once we apply the third boundary condition in (4.59). We calculate the q_x^4 contributions from Figs. C.2 (b) and (c) separately and define $\Sigma_3(\mathbf{q}) \equiv \Sigma_3^b(\mathbf{q}) + \Sigma_3^c(\mathbf{q})$. We first calculate the contribution from Fig. C.2(b). Using the same procedure as the one employed to calculate the $q_x^2 q_y^2$ contribution to $\Sigma(\mathbf{q})$, we find that $\Sigma_3^b(\mathbf{q})$ can be written in terms of the integral $I(s,t,v,x,q_z)$.

$$\begin{aligned}
\Sigma_3^b(\mathbf{q}) &= -\frac{w^{-3/2}}{8\pi^2} q_x^4 \int_0^1 dx \Big[-(1-x)(6I(4,0,3,x,q_z) + I(2,2,3,x,q_z) \\
&+ 18x^2 q_z^2 I(4,0,5,x,q_z) + 3x^2 q_z^2 I(2,2,5,x,q_z)) \\
&+ 3w^{-1}(1-x)^2 \Big(4I(8,0,5,x,q_z) + 20x^2 q_z^2 I(8,0,7,x,q_z) + 4I(6,2,5,x,q_z) \\
&+ 20x^2 q_z^2 I(6,2,7,x,q_z) + I(4,4,5,x,q_z) + 5x^2 q_z^2 I(4,4,7,x,q_z) \Big) \Big].
\end{aligned} \tag{D.13}$$

We note that three of the integrals in (D.13), $I(4,0,5,x,q_z)$, $I(8,0,7,x,q_z)$, and

$I(6,2,7,x,q_z)$, have leading order terms that scale as ϵ^0 and are dropped. Two integrals, $I(2,2,3,x,q_z)$ and $I(4,4,5,x,q_z)$, have $1/\epsilon^2$ as well as $1/\epsilon$ terms, while the remaining five integrals $I(4,0,3,x,q_z)$, $I(2,2,5,x,q_z)$, $I(8,0,5,x,q_z)$, $I(6,2,5,x,q_z)$, and $I(4,4,7,x,q_z)$ have leading order contributions that scale as $1/\epsilon$. We collect terms and perform the x integration to find

$$\Sigma_3^b(\mathbf{q}) = -\frac{1}{8\pi^2\epsilon} q_x^4 (w q_z^2)^{-\epsilon/4} \left[\frac{1}{\epsilon} + \ln[2] - \frac{1}{12}\right]. \tag{D.14}$$

Note that the dominant contribution to Σ_3^b is of order ϵ^{-2} rather than ϵ^{-1}. The undesirable ϵ^{-2} term and the $\ln[2]/\epsilon$ term will be cancelled by terms in Σ_3^c. The term proportional to $\ln[2]/\epsilon$ originates from the integrals $I(2,2,3,x,q_z)$ and $I(4,4,5,x,q_z)$. This can be seen by expanding $I(4,4,5,x,q_z)$ in powers of ϵ; we find

$$I(4,4,5,x,q_z) = \frac{2w^{-5/2}}{\epsilon^2}\left(1 - \frac{\epsilon}{2}\frac{\Gamma'(5/2)}{\Gamma(5/2)} + \frac{\epsilon}{2}\frac{\Gamma'(1)}{\Gamma(1)}\right)\left[x(1-x)wq_z^2\right]^{-\epsilon/4} \tag{D.15}$$

to order $\mathcal{O}(1/\epsilon)$, where $\Gamma'(x)$ is the derivative of the gamma function evaluated at x. The logarithm arises from evaluating the derivative of the gamma function at a half integer. For example, $\Gamma'(5/2)/\Gamma(5/2) = -\gamma + 8/3 - 2\ln[2]$ where γ is the Euler-Mascheroni constant.

We can also write $\Sigma_3^c(\mathbf{q})$ in terms of the integrals $I(s,t,w,x,q_z)$. We obtain

$$\begin{aligned}
\Sigma_3^c(\mathbf{q}) &= -\frac{w^{-3/2}}{8\pi^2} q_x^4 \int_0^1 dx \Big[(1-x)\Big(-10I(4,0,3,x,q_z) + 30x(1-x)q_z^2 I(4,0,5,x,q_z) \\
&- 3I(2,2,3,x,q_z) + 9x(1-x)q_z^2 I(2,2,5,x,q_z)\Big) + 3w^{-1}(1-x)^2\Big(4I(8,0,5,x,q_z) \\
&- 20x(1-x)q_z^2 I(8,0,7,x,q_z) + 4I(6,2,5,x,q_z) - 20x(1-x)q_z^2 I(6,2,7,x,q_z)
\end{aligned}$$

$$+ \quad I(4,4,5,x,q_z) - 5x(1-x)q_z^2 I(4,4,7,x,q_z)\Big)\Big], \tag{D.16}$$

which becomes

$$\Sigma_3^c(\mathbf{q}) = -\frac{1}{8\pi^2\epsilon} q_x^4 (w q_z^2)^{-\epsilon/4}\Big[-\frac{1}{\epsilon} - \ln[2] - \frac{7}{12}\Big] \tag{D.17}$$

when only terms proportional to $1/\epsilon^2$ and $1/\epsilon$ are retained. We see that when we add (D.14) to (D.17), the terms proportional to $1/\epsilon^2$ and $\ln[2]/\epsilon$ cancel and we are left with

$$\Sigma_3(\mathbf{q}) = \frac{1}{12\pi^2\epsilon} q_x^4 (w q_z^2)^{-\epsilon/4} \tag{D.18}$$

and

$$\left.\frac{d\Sigma_3(\mathbf{q})}{dq_x^4}\right|_{q_z=\mu^2, q_{x,y}=0} = (g\mu^\epsilon)^{-1} \frac{g}{12\pi^2\epsilon}. \tag{D.19}$$

Appendix E

SC One-Loop Diagrams with a Finite Wavenumber Cutoff

In this Appendix we show that employing a finite cutoff leads to ambiguities when we evaluate the sliding columnar one-loop diagrams. These diagrams are shown in Fig. C.2; (a) contributes to $\Sigma_1(\mathbf{q})$ and both (b) and (c) contribute to $\Sigma_2(\mathbf{q})$ and $\Sigma_3(\mathbf{q})$. The ambiguous result is that we obtain different answers for $\Sigma(\mathbf{q})$ depending on whether external momentum q is sent through the top or bottom part of the internal loop. The ambiguity develops when momentum q_x appears in the internal loop and the top and bottom paths through the internal loop are different. The diagram that causes this ambiguity is the q_x^4 part of Fig. C.2(b). We can see this by calculating the q_x^4 corrections to the vertex function, $\Sigma_3^b(\text{top})$ and $\Sigma_3^b(\text{bot})$, which result from sending $\mathbf{k}+\mathbf{q}$ through the top(bottom) sections of the internal loop.

$$\Sigma_3^b(\text{top}) = -q_x^2 \int_\Lambda \frac{d^3k}{(2\pi)^3} \left[k_z^2 (k_x + q_x)^2 G(-\mathbf{k}) G(\mathbf{k}+\mathbf{q}) \right], \tag{E.1}$$

and

$$\Sigma_3^b(\text{bot}) = -q_x^2 \int_\Lambda \frac{d^3k}{(2\pi)^3} \left[k_x^2 (k_z + q_z)^2 G(-\mathbf{k}) G(\mathbf{k}+\mathbf{q}) \right], \tag{E.2}$$

where Λ is a finite wavenumber cutoff and $G(\mathbf{q})$ was defined previously in (D.4). With $\Lambda \neq \infty$,

$$\Sigma_3^b(\text{top}) \neq \Sigma_3^b(\text{bot}). \tag{E.3}$$

If we employ dimensional regularization instead and send $\Lambda \to \infty$, these top and bottom amplitudes are identical.

Bibliography

[1] J. Als-Nielson, J. D. Lister, R. J. Birgeneau, M. Kaplan, C. R. Safinya, A. Lindegaard-Anderson, and S. Mathiseen. *Phys. Rev. B* **22**, 312 (1980).

[2] D. J. Amit, *Field theory, the renormalization group, and critical phenomena* (World Scientific, Singapore, 1984); J. Zinn-Justin, *Quantum field theory and critical phenomena* (Oxford University Press, New York, 1993).

[3] F. Artzner, R. Zantl, G. Rapp, and J. O. Rädler. *Phys. Rev. Lett* **81**, 5015 (1998).

[4] R. Bruinsma and J. Marshl, *Europhys. Lett.* **41**, 165 (1998).

[5] R. Bruinsma, *Eur. Phys. J. B* **4**, 75 (1998).

[6] P.M. Chaikin and T.C. Lubensky, *Principles of condensed matter physics*, Chapter 6, (Cambridge University Press, Cambridge, 1995).

[7] R. G. Crystal, *Science* **270**, 404 (1995).

[8] Seminal experiments using DNA-lipid complexes for gene therapy are discussed in P. L. Felgner, *et al.*, *Proc. Natl. Acad. Sci. USA* **84**, 7413 (1987).

[9] L. Golubović and Z.-G. Wang, *Phys. Rev. E* **49**, 2567 (1994).

[10] L. Golubović and M. Golubović, *Phys. Rev. Lett.* **80**, 4341 (1998). Erratum *ibid.* **81**, 5704 (1998).

[11] G. Grinstein and R. Pelcovits, *Phys. Rev. Lett.* **47**, 856 (1981); Phys. Rev. A **26** 915 (1982).

[12] B. I. Halperin, T. C. Lubensky, and S. Ma, Phys. Rev. Lett. **32**, 292 (1974).

[13] I. Koltover, T. Salditt, J. O. Rädler, C. R. Safinya. *Science* **281**, 78 (1998).

[14] I. Koltover, T. Salditt, J.-L. Rigaud, and C.R. Safinya. *Phys. Rev. Lett.* **81**, 2494 (1998); I. Koltover, (unpublished).

[15] J. M. Kosterlitz and D. J. Thouless. *J. Phys. C: Solid State Phys.* **6**, 1181 (1973); J. M. Kosterlitz. *J. Phys. C: Solid State Phys.* **7**, 1046 (1974).

[16] B. W. Lee, "Gauge Theory" in *Methods in Field Theory*, Les Houches Session XXVIII, (North-Holland Press, Amsterdam, 1976).

[17] F. Livolant, Physica A **176**, 117 (1991).

[18] See for example, D. R. Nelson and L. Radzihovsky, *Phys. Rev. A* **44**, 3525 (1991), D. Morse and T. C. Lubensky, *Phys. Rev. A* **45**, R2151 (1991), and L. Radzihovsky and J. Toner, *Phys. Rev. E* **57**, 1832 (1998).

[19] D. R. Nelson and J. Toner, *Phys. Rev. B* **24**, 363 (1981).

[20] C. S. O'Hern and T. C. Lubensky. Sliding Columnar Phase of DNA-Lipid Complexes. *Phys. Rev. Lett.* **80**, 4345 (1998).

[21] C.S. O'Hern and T. C. Lubensky. *Phys. Rev. E* **58**, 5948 (1998).

[22] C.S. O'Hern, T.C. Lubensky, and J. Toner, submitted to *Phys. Rev. Lett.*

[23] C. S. O'Hern, T. C. Lubensky, and J. Toner (unpublished).

[24] C.S. O'Hern, L. Golubović, and T.C. Lubensky (unpublished).

[25] F. Oosawa, *J. of Polym. Sci.* **23**, 421 (1957); G. S. Manning, *J. Chem. Phys.* **51**, 924 (1969); *ibid.* **51**, 3249 (1969); M. LeBret, B. Zimm, *Biopolym.* **23**, 287 (1984).

[26] J. O. Rädler, I. Koltover, T. Salditt, and C. R. Safinya. *Science* **275**, 810 (1997).

[27] C. R. Safinya, D. Roux, G. S. Smith, S. K. Sinha, P. Dimon, N. A. Clark, and A. M. Bellocq. *Phys. Rev. Lett.* **57**, 2718 (1986).

[28] T. Salditt, I. Koltover, J. O. Rädler, and C. R. Safinya. *Phys. Rev. Lett.* **79**, 2582 (1997).

[29] T. Salditt, I. Koltover, J. O. Rädler, and C. R. Safinya. *Phys. Rev. E* **58**, 889 (1998).

[30] H. Schiessel, *Eur. Phys. J. B* **6**, 373 (1998).

[31] J. Toner and D.R. Nelson, *Phys. Rev. B* **23**, 316 (1981).

[32] K. G. Wilson and J. Kogut, *Phys. Rep. C* **12**, 77 (1974); J. Rudnick and D. R. Nelson, *Phys. Rev. B* **13**, 2208 (1976).

[33] R. Zantl, F. Artzner, G. Rapp, and J. O. Rädler, *Eur. Phys. Lett.* **45**, 90 (1999).